NUREG/CR-4490 Vol. I
ANL-85-75 Vol. I

NUREG/CR-4490 Vol. I
ANL-85-75 Vol. I

LIGHT-WATER-REACTOR SAFETY MATERIALS ENGINEERING RESEARCH PROGRAMS: QUARTERLY PROGRESS REPORT

January–March 1985

ARGONNE NATIONAL LABORATORY, ARGONNE, ILLINOIS
Operated by THE UNIVERSITY OF CHICAGO

Prepared for the Office of Nuclear Regulatory Research
U. S. NUCLEAR REGULATORY COMMISSION
under Interagency Agreement DOE 40-550-75

Argonne National Laboratory, with facilities in the states of Illinois and Idaho, is owned by the United States government, and operated by The University of Chicago under the provisions of a contract with the Department of Energy.

Available from

Superintendent of Documents
U. S. Government Printing Office
Post Office Box 37082
Washington, D.C. 20013-7982

and

National Technical Information Service
Springfield, VA 22161

NUREG/CR-4490 Vol. I
ANL-85-75 Vol. I

(Distribution
Code: R5)

ARGONNE NATIONAL LABORATORY
9700 South Cass Avenue
Argonne, Illinois 60439

LIGHT-WATER-REACTOR SAFETY MATERIALS ENGINEERING RESEARCH PROGRAMS: QUARTERLY PROGRESS REPORT

January—March 1985

Date Published: March 1986

Previous reports in this series

ANL-8460 Vol. I	January—March 1984
ANL-8460 Vol. II	April—June 1984
ANL-85-33	October 1983—September 1984
ANL-85-20	October 1983—September 1984
ANL-84-60 Vol. III	October—December 1984

Prepared for the Division of Engineering Technology
Office of Nuclear Regulatory Research
U. S. Nuclear Regulatory Commission
Washington, D. C. 20555
Under Interagency Agreement DOE 40-550-75

NRC FIN Nos. A2212 and A2243

LIGHT-WATER-REACTOR SAFETY
MATERIALS ENGINEERING RESEARCH PROGRAMS:
QUARTERLY PROGRESS REPORT

January--March 1985

ABSTRACT

This progress report summarizes work performed by the Materials Science and Technology Division of Argonne National Laboratory during January, February, and March 1985 on water reactor safety problems. The research and development areas covered are Environmentally Assisted Cracking in Light-Water Reactors and Long-Term Embrittlement of Cast Duplex Stainless Steels in Light-Water-Reactor Systems.

NRC Fin No.	FIN Title
A2212	Environmentally Assisted Cracking in Light-Water Reactors
A2243	Long-Term Embrittlement of Cast Duplex Stainless Steels in LWR Systems

TABLE OF CONTENTS

TABLE OF CONTENTS (Contd.)

LIGHT-WATER-REACTOR SAFETY
MATERIALS ENGINEERING RESEARCH PROGRAMS:
QUARTERLY PROGRESS REPORT

January--March 1985

EXECUTIVE SUMMARY

I. ENVIRONMENTALLY ASSISTED CRACKING IN LIGHT-WATER REACTORS[a]

Analysis of reactor components has continued to verify the results of in-service inspections and to evaluate the effectiveness of remedial treatments applied to these components. Two 22-in. diameter recirculation header-endcap overlay weldments from the Hatch-2 BWR were evaluated by dye penetrant tests (PT). Axial, circumferential, and skewed-type PT indications were observed within 10 mm of the weld fusion line on the endcap side of one of the weldments and no indications were found on the other. Strain gages were mounted on one of the weldments to measure residual stresses. A Type 347 SS 16-in. diameter pipe weldment fabricated according to the German GTAW welding process was also examined. A weld defect (a cavity) and intergranular cracking to a depth of 75 μm were observed at the weld fusion line on the inner surface of the pipe. Sensitization measurements in the heat-affected zone by the ASTM A262-A and EPR techniques indicate that the weldment is resistant to sensitization as expected.

Microstructural changes resulting from welding and subsequent thermal exposure of austenitic stainless steels are collectively known as sensitization, which is one of the causitive factors in intergranular stress corrosion cracking (IGSCC) of these materials in LWR environments. The role of impurity elements, such as sulfur and phosphorus in the alloys, in SCC has been investigated to a lesser extent than chromium depletion by carbide precipitation at grain boundaries; however, impurity segregation may be a contributing factor to IGSCC. Scanning-transmission-electron microscopy measurements were performed on sulfur- and phosphorus-doped specimens of Type 304 SS after aging

[a]NRC FIN No. A2212; NRC Contact: A. Taboada.

for 300 h at 550°C. The results show that phosphorus promotes chromium depletion and carbide precipitation at grain boundaries whereas sulfur does not.

The effect of nitrogen concentration in several heats of Type 316 SS on SCC susceptibility has been investigated in CERT experiments in 289°C water containing dissolved oxygen and sulfate at low concentrations. The results show that nitrogen concentrations of >0.1 wt % have an adverse effect on transgranular stress corrosion cracking (TGSCC) of the materials. The SCC behavior of Type 347 NG SS was compared with that of Type 316 NG SS at the same temperature and water-chemistry conditions as in the previous experiments. The results of this work indicate that TGSCC in the Type 347 NG SS material occurred at lower strain rates, i.e., $<5 \times 10^{-7}$ s^{-1}, than were required for the other material, which is indicative of slightly better SCC resistance; however, the average crack growth rates were not very different for the two steels.

To obtain better insight into the effects of impurities on the SCC behavior of sensitized Type 304 SS, CERT tests were performed in 289°C water which contained different oxyacids (viz., HNO_3, H_3AsO_4, H_2SO_4, $HClO_4$, and H_3BO_3) at low dissolved-oxygen concentrations (<0.02 ppm). The crack growth rates were correlated with the conductivity and the concentrations of the various acids in the feedwater as well as the electrochemical potentials of the steel and platinum. The results indicate that the crack growth rate in these environments appears to be controlled by the rate of cathodic reduction of oxyacid anions that have a central atom which can assume different oxidation states. The acids mentioned above have this characteristic, with the exception of H_3BO_3. In the boric acid environments, the transgranular crack growth rate of the steel was relatively low and independent of the anion concentration over the range of 1 to 10,000 ppm.

The different oxyacids have a diverse effect on the open-circuit corrosion potential of the steel and the redox potential of the platinum electrode in high-temperature water at low dissolved-oxygen concentrations. For example, the potentials increase over a wide range [i.e., -450 to +500 mV(SHE)] when the concentrations of HNO_3, H_3AsO_4, or $HClO_4$ in the water

increase, whereas H_2SO_4 and H_3BO_3 cause a relatively small increase in the potentials [e.g., -550 to -450 mV(SHE)], owing to the decrease in the pH of the water. As a consequence of this behavior, IGSCC can proceed at a rapid rate for open-circuit corrosion potentials between -450 and +500 mV(SHE), depending upon the type and concentration of the impurity species in the water. Therefore, knowledge of only the corrosion or redox potential is not sufficient to predict whether the steel is susceptible to IGSCC in high-temperature water. The potential values must be used in conjunction with information on the type of impurities in the feedwater, in addition to dissolved oxygen.

To validate results from CERT tests on the effects of dissolved oxygen, hydrogen, and sulfate on SCC susceptibility of Type 304 SS, long-term crack growth experiments were performed on fracture-mechanics-type specimens of the steel under simulated BWR water chemistry conditions at 289°C. The water chemistry was varied from a reference condition (0.2 ppm dissolved oxygen and 0.1 ppm sulfate as H_2SO_4) to a lower dissolved-oxygen concentration (0.002 ppm) without and with 1.4 ppm hydrogen as well as to higher and lower sulfate concentrations at a fixed oxygen concentration in the water. The results showed that crack growth in the sensitized specimens virtually ceased when the dissolved-oxygen concentration was decreased to the low level, and also when sulfate was removed from the reference environment containing 0.2 ppm dissolved oxygen. Crack growth in the solution annealed as well as the sensitized specimens ceased when hydrogen was added to the low-oxygen feedwater containing 0.1 ppm sulfate. These crack growth results are consistent with the more extensive CERT data regarding the effects of water chemistry and corrosion potential on SCC susceptibility of the steel in high-temperature water.

II. LONG-TERM EMBRITTLEMENT OF CAST-DUPLEX STAINLESS STEELS IN LWR SYSTEMS[b]

Thermal aging, mechanical-property testing, and microstructural evaluations of cast duplex stainless steels are in progress to determine the possibility of in-service embrittlement of these steels under light-water

[b]NRC FIN No. A2243; NRC Contact: J. Muscara.

reactor operating conditions and to evaluate possible remedies to potential embrittlement problems for existing and future plants.

Material was obtained from nineteen small and six large experimental heats as well as six commercial heats of CF-3, -8, and -8M grades of cast-duplex stainless steels. Blanks for Charpy-impact, compact tension, and tensile specimens from the various materials are being aged at several temperatures between 290 and 450°C for time periods up to 50,000 h. A cover plate assembly of cast stainless steel from the recirculation pump of the KRB reactor, which was in service for ~12 yr, was also procured for microstructural characterization and mechanical testing.

Characterization of the six large experimental heats has been completed. All heats contain a mixed structure of columnar and equiaxed grains. The ferrite content and morphologies and hardness of these heats are similar to those observed for the small experimental heats with comparable chemical compositions.

Charpy-impact tests have been conducted on specimens from the experimental and commercial heats of the steels after aging for up to 3000 h at 320, 350, 400, and 450°C. The reduction in the room-temperature impact energy increases with the ferrite content of the material and the aging temperature. The low-carbon grades of the cast materials exhibit greater resistance to embrittlement than the CF-8 and -8M grades.

Microstructures of cast-duplex stainless steels subjected to long-term aging either in the laboratory or in reactor service have been characterized. The results indicate that at least two processes contribute to the low-temperature embrittlement of duplex stainless steels, viz., weakening of the ferrite/austenite phase boundary by carbide precipitation and embrittlement of the ferrite matrix by the formation of additional phases such as G-phase, Type X, or the α' phase.

I. ENVIRONMENTALLY ASSISTED CRACKING IN LIGHT-WATER REACTORS

Principal Investigators:
W. J. Shack, T. F. Kassner, P. S. Maiya,
J. Y. Park, and W. E. Ruther

The objective of this program is to develop an independent capability for prediction, detection, and control of intergranular stress corrosion cracking (IGSCC) in light-water reactor systems. The program is primarily directed at IGSCC problems in existing plants, but also includes the development of recommendations for plants under construction and future plants. The scope includes the following: (1) evaluation of the influence of metallurgical variables, stress, and the environment on IGSCC susceptibility, including the influence of plant operations on these variables; and (2) examination of practical limits for these variables to effectively control IGSCC in LWR systems. The experimental work concentrates primarily on problems related to pipe cracking in BWR systems. However, ongoing research work on other environmentally assisted cracking problems involving pressure vessels, nozzles, and turbines will be monitored and assessed, and where unanswered technical questions are identified, experimental programs to obtain the necessary information will be developed to the extent that resources permit.

The effort is divided into five subtasks: (A) Long-Term Aging and Analysis of Reactor Components; (B) Crack Growth Rate Studies; (C) Evaluation of Nonenvironmental Corrective Actions; (D) Evaluation of Environmental Corrective Actions; and (E) Mechanistic Studies. These subtasks reflect the major technical concerns associated with IGSCC in LWR systems, namely: the role of materials susceptibility, the role of stress in crack initiation and propagation, and the role of environment. The program seeks to evaluate potential solutions to IGSCC problems in LWRs, both by direct experimentation (including full-scale pipe tests) and through the development of a better understanding of the various phenomena.

A. Effects of Long-Term Aging and Analysis of Reactor Components (J. Y. Park and W. J. Shack)

1. Introduction

The microstructural changes resulting from thermal exposure that produce susceptibility to intergranular corrosion are collectively known as sensitization. Sensitization is one of the major causative factors in the IGSCC of austenitic stainless steels in LWR environments. Under normal isothermal heat treatments, sensitization of austenitic stainless steels (SS) such as Types 304 and 316 occurs in the temperature range of ∿500 to 850°C. However, Type 304 SS may be sensitized at temperatures below this range if carbide nuclei are present at grain boundaries. This low-temperature sensitization (LTS) phenomenon has been demonstrated in laboratory experiments in the temperature range from 350 to 500°C. Extrapolations to plant operating temperatures (288°C) yield estimated times for significant LTS to occur ranging from 10 to 1000 years. This wide variation has been attributed to differences in plastic strain levels, dislocation densities, and/or impurity element content, but with the current level of understanding, the susceptibility to LTS of arbitrary heats of material cannot be assessed. It is also not clear that the susceptibility to IGSCC produced by long, relatively low-temperature thermal aging can be adequately assessed by conventional measures of the degree of sensitization (DOS), such as the electrochemical potentiokinetic reactivation (EPR) technique or ASTM A262 Practices A through E. These tests have been developed and qualified primarily on the basis of the IGSCC susceptibility produced by high-temperature furnace sensitization or welding.

Analysis of in-reactor components is also a concern of this task. It has become increasingly important to verify the results of in-service inspections and to assess the effectiveness of remedial treatments under in-reactor conditions.

2. Technical Progress

a. Long-Term Aging

Scanning-transmission-electron microscopy (STEM) work is continuing on Type 304 SS (Heat No. 10285) specimens that have been given various heat treatments, and four other heats of Type 304 SS doped with sulfur (0.05 and 0.09 wt.%) and phosphorus (0.04 and 0.09 wt.%). Results from these analyses will help to assess the role of the irradiation-induced grain boundary segregants (phosphorus, sulfur, silicon, etc.) and the relative contribution of chromium depletion and grain boundary segregation to SCC susceptibility.

During this reporting period, sulfur- and phosphorus-doped materials were examined after aging at 550°C for 300 h and at 500°C for 1000 h. The STEM specimens were prepared by jet polishing of thin disks in a 25 vol.% HNO_3:75 vol.% methanol electrolyte with a current density of 16-22 mA/mm^2 at a temperature of -20 to -30°C. The phosphorus-doped specimens showed a large number of precipitates (~20-50 nm in diameter) at grain boundaries whereas the sulfur-doped specimens were virtually free of grain boundary precipitates for both aging conditions, as shown in Figs. 1.1 and 1.2.

Elemental concentration profiles across high-angle grain boundaries were measured for the specimens aged at 550°C for 300 h. The effect of electron beam size and broadening on the concentration profile was corrected by deconvolution of measured values. The results for chromium are shown in Fig. 1.3. Grain-boundary chromium depletion has occurred in the phosphorus-doped specimens in a region 200-300 nm in width, whereas no chromium depletion was found in the sulfur-doped specimens. ASTM A262-A tests confirm the STEM observations. The phosphorus-doped specimens showed ditching at grain boundaries, while the sulfur-doped specimens did not (Figs. 1.4 and 1.5). Phosphorus appears to strongly promote grain boundary carbide precipitation. In the next reporting period, chromium concentration profiles will be measured for the specimens aged at 500°C for 1000 h.

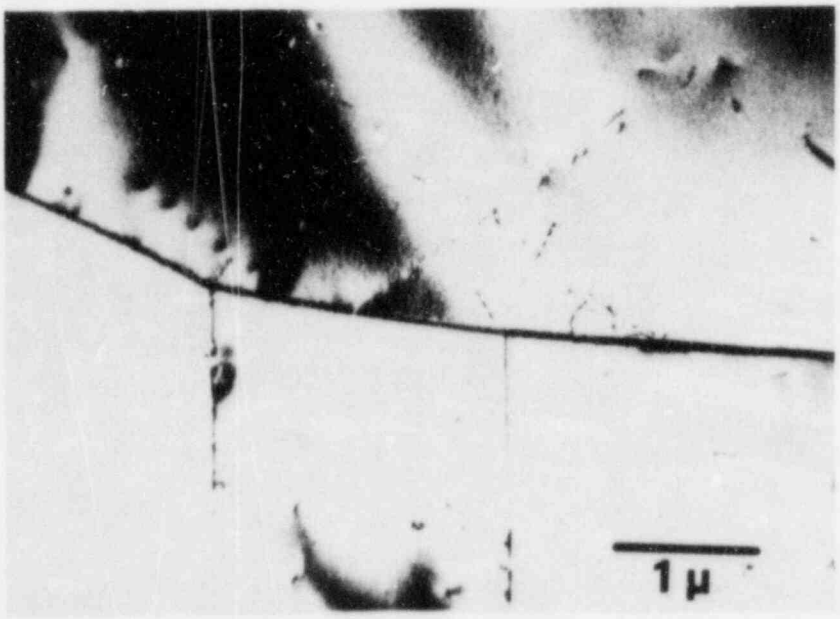

(a)

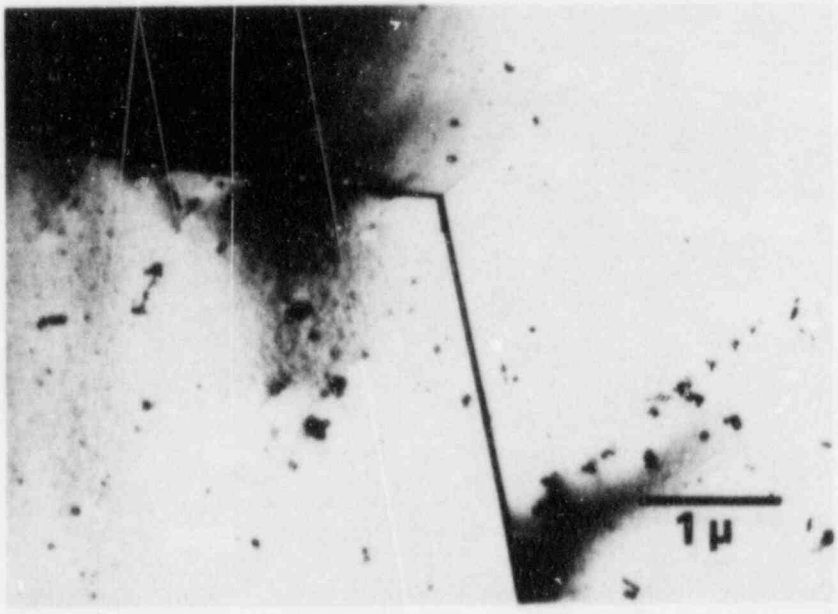

(b)

Fig. 1.1. Grain Boundaries of Doped Type 304 SS Aged at 550°C for 300 h. (a) 0.05% S, (b) 0.09% S, (c) 0.04% P and (d) 0.09% P. Sulfur-doped specimens are free of grain boundary precipitates while phosphorus-doped specimens show grain boundary carbide precipitates.

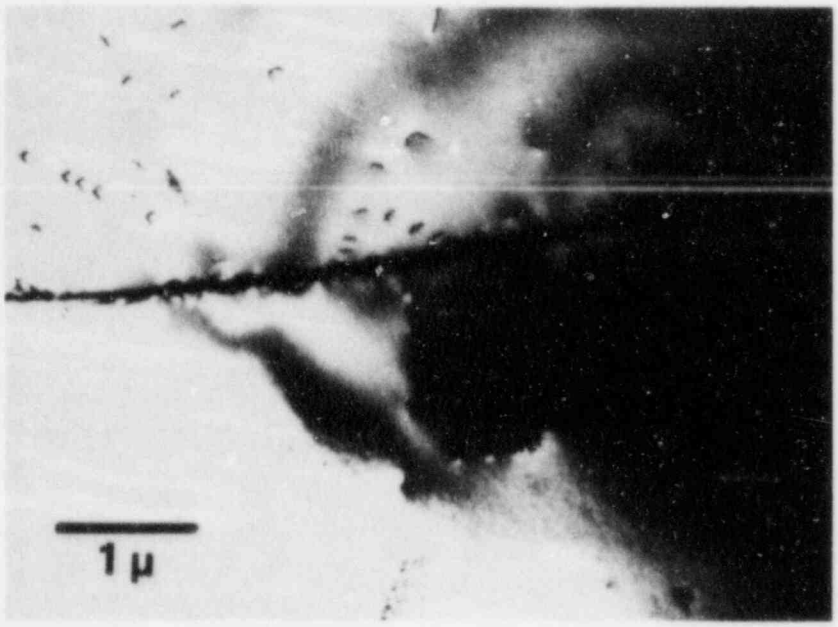

(c)

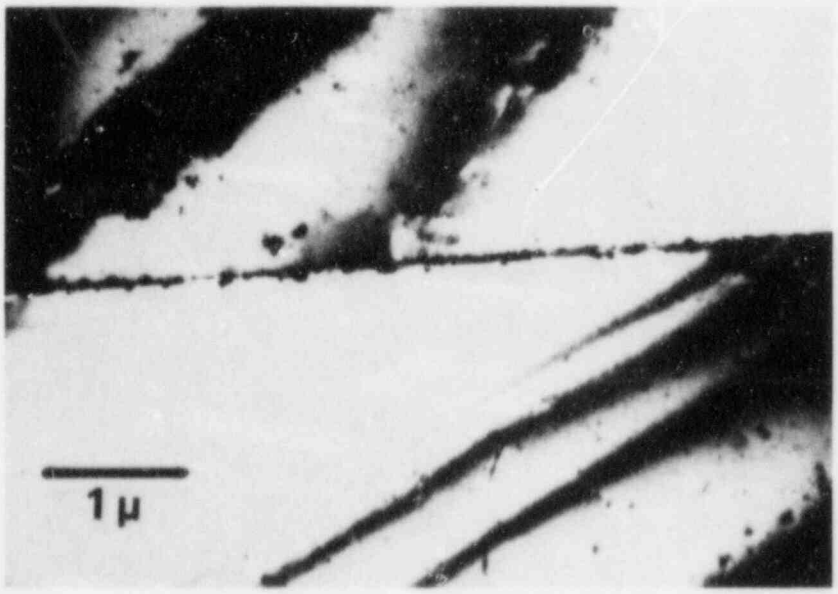

(d)

Fig. 1.1. Continued.

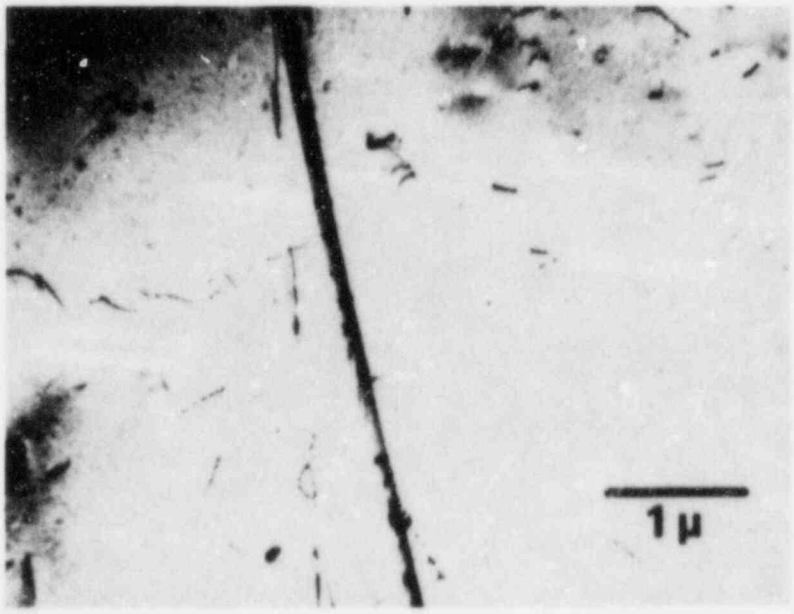

(a)

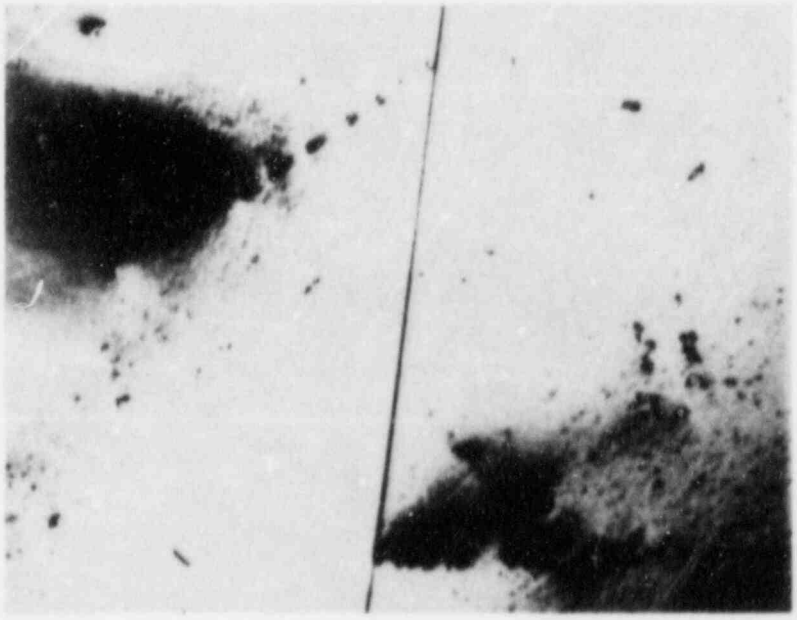

(b)

Fig. 1.2. Grain Boundaries of Doped Type 304 SS Aged at 500°C for 1000 h. (a) 0.05% S, (b) 0.09% S, (c) 0.04% P, and (d) 0.09% P. Phosphorus-doped specimens show grain boundary carbide precipitates.

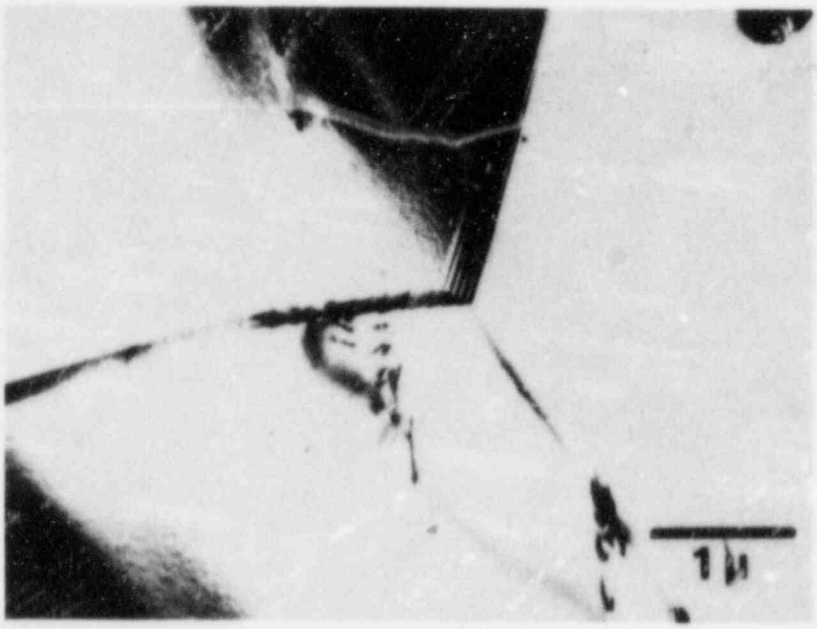

(c)

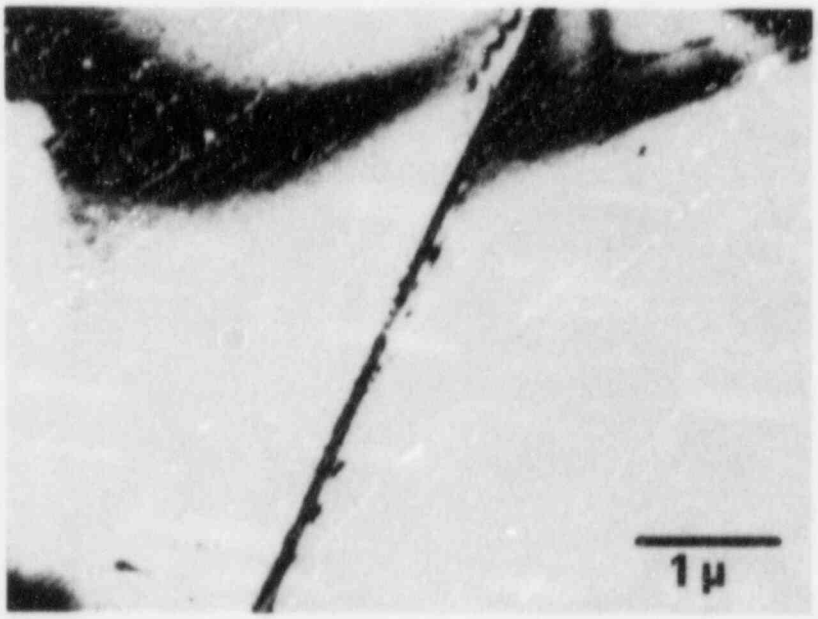

(d)

Fig. 1.2. Continued.

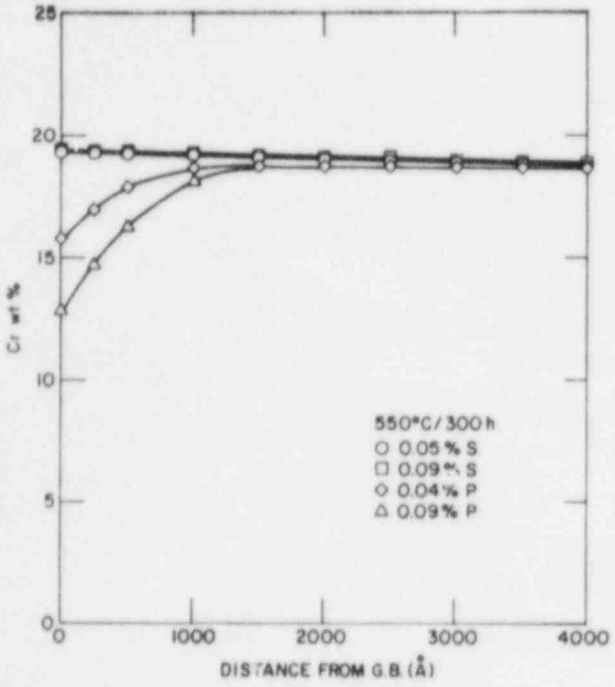

Fig. 1.3.

Chromium Concentration Profile for Doped Type 304 SS Aged at 550°C for 300 h.

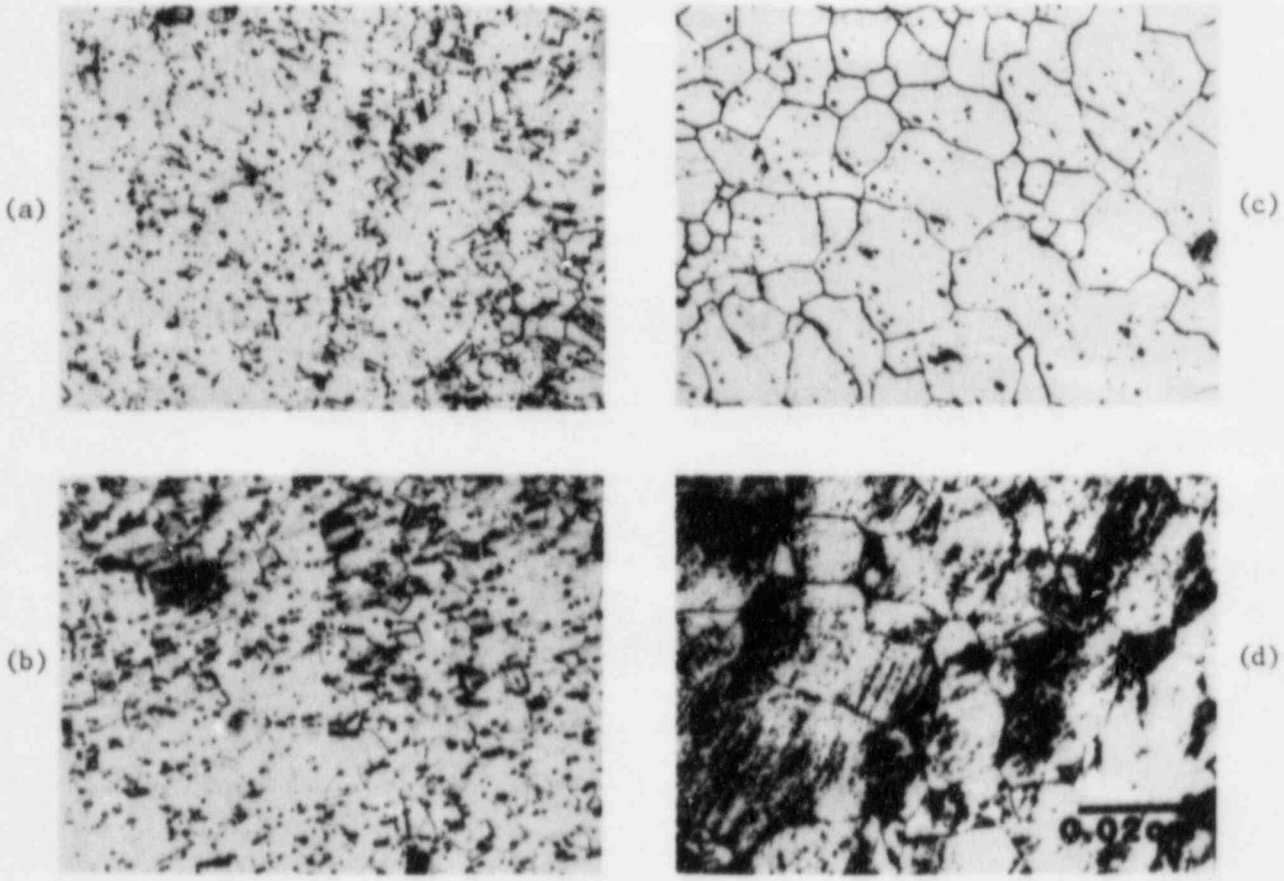

Fig. 1.4. ASTM A262-A Test Results for Doped Type 304 SS Aged at 550°C for 300 h. (a) 0.05% S, (b) 0.09% S, (c) 0.04% P, and (d) 0.09% P.

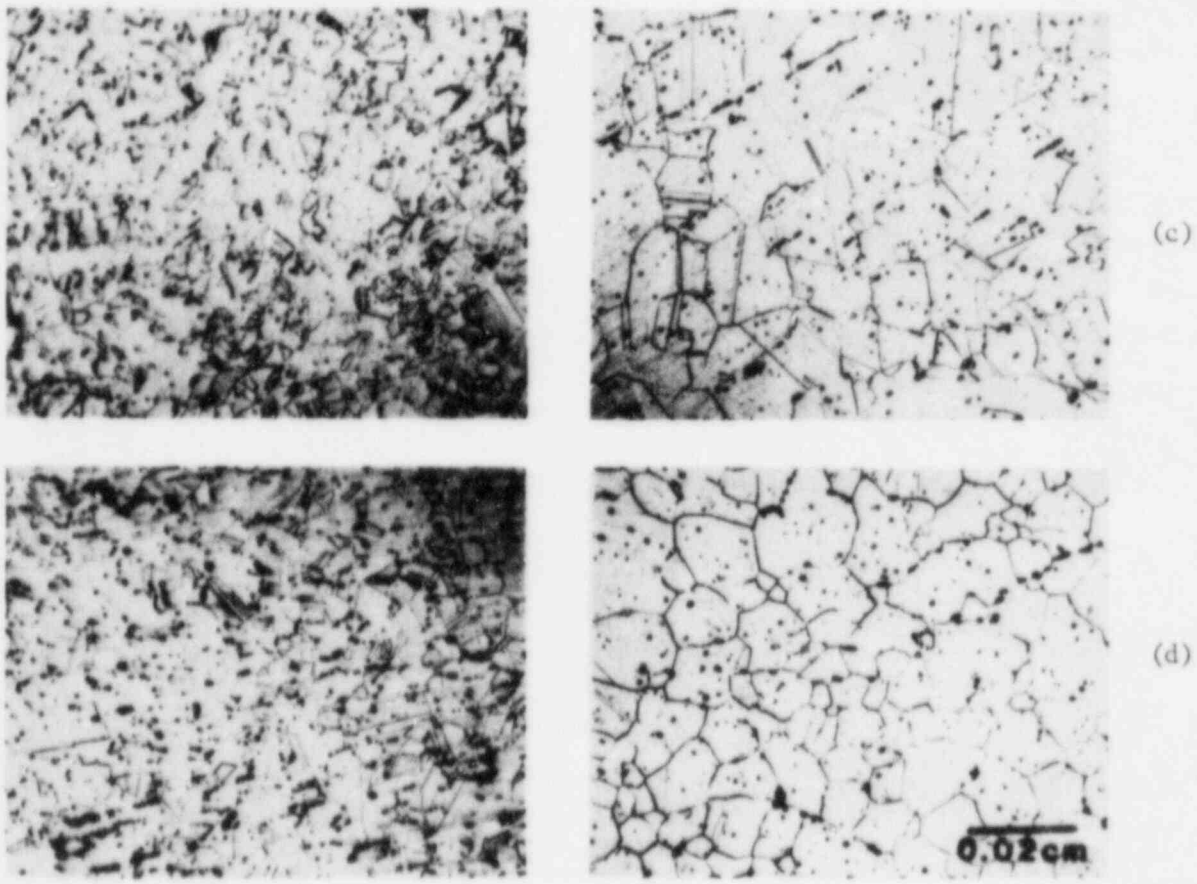

Fig. 1.5. ASTM A262-A Test Results for Doped Type 304 SS Aged at 500°C for 1000 h. (a) 0.05% S, (b) 0.09% S, (c) 0.04% P, and (d) 0.09% P.

A Type 347 SS (Mannesmann TP347 DIN 1.4550) 16-in.-diameter pipe weldment fabricated according to the German GTAW welding process was examined. Intergranular cracking to a depth of 75 μm was observed at the weld fusion line of the inner surface of the pipe (Figs. 1.6 and 1.7), and a weld defect (cavity) was also observed at the weld fusion line (Fig. 1.8). Sensitization of the material was examined by the ASTM A262-A test and EPR measurements. The ASTM A262-A test did not show grain boundary ditching except slight indications near the weld fusion line. Some intragranular precipitates were observed (Fig. 1.9). EPR values were measured in the HAZ, although no standard EPR measurement procedure has been established for Type 347 SS. The measurements were made using the prevailing procedure for Type 304 SS with 1- and 2-mv/s scan rates. The maximum EPR value (0.9 C/cm^2 at

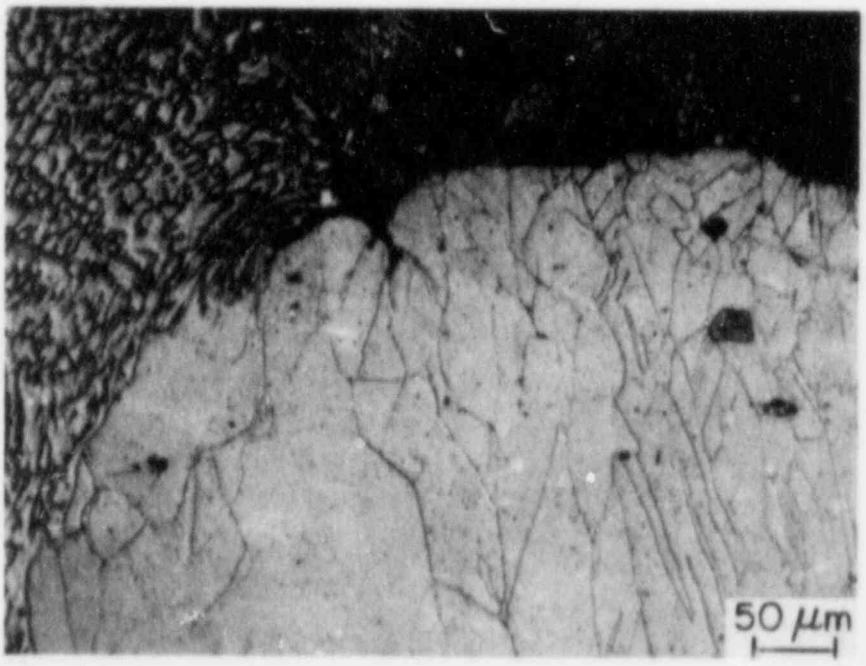

Fig. 1.6. Intergranular Crack At and Near Weld Fusion Line of Type 347 SS Weldment: Etched.

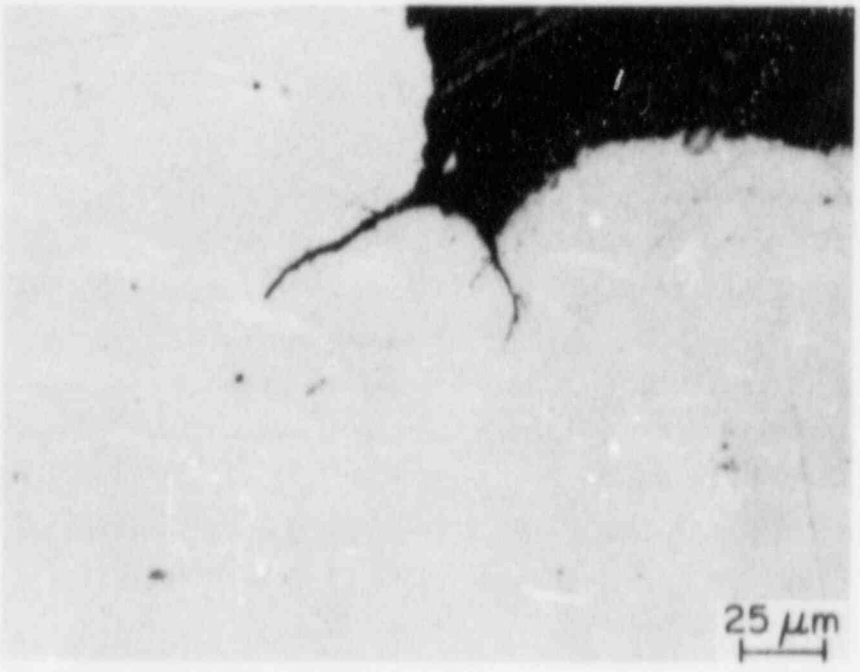

Fig. 1.7. Intergranular Crack At and Near Weld Fusion Line of Type 347 SS Weldment: As Polished.

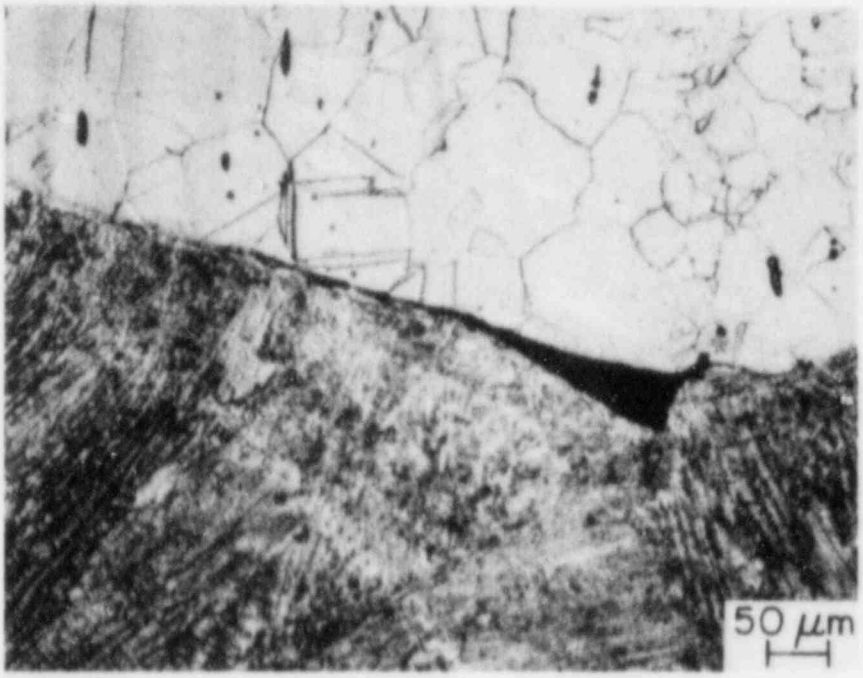

Fig. 1.8. Cavity at Weld Fusion Line of Type 347 SS Weldment.

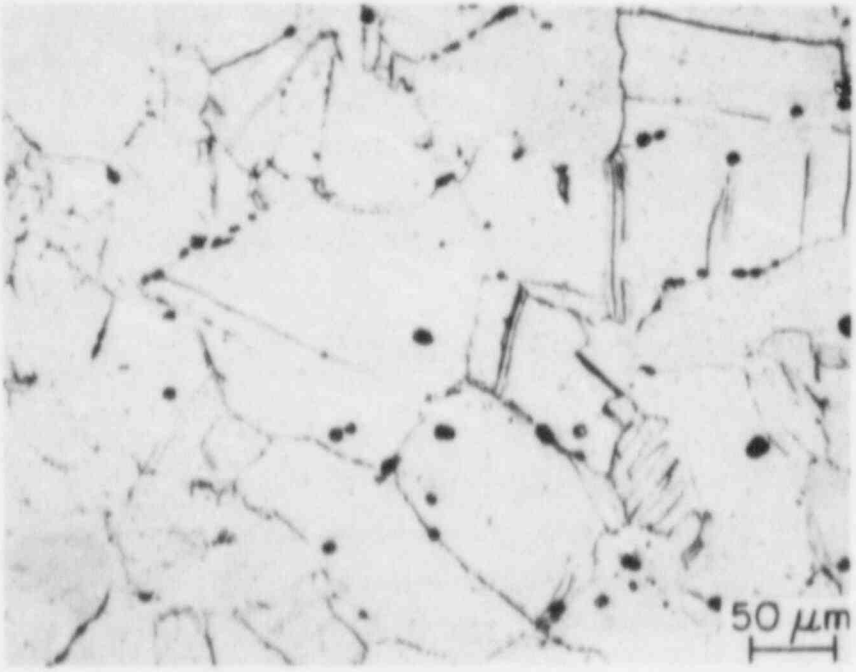

Fig. 1.9. Grain Boundary and Intragranular Precipitates Near Weld Fusion Line of Type 347 SS Weldment Revealed by ASTM A262-A Test.

1 mv/s) was observed in an area less than 0.2 mm from the weld fusion line, and then the values decreased to about 0.2 C/cm^2 (at 1 mv/s) beyond 1 mm from the weld fusion line (Fig. 1.10). The EPR results are consistent with the ASTM A262-A test results, and indicate that the Type 347 SS weldment is resistant to sensitization as expected.

IGSCC initiation in a furnace-sensitized (EPR 10 C/cm^2) Type 304 SS (Heat No. 10285) specimen was examined after a 1000-h test at a constant stress level of 1.5 σ_y in high-purity water with 8 ppm oxygen at 289°C. An intergranular crack had initiated at surface pits on a grain boundary (Fig. 1.11). Surface pits were also observed that were not on grain boundaries, but no cracks developed at these sites. The surface pitting appears to be due to the dissolution of precipitates or inclusions. The constant-load SCC test was resumed for an extended test period.

Low-temperature aging is continuing at 289, 315, 350, and 400°C of Type 304 SS specimens (Heat Nos. 10285 and 53319) subjected to controlled strains, Type 304 SS weld specimens (Heat No. 53319) treated by IHSI, HSW, and CRC, Type 347 SS (Mannesmann TP347 DIN 1.4550) weld specimens, and Type 316NG SS weld specimens (Heat No. P91576).

Type 304 SS (Heat No. 53319) pipe weldments were examined after aging at 400°C for 4000 h. An ASTM A262-A test produced a dual etch structure at a localized area far outside of the HAZ. This may be an indication of material inhomogeneity caused by long-term aging.

b. In-Reactor Components

Two 22-in.-diameter recirculation header-endcap overlay weldments (2B31-1RC-22BM-1 and 2B31-1RC-22AM-X) from the Hatch-2 reactor were received. The inner surfaces of the pipes were electrolytically polished by Quadrex Corporation before shipment to ANL. Postweld grinding marks were visible in some areas of the inner surface at the weld crown and the HAZ. The width of the overlay was approximately 200 mm for the weldment 22BM and 230 mm for the 22AM weldment. The thicknesses of the overlays were approximately 10-15 and 9-10 mm, respectively.

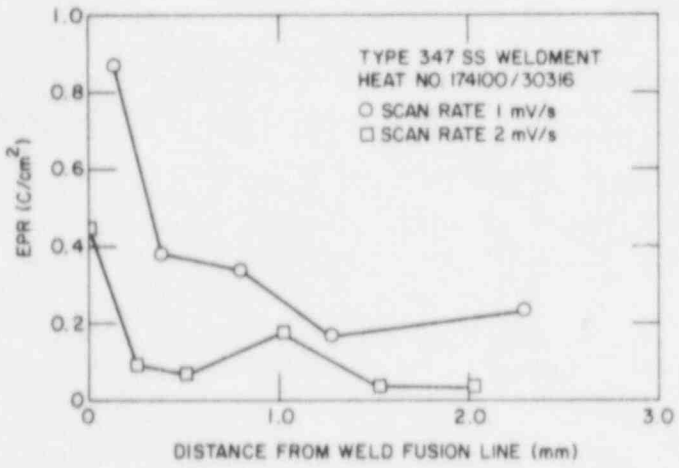

Fig. 1.10. EPR Measurements for Type 347 SS Weldment.

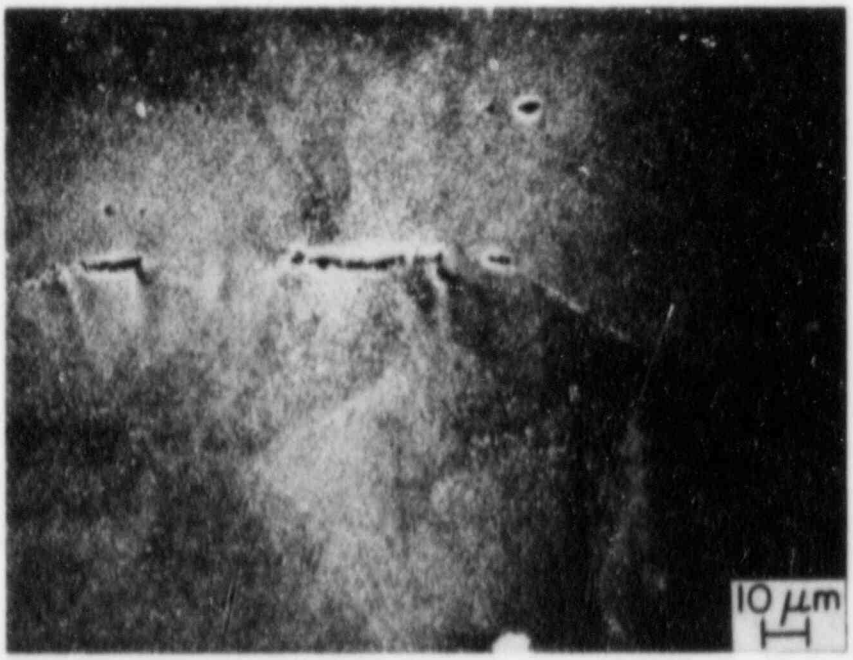

Fig. 1.11. IGSCC Initiation at Grain Boundary Pits after Constant-Load SCC Test in High-Purity Water for 1000 h.

Magnaflux dye penetrant was applied to the inner surface of both weldments. A number of PT indications were observed on the endcap side of weldment 22BM at circumferential positions between 129 cm and 147 cm. Postweld grinding was also evident in this region. The PT indications were axial, circumferential, and skewed types and were located within 10 mm from the weld fusion line. There were no PT indications in the weldment 22AM.

Strain gages were mounted on the complete 22-in.-diameter weldment 22BM to measure residual stresses. Two-inch-diameter throughwall plugs that surround the strain gages are being cut from the weldment. Metallographic examination will begin after residual stress measurements are completed.

B. Crack Growth Rate Studies (J. Y. Park and W. J. Shack)

1. Introduction

Early instances of IGSCC in operating BWRs generally occurred in small pipes, and the response to the detection of cracks was to repair or replace the cracked piping immediately. It is now clear that for reactors with standard Type 304 SS piping material, cracking can occur anywhere in the recirculation system, including the main recirculation line. Because of the severe economic consequences of long forced outages for repair or replacement, utilities must consider other approaches for dealing with cracked pipe. The possibilities include continued operation and monitoring for subsequent growth for an indefinite period, continued operation and monitoring until a repair can be scheduled to minimize outage, or immediate repair and replacement.

Understanding crack growth behavior is important for other reasons besides assessing the safety implications of flawed piping. A better understanding would permit a more rational extrapolation of laboratory test results to the prediction of behavior in operating plants. Current work on the measurement of crack growth rates seeks to characterize these rates in terms of the linear-elastic-fracture-mechanics (LEFM) stress intensity as well as the level of sensitization and the amount of oxygen present in the

coolant. The work in this subtask is aimed at a systematic evaluation of the validity of LEFM to predict IGSCC growth. The capability of data obtained under one type of loading history to predict crack growth under a different loading history is being investigated. The effect of flaw geometry on crack propagation rates will also be considered.

2. Technical Progress

Crack growth rate tests have continued on a Type 304 SS 1TCT weld overlay specimen (No. 304-01-01) in high-purity water with 8 ppm of dissolved oxygen at 289°C. The specimen was prepared from a 12-in.-diameter pipe weldment with a mockup weld overlay. The specimen was fabricated such that the crack will propagate through the HAZ of the original weld and into the overlay. The tests have been performed under cyclic loading (sawtooth waveform with an unloading time of 5 s at 2×10^{-3} Hz, K_{max} = 27-29 MPa·$m^{1/2}$, and R = 0.8-1.0. The crack length is being monitored by an a.c. potential system and by an in situ MTS clip gage. The results of the tests are summarized in Table 1.1. The crack, however, is in the HAZ and has not reached the overlay. The observed growth rates do not vary with R-value over this range. A negligible effect of small load fluctuations was also observed for furnace-sensitized Type 304 SS (Heat No. 10285).[1] The test will be continued to determine the crack growth rate in the overlay.

TABLE 1.1. Crack Growth Rates in the HAZ of a Weld Overlay Specimen

R	Frequency, Hz	K_{max}, MPa·$m^{1/2}$	Growth Rate, m/s
1.0	-	29	1.8×10^{-10}
0.95	2×10^{-3}	27-28	$1.2\text{-}2.2 \times 10^{-10}$
0.9	2×10^{-3}	27-28	1.3×10^{-10}
0.8	2×10^{-3}	28-29	1.5×10^{-10}

Additional fracture mechanics (1TCT) specimens were fabricated from a Type 304 SS (Heat No. 3083-5-1; 0.06% carbon; Schedule 140; 10-in. diameter) overlay pipe mockup prepared by NUTECH Engineers and

GAPCO Welding. The base material was furnace-sensitized at 600°C for 24 h before the overlay was applied.

C. Evaluation of Nonenvironmental Corrective Actions (P. S. Maiya and W. J. Shack)

1. Introduction

The fundamental premise of current efforts to prevent IGSCC in BWR piping is that IGSCC involves a complex interaction among material susceptibility (sensitization), the stresses acting on the material, and the environment and that suitable alteration or variation of these parameters can produce immunity to IGSCC. Nonenvironmental corrective actions seek to mitigate either the material susceptibility or the state of stress on the inside surface of the weldment. They include techniques for improving the margin against IGSCC of a susceptible material like Type 304 SS and the identification of alternative materials that are inherently more resistant to IGSCC.

The objective of the current work is an independent assessment of the proposed remedies developed by the utilities and the vendors. Additional research has been carried out to eliminate gaps in the existing data base on alternative materials and fabrication and to develop a better understanding of the relation between the existing laboratory results and satisfactory in-reactor operating performance. Current efforts in this task include additional screening tests for alternative materials and studies of the residual stress distributions associated with weld overlays.

2. Technical Progress

Previous work has[2-4] shown that Type 316NG SS cracks transgranularly in oxygenated water (0.2 ppm) with impurities (0.1 ppm sulfate, added as acid). The transgranular stress corrosion cracking (TGSCC) is associated with the presence of the sulfate impurity. Although the 0.1 ppm level used for much of the testing is within the Reg. Guide 1.56 limits, it is much higher than is typical for normal operation. CERT test

results for lower impurity concentrations and two strain rates, 4×10^{-7} and 2×10^{-7}/s, are summarized in Table 1.2. Although no cracking occurs in high-purity water, TGSCC occurs in low-conductivity water

TABLE 1.2. CERT Test Results for Type 316NC SS[a] in 289°C Oxygenated Water (~0.2 ppm) with Several Sulfate Concentrations

Test No.	Sulfate, ppm	Conductivity, μS/cm	t_f, h	σ_{max}, MPa	Failure Mode	$\dot{a}_{av}$, m/s
			$\dot{\varepsilon} = 4 \times 10^{-7}$ s^{-1}			
169	0.1	0.90	217.4	462	TGSCC	9.74×10^{-10}
216	0.075	0.69	559.4	449	TGSCC	2.03×10^{-10}
			$\dot{\varepsilon} = 2 \times 10^{-7}$ s^{-1}			
187	0.00	<0.2	483.3	460	Ductile	-
207	0.01	<0.2	497.3	468	Ductile	-
228	0.025	0.25	473.8	462	TGSCC	4.71×10^{-10}
210	0.025	0.25	532.4	458	TGSCC	6.33×10^{-10}
199	0.050	0.47	588.7	449	TGSCC	2.21×10^{-10}
228	0.075	0.64	562.8	456	TGSCC	4.52×10^{-10}
172	0.10	0.90	474.0	461	TGSCC	7.35×10^{-10}

[a]Heat No. P91576 after a heat treatment of 1050°C for 0.5 h plus 650°C for 24 h.

(0.25 μS/cm) containing sulfate levels as low as 0.025 ppm. These results indicate that at a strain rate of 2×10^{-7}/s, the critical sulfate concentration needed to induce cracking is between 0.01 and 0.025 ppm, and this concentration level could even be lower at slower strain rates. There is some scatter in the data, but it appears that, although cracking occurs even at low impurity levels, the crack growth rates decrease with decreasing impurity concentration. TGSCC does not appear to be a significant problem in existing Type 304 SS piping systems. However, it is possible that, at present, cracking incidents are dominated by the more severe IGSCC in sensitized stainless steels, and TGSCC could occur in nuclear-grade materials, albeit at a lower frequency, unless other measures are taken, such as good water chemistry control or residual stress remedies.

To assure that TGSCC in impurity environments is not an artifact associated with the large plastic strains achieved in CERT tests, interrupted tests were performed on Types 316NG and 316 SS in oxygenated water (0.02-0.25 ppm) containing 0.1 ppm sulfate at strain rates between 10^{-6} and 10^{-7}/s. In these tests cracks 50-200 μm long are observed at relatively small strains (<5%). The results in general are consistent with predictions of our phenomenological model for crack growth in CERT tests and the assumption that initiation of smaller cracks (~1 μm deep) occurs at much lower strains (~1%)[3,5], but direct observation at lower strains is difficult. To improve the sensitivity of detecting cracks at lower strains, plastic replica techniques similar to those employed in observing crack initiation in high-temperature fatigue studies[6] of Type 304 SS are being initiated.

A phenomenological model that describes the effects of applied strain rate $\dot{\epsilon}$ on SCC behavior in CERT tests has been discussed in previous reports.[2,3] The correlations obtained can be represented in a generalized form:

$$P = A^{p}(J_c/C)^{q}(\dot{\epsilon})^{r} \qquad (1)$$

where $P = \epsilon_f$, a_f, t_f, or $\dot{a}_{av}$; A depends on the environment and material microstructure but is independent of $\dot{\epsilon}$; J_c/C is a fracture-characterizing parameter that is nearly independent of both environment and $\dot{\epsilon}$; and the exponents p, q, and r are given by the model. In addition to strain rate effects, Eq. (1) can also account for environmental and microstructural effects[7] through the parameter A. There is good agreement between the model predictions and laboratory CERT results, and the description of strain rate effects on SCC susceptibility given by the model is also in good agreement with in-reactor measurements,[8] an example of which is shown in Fig. 1.12. We have, in addition, used the model to compare the results pertaining to the effects of dissolved oxygen or open-circuit corrosion potential on the SCC of Type 304 SS, obtained at ANL with those obtained by Indig and Weber.[9] The latter results were generated in the Dresden-II boiling water reactor. This comparison is shown in Table 1.3. Although the excellent agreement between the predictions based on ANL results and the in-reactor data

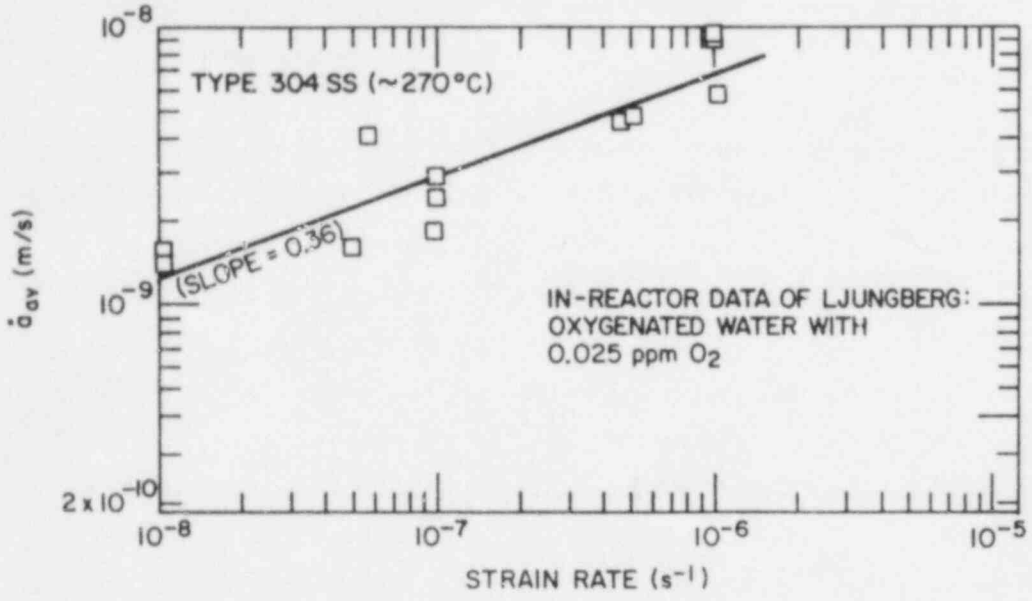

Fig. 1.12. Average Crack Growth Rate as a Function of Strain Rate for Type 304 SS. Data were obtained in the Ringhals-1 reactor in Sweden.[8]

TABLE 1.3. CERT Test Results in High Purity Water at ~274°C and a Strain Rate of $\dot{\varepsilon} \sim 3.5 \times 10^{-7}$ s^{-1} (Indig and Weber, 1985)

Dissolved O_2, ppm	t_f, h Exp (Pred)[a]	ε_f, % Exp (Pred)[a]
Laboratory Results (Type 304 SS, Welded + LTS)		
0.18	224.0 (225)	26.8 (26.6)
0.09	293.5 (280)	36.3 (33.2)
In-Reactor Results[b] (Type 304 SS, SA + 621°C/24 h)		
0.2	108.0 (112.0)	12.1 (14.8)
0.04	143.0 (139.5)	20.3 (18.4)

[a] Based on ANL model.

[b] Reference 9.

may be fortuitous, the consistency regarding the benefits of reducing the dissolved-oxygen concentration in laboratory tests and in-reactor experiments is encouraging.

The effects of reduction in the dissolved-oxygen content on SCC of Type 316NG SS have been investigated. The dissolved oxygen was varied between 8 and 0.02 ppm in tests at a strain rate of 2×10^{-7}/s. To compare these results with similar data for Type 304 SS obtained at a higher strain rate of 10^{-6}/s, the model was used to account for the differences in strain rate. A comparison of the results for the two materials is shown in Fig. 1.13. With a decrease in oxygen content, $\dot{a}_{av}$ decreases by a factor of ~8 for Type 304 SS and by a factor of ~4 for Type 316NG SS. The degree of improvement for Type 316NG SS is smaller but significant. Thus the use of hydrogen-water chemistry can also improve the SCC resistance for Type 316NG SS.

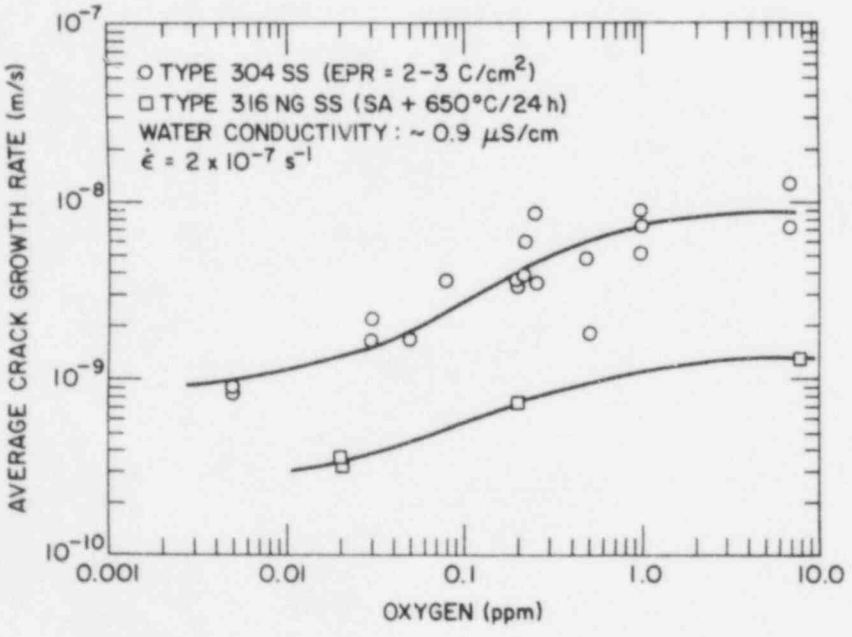

Fig. 1.13. Comparison of the Effects of Dissolved Oxygen in Water on the SCC Susceptibility of Types 316NG and 304 SS. The 304 data were obtained in Subtask D.

More extensive results are being obtained for alternative materials to establish definitive correlations between corrosion potential (or dissolved-oxygen concentration) and water conductivity (or impurity concentration). Such correlations are fundamental to the determination of cracking versus no-cracking zones relevant to reactor operating conditions.

Nitrogen levels in Types 316NG, 316 and 304 SS are required to be <0.1 wt.%, although the nuclear-grade material also has a minimum requirement so that $0.06 < N < 0.1$ wt.% to compensate for the loss of strength properties resulting from the reduction in carbon. An increase in nitrogen content is known to increase SCC susceptibility. This detrimental effect appears to be associated with the observation that nitrogen promotes slip planarity and hence assists the film rupture process required for SCC. To obtain better understanding of the role of nitrogen, CERT tests were performed on four heats of Type 316LN SS. The LN-grade materials contain nitrogen levels >0.1 wt.%. The data obtained for the NG and LN grades as well as conventional steels are presented in Fig. 1.14, which shows the variation of $\dot{a}_{av}$ (TGSCC) with nitrogen content. Nitrogen levels in excess of approximately 0.1 wt.% appear to have an adverse effect on TGSCC. These preliminary results suggest that the nuclear-grade Type 316 SS is superior to the LN grade of Type 316 SS insofar as TGSCC resistance is concerned.

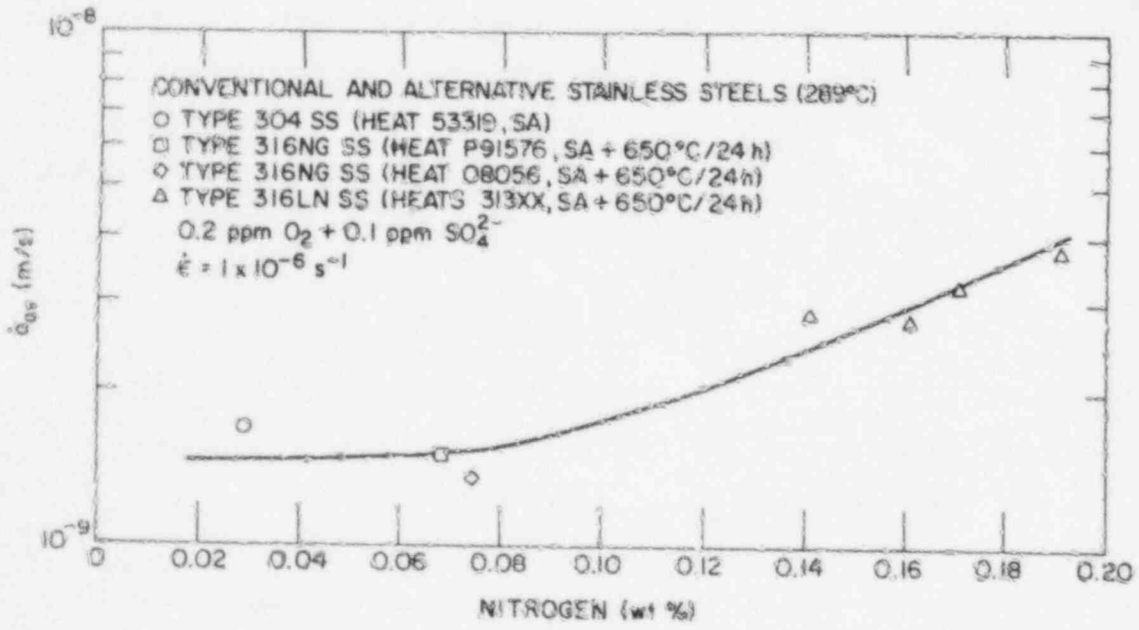

Fig. 1.14. Influence of Nitrogen on Average Transgranular Crack Growth Rates for Austenitic Stainless Steels.

In a cooperative effort with the EPRI Nondestructive Evaluation (NDE) Center, studies are being carried out on the German Type 347NG SS (Mannesmann TP347 DIN 1.4550). The work at the NDE Center focuses on weldability, and the work at ANL focuses on the SCC susceptibility of the material. Chemical analyses of the base and filler metals (Heat Nos. 174100 and 30316, respectively) from a weldment supplied by the NDE Center are shown in Table 1.4. This weldment was fabricated by the prescribed German practice. CERT tests have been performed in 289°C water with ~0.23 ppm oxygen and 0.1 ppm sulfate on this material in the as-welded condition and after an additional heat treatment (i.e., as-welded + 500°C/24 h) over a range of strain rates. The results are shown in Table 1.5. TGSCC was observed at strain rates of $\leq 5 \times 10^{-7}$/s, which are slower than those required to produce TGSCC in CERT tests on Type 316NG SS. Hence, based on this observation, this heat of Type 347 SS, although not immune to TGSCC, appears slightly superior to Type 316NG SS (Heat No. P91576). However, TGSCC susceptibility, as quantified by average crack growth rates, does not appear to be very different from that of Type 316NG SS. For example, the values of $\dot{a}_{av}$ for Type 347 and 316NG SS tested in a sulfate solution at a strain rate of 10^{-7}/s are 7×10^{-10} to 1×10^{-9} m/s and $\sim 6 \times 10^{-10}$ m/s, respectively. Furthermore, the low-temperature heat treatment does not appear to have any significant effect on the SCC susceptibility. Visual examination of the gage length of failed specimens suggests that, in most cases, failure occurred in the base metal (Heat No. 174100), away from the weld fusion line (the "knife-line attack" region). The enhanced resistance of the filler material, which is a different heat of Type 347 SS (Heat No. 30316), is most likely associated with a higher ferrite content. Although no detailed microstructural examination has been made to verify this, empirical correlations of composition with ferrite number[10] suggest that the ferrite number of the filler is about 5 while that of the base metal is about 1-2.

To compare the behavior of materials in our studies with those at SRI in EPRI-sponsored work, three exploratory CERT tests have been performed on another heat of Type 316NG SS (Heat No. 59076), whose chemical composition is listed in Table 1.6. This heat is also susceptible to TGSCC in impurity environments, similar to the behavior of our reference

TABLE 1.4. Chemical Analysis (wt.%) of Nuclear Grade SS

Element	Type 347 (No. 174100)[a]		Type 347 (No. 90316)[b]	Type 316 (No. 59076)
	Vendor	ANL	Vendor	ANL
Si	0.33	0.33	0.8	0.60
Mn	1.65	1.7	1.61	1.44
C	0.027	0.023	0.017	0.018
P	0.03	0.036	0.018	0.022
S	0.015	0.012	0.002	0.018
Ni	10.85	11.00	10.85	12.83
Cr	18.00	18.15	19.53	17.41
Mo	-	0.48	0.03	2.48
Nb	0.43	0.44	0.61	-
Cu	-	0.12	0.04	0.48
Mg[c]	-	0.005	-	0.005
N	0.031	0.029	-	0.0715
O	-	0.0046	-	0.0044
B	-	0.0005	-	0.0008
Co	-	-	0.03	-

[a]Base metal.

[b]Filler metal (welded at the EPRI NDE Center).

[c]Obtained from SRI.

TABLE 1.5. CERT Test Results for Type 347 Stainless Steel in 289°C Water Containing ~0.23 ppm Oxygen and 0.1 ppm Sulfate[a]

Specimen No.	Heat Treatment	t_f, h	ϵ_f, %	$\epsilon_{uniform}$, %	$\Delta A/A$, %	σ_{max}, MPa	$\dot{\epsilon}$, s^{-1}	Failure Mode	$\dot{a}_{SCC}$, m/s
174-1	AW	77.5	27.9	19.4	62	435	1×10^{-6}	Ductile	-
174-4	AW + 500°C/24 h	65.5	23.6	18.2	65	432	1×10^{-6}	Ductile	-
174-2	AW	136.6	24.6	19.0	51	428	5×10^{-7}	TGSCC	1.40×10^{-9}
174-5	AW + 500°C/24 h	114.5	20.6	16.6	47	417	5×10^{-7}		1.63×10^{-9}
174-8	AW	328.5	23.7	[illegible]	41	434	2×10^{-7}		1.00×10^{-9}
174-3[b]	AW + 500°C/24 h	301.5	21.7	17.8		448	2×10^{-7}		1.10×10^{-9}
174-9	AW	676.5	24.4	21.6	41	443	1×10^{-7}		1.05×10^{-9}
174-6	AW + 500°C/24 h	574.5	20.7	16.4	47	451	1×10^{-7}		7.58×10^{-10}

[a]Steady-state open-circuit corrosion potential: ~30 mV(SHE).

TABLE 1.6. Exploratory CERT Test Results on Type 316NG SS (Heat No. 59076)[a] 289°C

Test No.	Environment	t_f, h	ϵ_f, %	σ_{max}, MPa	$\dot{\epsilon}$, s^{-1}	Failure Mode	$\dot{a}_{av}$, m/s
282	0.2 ppm O_2	626.5	45	500	2×10^{-7}	TGSCC	3.2×10^{-10}
280	0.2 ppm O_2 + 0.1 ppm SO_4^{2-}	114.5	41	484	1×10^{-6}	TGSCC	-
231	0.2 ppm O_2 + 0.1 ppm SO_4^{2-}	250	36	487	4×10^{-7}	TGSCC	2.6×10^{-9}

[a]Heat treatment: 1050°C/0.5 h + 650°C/24 h.

heat of 316NG SS (No. P91576). However, based on a test at a strain rate of 2×10^{-7}/s, the SRI material shows TGSCC susceptibility even in high-purity water, although the apparent TG crack growth rate is considerably slower than that in impurity environments (Table 1.5). Additional tests are required to better characterize the nature of this cracking.

D. Evaluation of Environmental Corrective Actions (W. E. Ruther, W. K. Soppet, and T. F. Kassner)

1. Introduction

The objective of this subtask is to evaluate the potential effectiveness of proposed actions to solve or mitigate the problem of IGSCC in BWR piping and safe ends through modifications of the water chemistry. In this regard, the synergistic effects of dissolved oxygen (produced by radiolytic decomposition of the water) and impurities (e.g., oxyacids from decomposition of ion exchange resins during periodic intrusions into the primary system) on the IGSCC susceptibility and crack growth properties of sensitized Type 304 SS are being evaluated. The potential benefits associated with small additions of hydrogen to the coolant are also being evaluated under conditions in which ionic impurities at low concentrations are also present in the high-temperature water.

During this reporting period, additional information is presented on the effects of dissolved oxygen and several oxyanion impurity species at low dissolved-oxygen concentrations on the electrochemical potential and SCC susceptibility of sensitized Type 304 SS in 289°C water. The effects of dissolved oxygen, hydrogen, and sulfate (as H_2SO_4) in 289°C water on crack growth rates of the steel in the solution annealed and sensitized conditions also were determined from fracture-mechanics-type specimens under low-frequency, moderate-stress intensity, and high-R loading conditions.

2. Technical Progress

a. Influence of Several Oxyanion Species on the Electrochemical Potential of Type 304 SS and Platinum in 289°C Water at Low Dissolved-Oxygen Concentrations

The manner in which different impurity species at low concentrations, along with dissolved oxygen, in the bulk-coolant environment influence the open-circuit corrosion potential and SCC behavior of reactor materials is not well known, although the relative effects of several anions, in conjunction with sodium and hydrogen cations, on SCC of sensitized Type

304 SS has been investigated.[11-15] To obtain additional insight into the effects of impurities on the corrosion potential and SCC behavior of this material, numerous CERT experiments were performed in 289°C water containing different oxyacids (viz., HNO_3, H_3AsO_4, H_2SO_4, $HClO_4$, and H_3BO_3) at low dissolved-oxygen concentrations (<0.02 ppm). An investigation of the influence of the various species on the corrosion potential of the material in high-temperature water hopefully will provide better insight into the SCC behavior of the steel in reactor-coolant environments.

Table 1.7 summarizes the CERT data and the effects of the various oxyacids on the electrochemical potentials of the Type 304 SS and platinum for the different feedwater chemistries. The anion concentrations in the feedwater ranged from 1 to 10,000 ppm for H_3BO_3 and from ~0.1 to 100 ppm for the other oxyacids. The dependence of the electrochemical potentials of the steel and platinum on the conductivity of the feedwater containing the various oxyacids is shown in Fig. 1.15 along with similar information for dissolved oxygen in high-purity water, which was reported previously.[16] The potentials of Type 304 SS and platinum in water that contains HNO_3, H_3AsO_4, or $HClO_4$ at low dissolved-oxygen concentrations exhibit the same dependence on conductivity, i.e., the concentration of the oxyacids. The potential values obtained with HNO_3 or H_3AsO_4 at anion concentrations of >20 ppm (conductivity values >100 μS/cm) are almost a factor of two higher than those in high-purity water containing ~20-40 ppm dissolved oxygen [i.e., +500 vs +250 mV(SHE)]. In contrast, the potentials of the steel and platinum in high-temperature water containing low dissolved-oxygen concentrations (<0.01 ppm) and H_2SO_4 or H_3BO_3 are quite negative over a wide range of conductivity or concentration. The slight increase in potential as the conductivity or concentration of the acid increases can be attributed to the decrease in the pH of the water, i.e., the values tend to follow the pH dependence of the hydrogen evolution reaction ($2H^+ + 2e^- = H_2$) given by the expression

$$E_{289°C}(SHE) = -0.1113\ pH_{289°C} - 0.0557\ \log\ C_H/C_H^o, \qquad (2)$$

where C_H^o is the solubility of hydrogen in water at 289°C (viz., 7.55 ppm)[17] and C_H is the dissolved-hydrogen concentration of the water. The $pH_{289°C}$ values for high-purity water and water containing 0.1, 1.0, 10, 50, and

TABLE 1.7. Influence of Several Oxyacids at Low Dissolved-Oxygen Concentrations on the SCC Susceptibility of Sensitized (EPR = 2 C/cm^2) Type 304 SS Specimens[a] (Heat No. 30956) in 289°C Water

Test No.	Feedwater Chemistry: Oxygen, ppm	Impurity Species	Anion Conc., ppm	Cond. at 25°C, μS/cm	pH at 25°C	CERT Parameters: Failure Time, h	Maximum Stress, MPa	SCC Growth Rate,[b] mm·h^{-1}	SCC Growth Rate,[b] m·s^{-1}	Fracture Morphology[c]	Potentials: Type 304 SS, mV(SHE)	Potentials: Pt, mV(SHE)
A105	0.005	$HClO_4$	80.0	315.0	3.12	19	245	1.9×10^{-1}	5.1×10^{-8}	1.00I	319	309
A104	0.005		20.0	85.0	3.73	17	237	2.2×10^{-1}	6.1×10^{-8}	0.03D, 0.97I	209	-95
A110	0.005		10.0	42.0	4.03	20	226	2.3×10^{-1}	6.4×10^{-8}	0.12D, 0.88I	169	-98
A101	0.005		7.0	29.0	4.21	26	241	2.4×10^{-1}	6.6×10^{-8}	0.14D, 0.86I	120	-156
A109	0.005		5.0	22.0	4.34	20	233	2.5×10^{-1}	7.0×10^{-8}	0.08D, 0.92I	107	-149
A106	0.005		3.0	13.7	4.55	35	305	1.0×10^{-1}	2.8×10^{-8}	0.22D, 0.78I	-3	-
A108	0.005		2.0	8.5	4.78	70	428	3.1×10^{-2}	8.7×10^{-9}	0.45D, 0.55I	-48	-215
A111	0.005		1.5	6.3	4.90	97	476	2.3×10^{-2}	6.4×10^{-9}	0.56D, 0.44I	-89	-226
A102	0.005		1.0	3.9	5.17	136	530	8.0×10^{-3}	2.2×10^{-9}	0.64D, 0.36T	-111	-263
A103	0.005		0.1	0.56	6.27	120	503	9.0×10^{-3}	2.5×10^{-9}	0.68D, 0.32T	-356	-444
A98	0.010	HNO_3	63.0	390.0	3.02	33	312	1.0×10^{-1}	2.8×10^{-8}	0.07D, 0.93I	577	555
A99	0.010		7.0	43.0	3.99	38	317	9.5×10^{-2}	2.6×10^{-8}	0.26D, 0.74I	333	-134
A100	0.010		0.7	4.5	5.06	154	520	0	0	1.00D	-147	-309
A88	0.017	H_3AsO_4[d]	70.0	410.0	3.03	42	352	7.6×10^{-2}	2.1×10^{-8}	0.07D, 0.93I	419	413
A87	0.018		20.0	111.0	3.57	42	340	7.3×10^{-2}	2.0×10^{-8}	0.13D, 0.87I	310	225
A90	0.013		7.0	40.0	4.05	63	404	5.6×10^{-2}	1.6×10^{-8}	0.31D, 0.69I	131	75
A89	0.013		1.0	14.3	4.54	95	483	1.9×10^{-2}	5.3×10^{-9}	0.49D, 0.51G_3	-79	-184
A27	<0.01	H_2SO_4	100.0	800.0	2.74	45	287	9.1×10^{-2}	2.5×10^{-8}	0.14D, 0.86G_3	-420	-366
A28	<0.01		100.0	785.0	2.76	41	301	9.4×10^{-2}	2.6×10^{-8}	0.12D, 0.88G_3	-370	-330
A36	<0.01		50.0	425.0	3.01	56	342	6.0×10^{-2}	1.7×10^{-8}	0.16D, 0.84G_3	-392	-340
53	0.03		10.0	71.0	3.80	65	384	4.0×10^{-2}	1.1×10^{-8}	0.25D, 0.75I	-405	-365
62	0.03		10.0	72.0	3.80	72	373	5.7×10^{-2}	1.6×10^{-8}	0.21D, 0.79G_3	-419	-416
49	0.03		1.0	8.0	4.80	119	495	1.8×10^{-2}	5.0×10^{-9}	0.45D, 0.55G_2	-450	-470
60	0.01		1.0	8.3	4.80	103	478	1.4×10^{-2}	3.9×10^{-9}	0.56D, 0.44G_2	-496	-515
68	<0.005[e]		0.1	1.1	8.40	147	518	5.9×10^{-3}	1.6×10^{-9}	0.77D, 0.23T	-573	-575
A114	0.005	H_3BO_3	10,000	7.40	4.85	125	504	1.3×10^{-2}	3.4×10^{-9}	0.52D, 0.48T	-469	-372
A113	0.005		1,000	1.54	5.63	122	509	1.3×10^{-2}	3.7×10^{-9}	0.58D, 0.42T	-432	-432
A112	0.005		100.0	0.42	6.05	123	504	8.8×10^{-3}	2.4×10^{-9}	0.65D, 0.35T	-531	-521
A116	0.005		10.0	0.16	6.34	118	505	9.2×10^{-3}	2.6×10^{-9}	0.66D, 0.34T	-491	-435
A117	0.005		1.0	0.10	6.37	123	506	1.1×10^{-2}	3.0×10^{-9}	0.71D, 0.29T	-566	-505

[a] Specimens were exposed to the environment for ~20 h at 289°C before straining at a rate of 1×10^{-6} s^{-1}.

[b] SCC growth rates are based on measurement of the depth of the longest crack in an enlarged micrograph of the fracture surface and the time period from the onset of yield to the point of maximum load on the tensile curve.

[c] Ductile (D), transgranular (T), granulated (G), intergranular (I), in terms of the fraction of the cross-sectional area. Characterization of the fracture surface morphologies is in accordance with the illustrations and definitions in Corrosion 40(9), pp. 493-506 (1984), "Transgranular, Granulated, and Intergranular Stress Corrosion Cracking in AISI 304 SS," by H. D. Solomon.

[d] H_3AsO_4 master solutions were prepared by the addition of concentrated HNO_3 to arsenic (III) oxide according to the reaction $2As_2O_3 + 8HNO_3 + 2H_2O \rightarrow 4H_3AsO_4 + 8NO_2\uparrow$; consequently, the H_3AsO_4 solutions may contain NO_3^- in addition to $H_2AsO_4^-$.

[e] Hydrazine was added to the feedwater to decrease the oxygen level to <0.005 ppm.

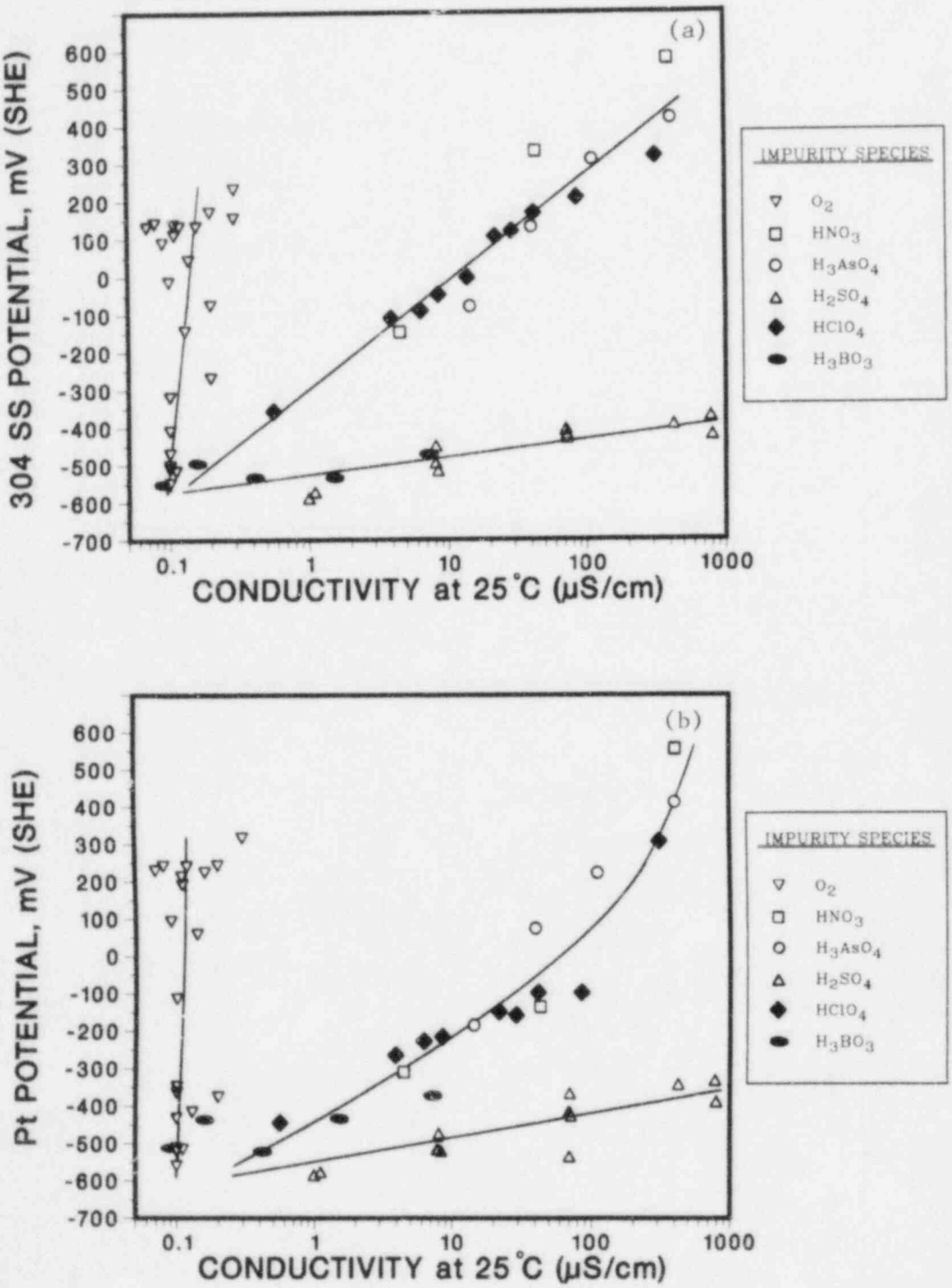

Fig. 1.15. Effect of Dissolved Oxygen in High-Purity Water and Several Oxyacids at Low Dissolved-Oxygen Concentrations on the Electrochemical Potentials of (a) Type 304 SS and (b) Platinum at 289°C.

100 ppm sulfate as H_2SO_4 are 5.63, 5.49, 4.95, 4.00, 3.30, and 3.00, respectively, from information on the dissociation of water[18] and the second dissociation constant of sulfuric acid[19] at high temperature.

The diverse effect of the various species on the open-circuit corrosion potential of the steel can be rationalized in terms of the Wagner-Traud mechanism[20] for electrochemical corrosion. According to that theory, dissolution or oxidation of a metal in an aqueous environment does not occur directly but by the superposition of electrochemical anodic and cathodic partial processes. Furthermore, the two processes can occur at different local anodic and cathodic areas on the metal surface. The mechanism also indicates that the corrosion or mixed potential normally lies closest to the potential of the partial process that has the highest exchange current density, or alternatively, farthest from the equilibrium potential for the rate-determining partial process.

In the case of stainless steel exposed to high-temperature water, a highly passive oxide film forms on the surface and metal dissolution or oxidation proceeds at a low rate. Under this condition the rate of the anodic partial process apparently is very slow compared with that of a number of cathodic reduction processes involving dissolved oxygen or various oxyacids listed in the next section. Consequently, the open-circuit corrosion or mixed potential for the steel in Fig. 1.15a is indicative of that for the cathodic reduction of various species at the surface of the electrode. Under most of the water chemistry conditions in Table 1.7, the values are not very different from those obtained from a platinum electrode, which frequently serves as an "inert" redox electrode in electrochemical studies.

b. Effect of Dissolved Oxygen and Several Oxyacids on the Crack Growth Rate of Sensitized Type 304 SS from CERT Tests in 289°C Water

The rate of intergranular or transgranular crack growth of sensitized Type 304 SS CERT specimens was evaluated from the maximum depth of stress-corrosion crack propagation on an enlarged photomicrograph of the fracture surface and the time interval from the onset of yield to the time of maximum load on the load versus time curve. The dependence of the crack

growth rate of Type 304 SS specimens (EPR = 2-30 C/cm^2) on the dissolved-oxygen concentration in high-purity water and on the sulfate concentration in water with low dissolved-oxygen concentrations is shown in Fig. 1.16.[15] Within the scatter of the data, the slope of the lines on the logarithmic plots of crack growth rate versus oxygen or sulfate concentration in Figs. 1.16(a) and (b) are 1/4 and 1/2, respectively, over three orders of magnitude of the concentration of the dissolved species. For comparison with these results, the crack growth rates of lightly sensitized (EPR = 2 C/cm^2) Type 304 SS specimens (Heat No. 30956) on the concentrations of HNO_3, H_3AsO_4, and H_2SO_4 and the conductivity of the feedwater containing these oxyacids (Table 1.7) are shown in Fig. 1.17. Lines with a slope of 1/2 are also depicted on the figure, which are a reasonable representation of the combined data for the three acids.

The dependence of the crack growth rates of the steel on the conductivity and the concentrations of $HClO_4$ and H_3BO_3 in the feedwater is shown in Fig. 1.18. In contrast to the results for the other acids, the crack growth rate exhibits a strong dependence on the perchlorate ion concentration over the range of 1 to 7 ppm and becomes independent of concentration at higher levels, whereas the transgranular crack growth rate is relatively low and independent of the borate concentration over the range of 1 to 10,000 ppm. The crack growth rate exhibits a power of 2 dependence on the perchlorate concentration over a relatively narrow range and zero-power dependence in the case of the borate species.

A possible rationale for the role of the different oxyacids in the SCC behavior of sensitized Type 304 SS is analogous to that proposed for oxyanions of several acids and sodium salts of arsenic.[16] If one postulates that crack growth occurs via a slip-dissolution process at the crack tip,[21,22] the anodic dissolution reaction and hydrolysis equilibria at the crack tip are given by

$$Me = Me^{z+} + ze^{-} \qquad (3)$$

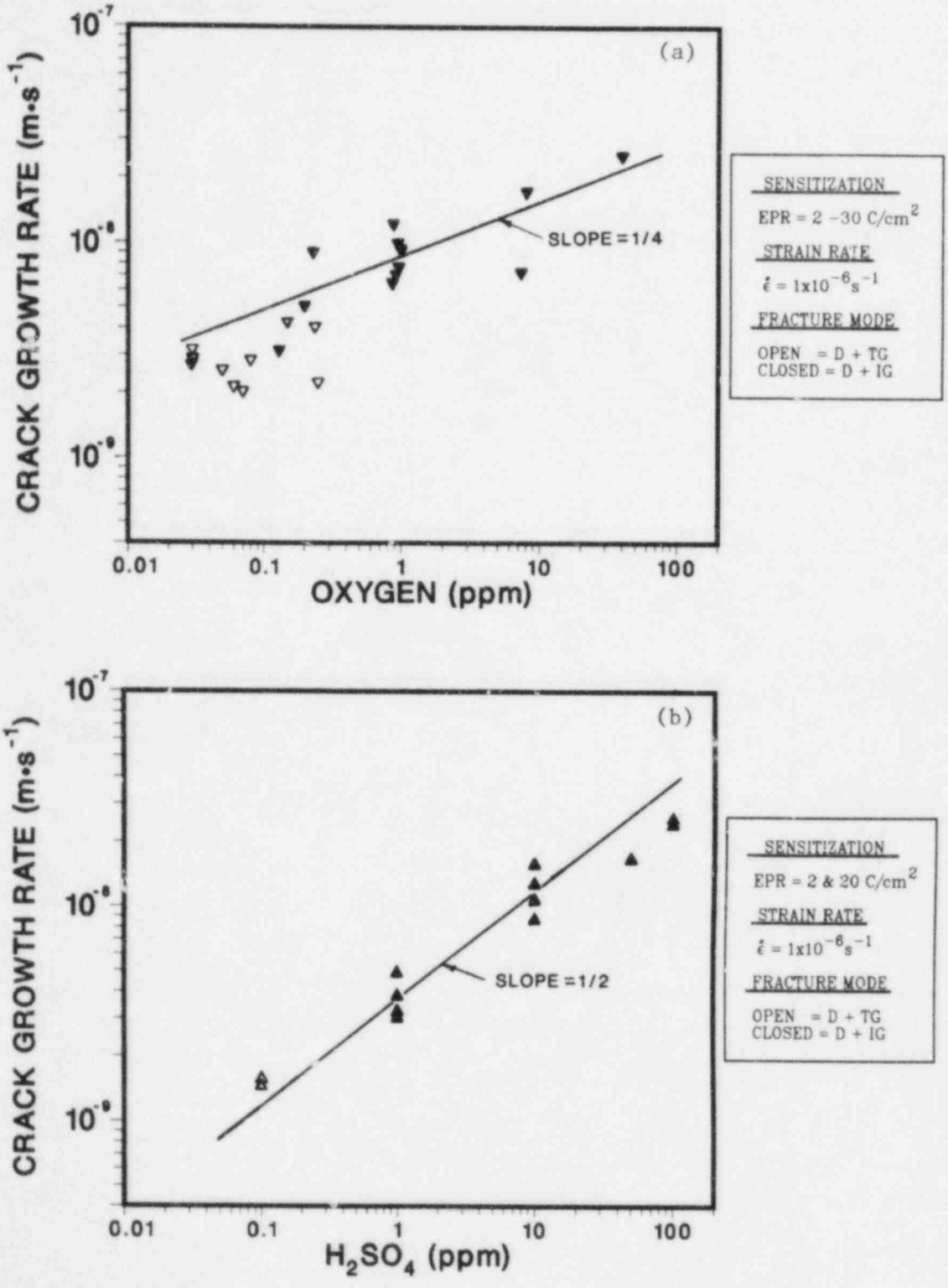

Fig. 1.16. Dependence of the Crack Growth Rate of Sensitized Type 304 SS CERT Specimens on the Concentrations of (a) Dissolved Oxygen and (b) H_2SO_4 in 289°C Water. Open and closed symbols denote ductile plus transgranular and intergranular fracture morphologies, respectively.

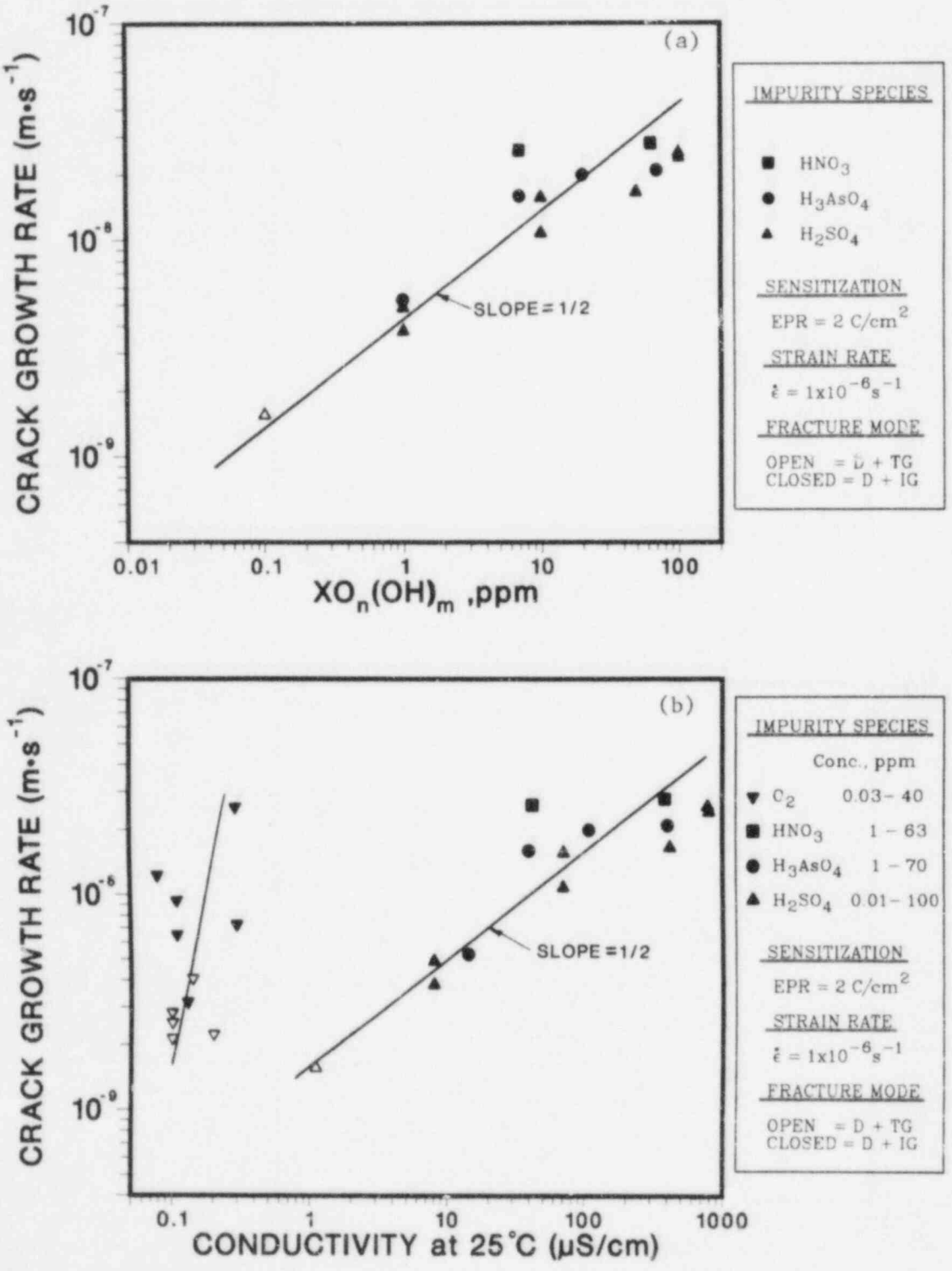

Fig. 1.17. Dependence of the Crack Growth Rate of Sensitized Type 304 SS CERT Specimens on (a) the Concentration of Several Oxyacids in 289°C Water and (b) the Conductivity of the Low-Oxygen Feedwater Containing the Various Species. Open and closed symbols denote ductile plus transgranular and intergranular fracture morphologies, respectively. $XO_n(OH)_m$ is a general formula for an oxyacid where X denotes the central atom, e.g., N, As, S, etc.

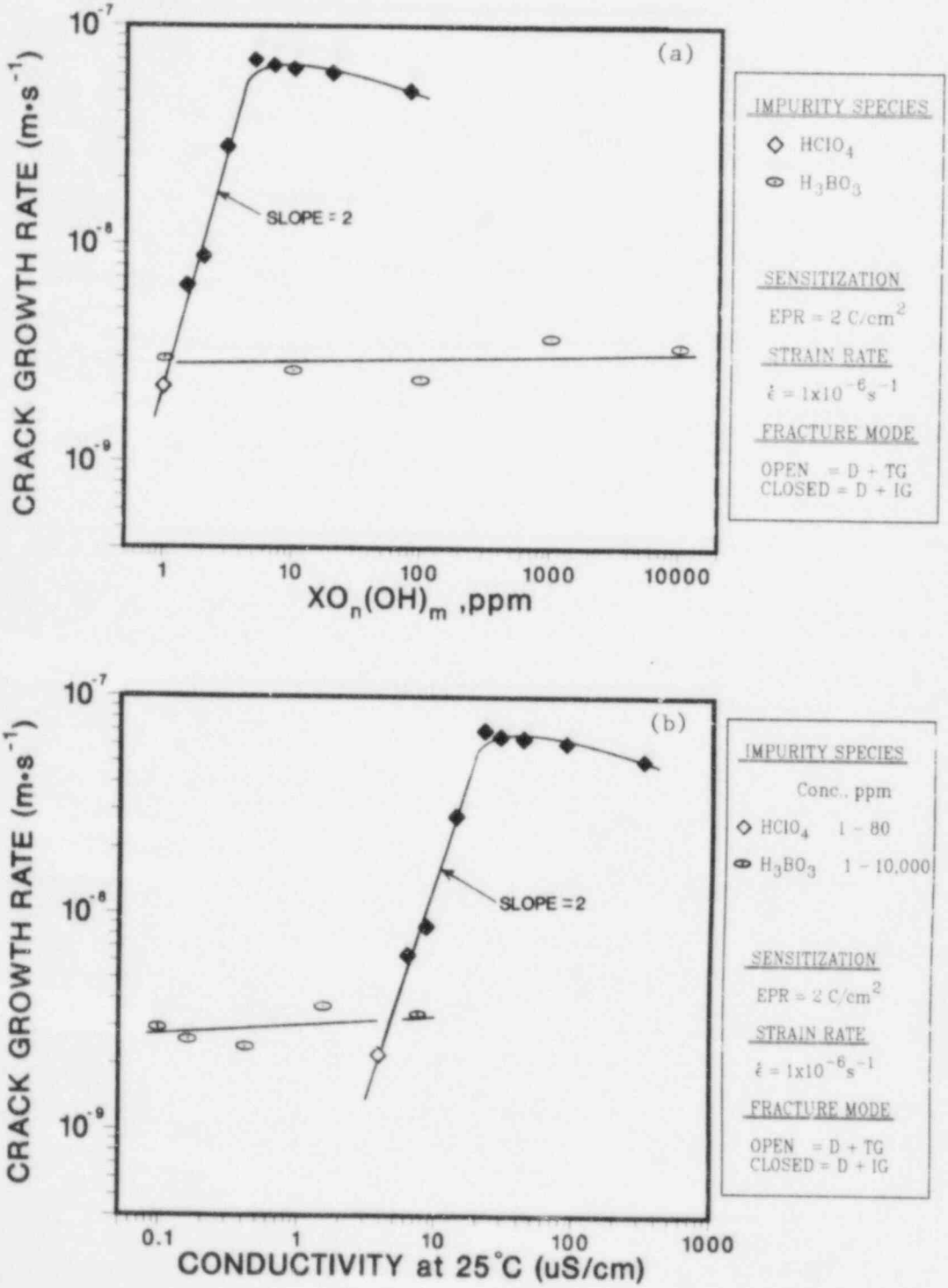

Fig. 1.18. Dependence of the Crack Growth Rate of Sensitized Type 304 SS CERT Specimens on (a) the Concentration of $HClO_4$ or H_3BO_3 in 289°C Water and (b) the Conductivity of the Low-Oxygen Feedwater Containing these Species. Open and closed symbols denote ductile plus transgranular and intergranular fracture morphologies, respectively. $XO_n(OH)_m$ is a general formula for an oxyacid where X denotes the central atom, e.g., Cl, B, etc.

and

$$Me^{z+} + H_2O = Me(OH)^{(z-1)+} + H^+, \quad (4)$$

$$Me(OH)^{(z-1)+} + H_2O = Me(OH)_2^{(z-2)+} + H^+,$$

$$\vdots \qquad\qquad \vdots$$

$$Me(OH)_{z-2}^{2+} + H_2O = Me(OH)_{z-1}^{+} + H^+,$$

$$Me(OH)_{z-1}^{+} + H_2O = Me(OH)_z + H^+.$$

where each step occurs by the loss of successive protons.

The cathodic reactions can involve the reduction of dissolved oxygen, hydrogen ions, and certain oxyanions that contain a central atom that assumes different oxidation states, e.g., S, N, As, Cl, P, and I, but not C, B, or Si. Typical cathodic reactions involving some of these species are as follows:

$$O_2 + 2H_2O + 4e^- = 4OH^- \quad (5)$$

$$2H^+ + 2e^- = H_2, \quad (6)$$

and

$$SO_4^{2-} + H_2O + 2e^- = SO_3^{2-} + 2OH^- \quad (7)$$

$$NO_3^- + H_2O + 2e^- = NO_2^- + 2OH^- \quad (8)$$

$$AsO_4^{3-} + 2H_2O + 2e^- = AsO_2^- + 4OH^-. \quad (9)$$

A number of cathodic reduction reactions can be written for the perchlorate oxyanion and these are given below:

$$ClO_4^- + 4H_2O + 8e^- = Cl^- + 8OH^- \quad (10)$$

$$ClO_4^- + 2H_2O + 4e^- = ClO_2^- + 4OH^- \quad (11)$$

$$ClO_4^- + H_2O + 2e^- = ClO_3^- + 2OH^- \quad (12)$$

$$4ClO_4^- + 2H_2O + 4e^- = 4ClO_3^- + 4OH^- + O_2 \quad (13)$$

$$8ClO_4^- + 2H_2O + 4e^- = 8ClO_3^- + 4OH^- + 3O_2. \quad (14)$$

For the purpose of analyzing the dependence of the SCC growth rates on the concentrations of the various species in the feedwater, the following equilibria and concentration-dependence relations can be written from Eqs. (5) to (14):

Species	Equilibria	Concentration Dependence	
O_2	$K_{eq} = \frac{[OH^-]^4}{[e^-]^4[O_2]}$	$\frac{1}{[e^-]} = \frac{k_1 [O_2]^{1/4}}{[OH^-]}$	(15)
H_2	$K_{eq} = \frac{[H_2]}{[e^-]^2[H^+]^2}$	$\frac{1}{[e^-]} = \frac{k_2 [H^+]}{[H_2]^{1/2}}$	(16)
SO_4^{2-}	$K_{eq} = \frac{[OH^-]^2}{[e^-]^2}\left[\frac{SO_3^{2-}}{SO_4^{2-}}\right]$	$\frac{1}{[e^-]} = \frac{k_3}{[OH^-]}\left[\frac{SO_4^{2-}}{SO_3^{2-}}\right]^{1/2}$	(17)
NO_3^-	$K_{eq} = \frac{[OH^-]^2}{[e^-]^2}\left[\frac{NO_2^-}{NO_3^-}\right]$	$\frac{1}{[e^-]} = \frac{k_4}{[OH^-]}\left[\frac{NO_3^-}{NO_2^-}\right]^{1/2}$	(18)
AsO_4^{3-}	$K_{eq} = \frac{[OH^-]^4}{[e^-]^2}\left[\frac{AsO_2^-}{AsO_4^{3-}}\right]$	$\frac{1}{[e^-]} = \frac{k_5}{[OH^-]^2}\left[\frac{AsO_4^{3-}}{AsO_2^-}\right]^{1/2}$	(19)
ClO_4^-	$K_{eq} = \frac{[OH^-]^8}{[e^-]^8}\left[\frac{Cl^-}{ClO_4^-}\right]$	$\frac{1}{[e^-]} = \frac{k_6}{[OH^-]}\left[\frac{ClO_4^-}{Cl^-}\right]^{1/8}$	(20)
ClO_4^-	$K_{eq} = \frac{[OH^-]^4}{[e^-]^4}\left[\frac{ClO_2^-}{ClO_4^-}\right]$	$\frac{1}{[e^-]} = \frac{k_7}{[OH^-]}\left[\frac{ClO_4^-}{ClO_2^-}\right]^{1/4}$	(21)
ClO_4^-	$K_{eq} = \frac{[OH^-]^2}{[e^-]^2}\left[\frac{ClO_3^-}{ClO_4^-}\right]$	$\frac{1}{[e^-]} = \frac{k_8}{[OH^-]}\left[\frac{ClO_4^-}{ClO_3^-}\right]^{1/2}$	(22)

$$ClO_4^- \qquad K_{eq} = \frac{[OH^-]^4[O_2]}{[e^-]^4}\left[\frac{ClO_3^-}{ClO_4^-}\right]^4 \qquad \frac{1}{[e^-]} = \frac{k_9}{[OH^-][O_2]^{1/4}}\left[\frac{ClO_4^-}{ClO_3^-}\right] \tag{23}$$

$$ClO_4^- \qquad K_{eq} = \frac{[OH^-]^4[O_2]^3}{[e^-]^4}\left[\frac{ClO_3^-}{ClO_4^-}\right]^8 \qquad \frac{1}{[e^-]} = \frac{k_{10}}{[OH^-][O_2]^{3/4}}\left[\frac{ClO_4^-}{ClO_3^-}\right]^2 \tag{24}$$

The concentration dependence relations are written in terms of $1/[e^-]$ to illustrate the exponential power for the concentration of the species according to each of the possible cathodic reactions.

In the case of crack advance by an anodic dissolution partial process at the crack tip, the crack growth rate can be expressed in terms of Faraday's Law,

$$\dot{a}\ (m \cdot s^{-1}) = Mi_a/z\rho F \approx 3.7 \times 10^{-7}\ i_a, \tag{25}$$

where M is the molecular weight of the metal (i.e., Fe), i_a is the anodic current density (A/cm^2), z is the charge of the metal ion, ρ is the density of the metal, and F is Faraday's constant. The rate is also proportional to the concentration of metal ions in solution at the crack tip; i.e.,

$$\dot{a} \approx [Me^{z+}] = K_{eq}/[e^-]^z, \tag{26}$$

from Eq. (3), where the metal ions either hydrolyze and diffuse from the crack tip and/or are removed from solution by the hydrolysis reactions in Eq. (4). The rate of crack advance increases under conditions where mass transport is enhanced, i.e., a higher metal ion or metal-ion complex concentration at the crack tip provides a larger driving force for diffusion and electromigration. Since the hydrolysis reactions are rapid,[23,24] the crack growth rate, conceivably, can increase as the concentration of electrons decreases [Eq. (26)] by means of the cathodic reactions listed in Eqs. (5)-(14), provided the species are present in the water. In terms of the Wagner-Traud mechanism[20] the cathodic partial processes can occur away from the crack tip, i.e., within the crack or at the crack mouth (external cathode), since electron transport through the metal is rapid compared to ionic charge transport within the crack solution.

If, in contrast to slow uniform corrosion of the passive steel surface, the rate of the anodic-dissolution partial reaction at the crack tip is very rapid following a film-rupture event until repassivation occurs, the equal but opposite current density i_c for the cathodic-reduction partial reaction may conceivably limit the dissolution rate. Under this scenario the crack growth rates could be expected to follow the exponential dependence of the concentrations of the individual species in Eqs. (15)-(24). The relative rates of the various cathodic partial reactions will depend on the concentration of the reactants (i.e., dissolved oxygen in the case of high-purity water and the oxyanions in impurity environments), the kinetics of adsorption/desorption reactions involving these species and their products at the metal-oxide/electrolyte interface, the rate of electron transfer through the oxide layer or across the interface, and the pH of the solution. Based on the law of mass action, all of the cathodic reactions are more favorable in acidic solutions.

Some insight into the relative efficiency of the various cathodic reactions in high-temperature water can be obtained from the dependence of the crack growth rates on the concentrations of the various species in the bulk feedwater (i.e., Figs. 1.16, 1.17a, and 1.18a). For example, in high-purity water, the crack growth rate of sensitized Type 304 SS is proportional to the 1/4 power of the dissolved-oxygen concentration. Presumably, the solution at the crack tip rapidly becomes deoxygenated and the crack-tip solution acidifies via the hydrolysis reaction. Consequently, the crack growth rate could, in principle, be independent of the dissolved-oxygen concentration of the bulk feedwater if the hydrogen-ion reduction reaction (accompanied by possible hydrogen adsorption in the metal and evolution of hydrogen from the crack) was the rate-limiting step. Similarly, based on the law of mass action, the addition of hydrogen to the feedwater either with or without dissolved oxygen could decrease the rate of hydrogen ion reduction in Eq. (6). However, hydrogen additions of up to 2 ppm to feedwater containing either 0.02 or 0.2 ppm dissolved oxygen did not produce a measurable decrease in the crack growth rate of sensitized Type 304 SS in 289°C water in laboratory CERT experiments.[15] In view of the dependence of the crack growth rate on the 1/4 power of the dissolved-oxygen concentration and the observation that IGSCC is essentially mitigated in low-oxygen, low-conductivity water, the

relative rate of the oxygen reduction [Eq. (5)] is apparently much greater than that for hydrogen ion reduction [Eq. (6)].

With regard to the effect of the oxyacids on IGSCC of sensitized Type 304 SS in 289°C water at low dissolved-oxygen concentrations, the crack growth rate depends on the 1/2 power of the sulfate, nitrate, and arsenate concentrations of the feedwater; which is consistent with the cathodic reduction reactions [Eqs. (7)-(9)] and the corresponding equilibria relations [Eqs. (17)-(19)]. In the dilute acid environments (pH of 2.7 to 4.8), hydrogen ions are present in the bulk water as well as in the crack, and thus, could provide an alternate cathodic reaction to couple with anodic dissolution at the crack tip. An extensive CERT study of the effects of pH of H_2SO_4-Na_2SO_4 solutions on the SCC behavior of sensitized Type 304 SS in 289°C water containing 0.2 ppm dissolved oxygen showed that pH per se had a minimal effect on IGSCC; i.e., the time to failure of the specimens was virtually independent of $pH_{25°C}$ or $pH_{289°C}$ at a given sulfate concentration, but decreased as the sulfate concentration increased for any given pH of the water.[25] These results also imply that the reduction kinetics of the oxyanion (viz., SO_4^{2-}) and dissolved oxygen are more favorable compared to the cathodic reduction of hydrogen ions.

The situation with regard to perchloric acid is quite interesting since the chlorine atom can assume several different oxidation states in the oxyacid, and conceivably, could be reduced from Cl^{+7} to Cl^- according to Eq. (10); however, other reactions are also possible [Eqs. (11)-(14)]. The crack growth rate results in Fig. 1.18 suggest that cathodic reduction of the perchlorate anion occurs via Eq. (14), in which the dependence on the ion concentration is to the power of 2 in Eq. (24). Since this reaction yields dissolved oxygen as well as hydroxyl ions, the effluent dissolved-oxygen concentration of the water from the autoclave was analyzed on numerous occasions; however, the values did not increase from those present in the low-oxygen feedwater. In retrospect, this is not surprising since the quantity of oxygen that could be produced via this reaction is coupled with the amount of dissolution at the crack tip in the CERT specimen and by general corrosion of the passivated autoclave system. The production of oxygen from both regions would be small in relation to the flow rate of low-oxygen water in the once-through system.

In the case of boric acid, the boron atom is in the +3 state and cannot participate in reduction reactions similar to those in Eqs. (5)-(14). This species has virtually no effect on the crack growth rate of the steel either in the presence of 8 ppm of dissolved oxygen[26] or in the low-oxygen environments (Table 1.7 and Fig. 1.18). Carbon and silicon in the CO_2^{2-}, HCO_2^-, or SiO_3^{2-} anions, which may be present in BWR water, are in the +4 state and it is unlikely that these anions can be reduced in high-temperature water, although carbon assumes different oxidation states in various organic acids.

In summary, CERT experiments on sensitized Type 304 SS in 289°C water that contains either dissolved oxygen or several oxyacids at low dissolved-oxygen concentrations indicate that the crack growth rates may be controlled by the concentrations of the various species in the bulk feedwater through the rate of the respective cathodic reduction reactions, which can occur at the specimen surface as well as within the crack itself. Plots of the crack growth rate as a function of the open-circuit corrosion potential of the steel or the redox potential of a platinum electrode in Figs. 1.19 and 1.20 show that cracking can proceed at a rapid rate ($2\text{-}3 \times 10^{-8}$ m·s^{-1}) at corrosion potentials of -450, 0, and +300 to 500 mV(SHE) in the presence of H_2SO_4, $HClO_4$, and either dissolved oxygen, HNO_3, or H_3AsO_4, respectively. These results suggest that the rate of the cathodic reactions involving the different species, at their respective concentrations in the water, is the same (i.e., they produce the same crack growth rate), although the corrosion potential at which this occurs is vastly different for the various species. Even higher growth rates (7×10^{-8} m·s^{-1}) occur at corrosion potentials between 100 and 325 mV(SHE) in dilute perchloric acid solutions at the same strain rate (1×10^{-6} s^{-1}) and degree of sensitization of the steel (EPR = 2 C/cm^2). Therefore, a knowledge of just the corrosion or redox potential is not sufficient to predict whether a material such as sensitized Type 304 SS is susceptible to IGSCC in high-temperature water, or the rate at which crack growth will occur. The corrosion potential must be used in conjunction with a knowledge of the type and concentration of impurities in the water [e.g., dissolved oxygen, oxyanions (particularly those having a central atom with multiple oxidation states), and pH (which has a bearing on whether the

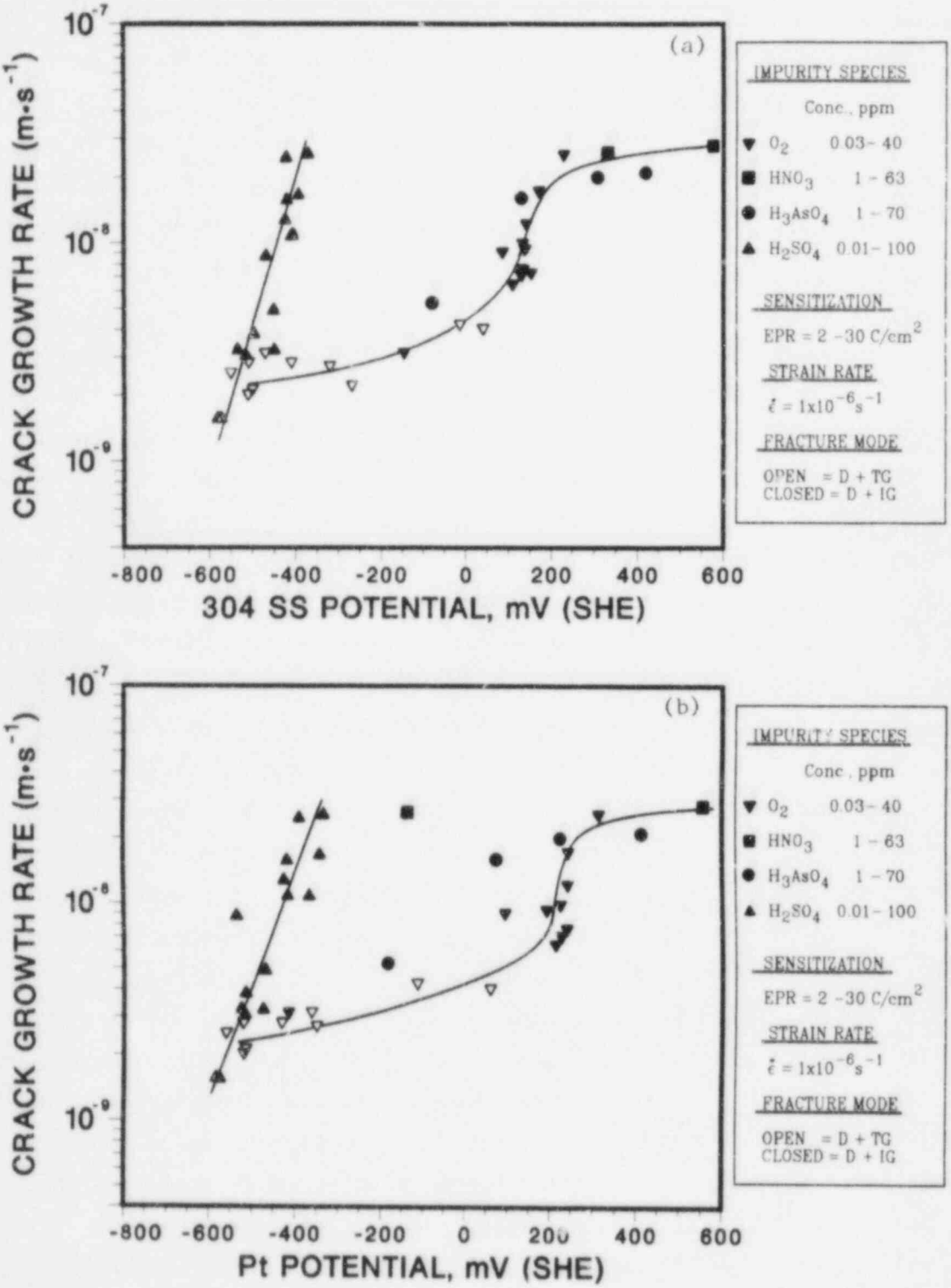

Fig. 1.19. Dependence of the Crack Growth Rate of Sensitized Type 304 SS CERT Specimens on the Electrochemical Potentials of (a) Type 304 SS and (b) Platinum in 289°C Water Which Contains Dissolved Oxygen or Several Oxyacids at Low Dissolved-Oxygen Concentrations. Open and closed symbols denote ductile plus transgranular and intergranular fracture morphologies, respectively.

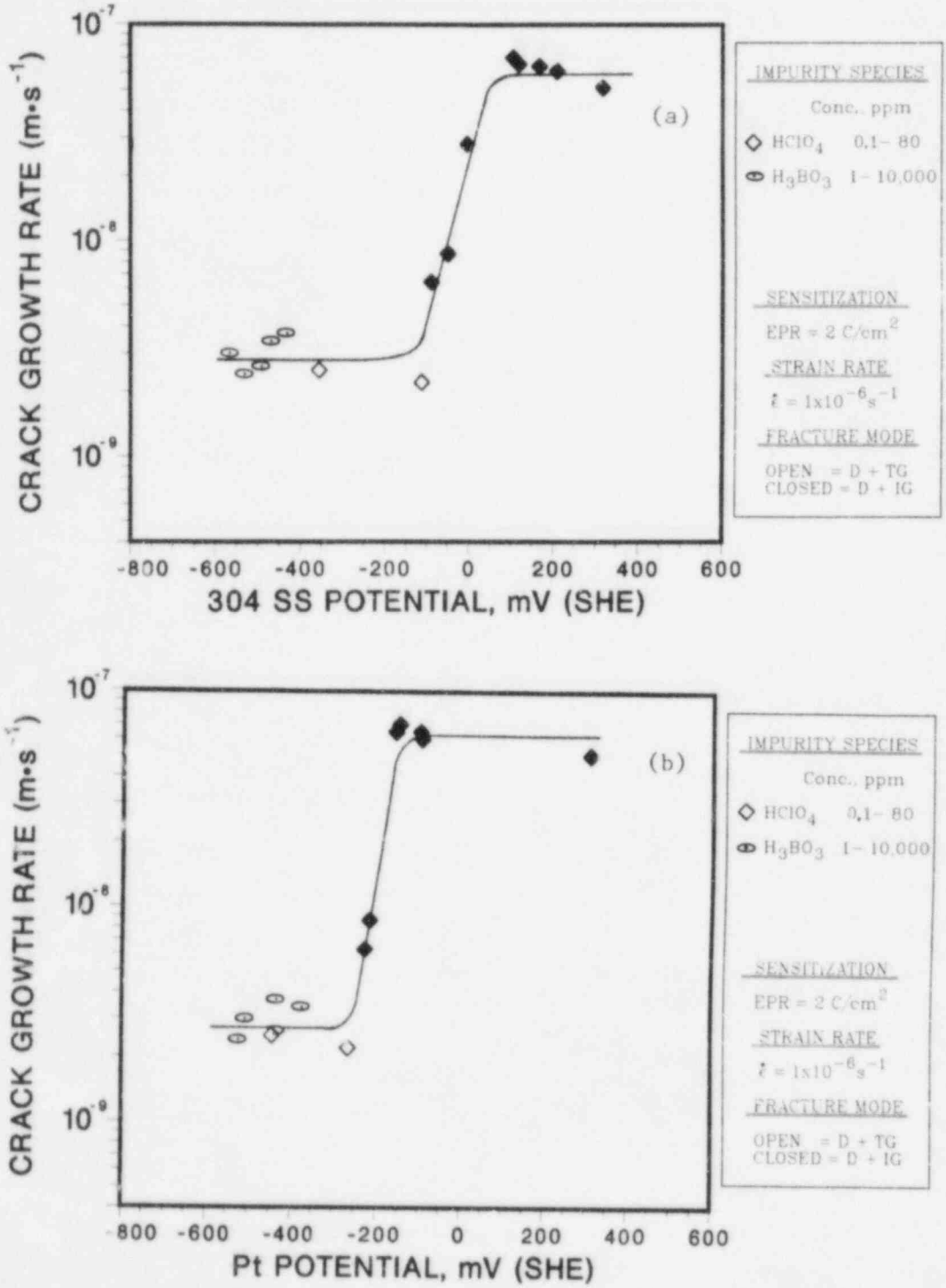

Fig. 1.20. Dependence of the Crack Growth Rate of Sensitized Type 304 SS CERT Specimens on the Electrochemical Potentials of (a) Type 304 SS and (b) Platinum in 289°C Water Which Contains $HClO_4$ or H_3BO_3 at Low Dissolved-Oxygen Concentrations. Open and closed symbols denote ductile plus transgranular and intergranular fracture morphologies, respectively.

cathodic reduction reactions will proceed in the various environments). In the latter regard, it was shown that IGSCC of sensitized Type 304 SS was inhibited completely in basic ($pH_{25°C}$ = 9) $NaAsO_2$ and Na_2HAsO_4 solutions at anion concentrations of greater than approximately 5 and 20 ppm, respectively,[16] although arsenic in the latter salt is in the As^{+5} state and thus, is capable of being reduced to As^{+3} according to Eq. (9)].

On the basis of this work, it may be possible to establish the synergistic effect of different impurity species along with dissolved oxygen on the SCC susceptibility of sensitized Type 304 SS. The manner in which the different cathodic reactions couple with the anodic-dissolution reaction at the crack tip and contribute to the overall crack growth rate may be as follows:

$$\dot{a}\ (m \cdot s^{-1}) = k_1'/[e^-]_{O_2} + k_3'/[e^-]_{SO_4^{2-}} + k_4'/[e^-]_{NO_3^-} + \ldots\ldots, \qquad (27)$$

where the contributions to crack growth are obtained from the concentration dependence for the individual species, i.e., the curves in Figs. 1.16-1.18. Similarly, species that do not appear to have a major influence on the crack growth process by themselves (viz., BO_3^{3-}, CO_3^{2-}, Cl^-) could receive lesser consideration when assessing the amount of crack propagation in a susceptible material in a particular environment. The range of dissolved-oxygen and impurity concentrations over which Eq. (27) may be applicable is limited to relatively low levels because the crack growth rate at a given strain rate (e.g., 1 x 10^{-6} s^{-1}) tends to become independent of the concentration of the various species at high concentrations (e.g., Fig. 1.18a). Some indication of this is also evident in Figs. 1.16b and 1.17a for H_2SO_4 and the other oxyacids where the data points at high concentrations fall below the line. In terms of the slip-dissolution model, the film rupture rate at the crack tip is probably not sufficient to sustain larger crack growth rates in the presence of higher oxygen and/or impurity concentrations. However, in simulated BWR environments (low-conductivity water with 0.2-0.3 ppm dissolved oxygen), small concentrations (<0.1 ppm) of the various oxyanions and other species in the water have a measurable effect on the crack growth rate of sensitized Type 304 SS at 289°C.[27]

c. Influence of Environment on Crack Growth of Type 304 SS under Cyclic Loading in Simulated BWR-Quality Water

To further investigate the effects of dissolved oxygen, hydrogen, and sulfate on the crack growth properties of Type 304 SS, an experiment was performed on fracture-mechanics-type specimens of the steel in the solution annealed and sensitized conditions. In different phases of the test, the water-chemistry conditions were varied from a reference condition of 0.2 ppm dissolved oxygen plus 0.1 ppm sulfate (as H_2SO_4) to lower oxygen concentrations at this sulfate level as well as higher and lower sulfate concentrations at a fixed dissolved-oxygen concentration in the feedwater. Measurements of the steady-state open-circuit corrosion potential of the steel and the redox potential of a platinum electrode located at the outlet of the autoclave were made. Analyses of the inlet and effluent dissolved-oxygen concentrations of the water were obtained during each water-chemistry condition. The steady-state crack growth rates were determined over time intervals of ~600-1000 h under low-frequency (8×10^{-2} Hz), moderate stress-intensity (K_{max} = 27-34 MPa$\cdot m^{1/2}$), and high-R (0.95) loading conditions at 289°C. The crack growth data for specimens sensitized to EPR values of 0, 2, and 20 C/cm^2 are given in Table 1.8 along with the electrochemical-potential results and the dissolved oxygen, hydrogen, and sulfate concentrations of the feedwater during each phase of the experiment, i.e., (1) through (7). The crack growth rates for each specimen under the different water-chemistry conditions are shown in Fig. 1.21. The open-circuit corrosion potential of the steel and the conductivity of the feedwater for each phase of the test are shown in the insert panel of the figure, where the region above the curve defines the regime for IGSCC based on CERT data at 289°C and a strain rate of 1×10^{-6} s^{-1} for this heat of steel.[16,25]

The crack growth rates under the reference water-chemistry condition of 0.2 to 0.3 ppm dissolved oxygen and 0.1 ppm sulfate [(1, 3, and 5) in Fig. 1.21] ranged from 2.8 to 5.0 $\times 10^{-10}$ m$\cdot$s^{-1} for the three levels of sensitization of the material. In moving from condition (1) to (2), in which the dissolved-oxygen concentration of the water was decreased from 0.2 to 0.002 ppm, crack growth in the sensitized specimens ceased and the rate in the solution annealed specimen decreased by a factor of 10. Upon returning to the

TABLE 1.8. Crack Growth Results for Type 304 SS Specimens[a] during an Experiment[b] in Which the Dissolved Oxygen and Sulfate Concentrations of the Feedwater Were Cycled between a Reference Condition and Several Different Chemistries Including Hydrogen Additions to the Water

TABLE 1.8. Crack Growth Results for Type 304 SS Specimens[a] during an Experiment[b] in Which the Dissolved Oxygen and Sulfate Concentrations of the Feedwater Were Cycled between a Reference Condition and Several Different Chemistries Including Hydrogen Additions to the Water

Test Cond.	Test Time, h	Water Chemistry				Electrode Potentials		Specimen #27 (EPR = 0 C/cm^2)			Specimen #28 (EPR = 2 C/cm^2)			Specimen #29 (EPR = 20 C/cm^2)		
		Oxygen,[c] ppm	Hydrogen, ppm	Sulfate, ppm	Cond., µS/cm	304 SS, mV(SHE)	Pt, mV(SHE)	Crack Length, mm	K_{max}, MPa·m$^{1/2}$	Growth Rate, m·s^{-1}	Crack Length, mm	K_{max}, MPa·m$^{1/2}$	Growth Rate, m·s^{-1}	Crack Length, mm	K_{max}, MPa·m$^{1/2}$	Growth Rate, m·s^{-1}
1	5 840	0.2–0.3	–	0.1	0.88	+80	+180	0.84 1.65	26.5	2.8×10^{-10}	1.17 2.67	27.0	5.0×10^{-10}	1.24 2.51	27.1	4.2×10^{-10}
2	1007 2184	0.002	–	0.1	0.88	-545	-520	1.73 1.80	27.8	2.0×10^{-11}	2.67 2.62	29.1	0	2.51 2.49	28.9	0
3	2357 3024	0.2–0.3	–	0.1	0.88	+120	+215	2.01 3.04	28.1	4.2×10^{-10}	3.25 4.06	30.0	3.4×10^{-10}	2.79 3.61	29.3	3.4×10^{-10}
4	3196 4200	0.2–0.3	–	–	0.16	+110	+230	3.25 4.39	30.0	3.2×10^{-10}	4.06 4.09	31.5	0	3.58 3.58	30.5	0
5	4393 5040	0.2–0.3	–	0.1	0.88	+120	+190	4.72 5.69	32.3	4.2×10^{-10}	4.78 5.46	32.4	2.9×10^{-10}	4.11 4.72	31.4	2.6×10^{-10}
6	5208 5216	0.002	1.4	0.1	0.88	-635	-640	5.74 5.77	34.0	0	5.46 5.41	33.7	0	4.70 4.62	32.3	0
7	6385 7011	0.002	1.4	1.0	8.1	-575	-565	5.79 5.82	34.1	3.0×10^{-11}	5.41 5.25	33.4	0	4.64 4.67	32.2	1.3×10^{-11}

[a]Compact tension specimens (1TCT) from Heat No. 30956 were solution annealed at 1050°C for 0.5 h (EPR = 0), sensitized at 700°C for 12 h (EPR = 20 C/cm^2), and 700°C for 25 h plus 500°C for 24 h (EPR = 2 C/cm^2).

[b]The load ratio and frequency of the positive sawtooth waveform were 0.95 and 8×10^{-2} Hz, respectively.

[c]Feedwater oxygen concentration at the 0.2–0.3 ppm level was approximately a factor of 3 higher to compensate for oxygen depletion by corrison of the autoclave system.

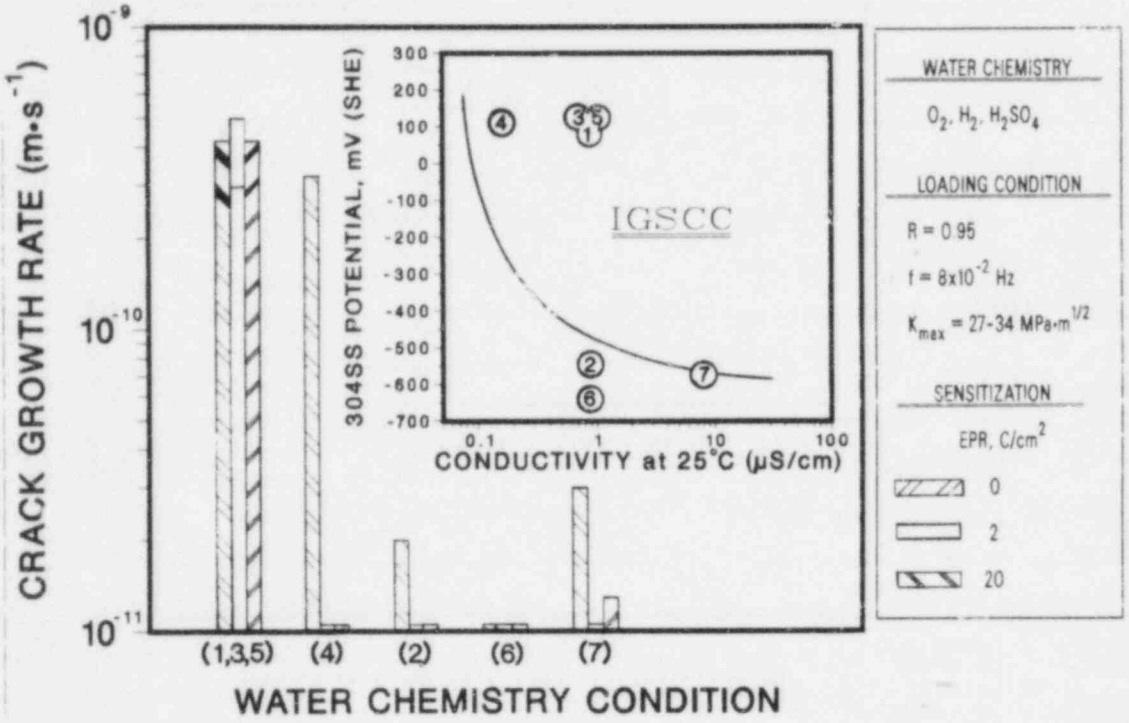

Fig. 1.21. Effect of Several Simulated BWR Water Chemistries Within and Outside of the IGSCC Regime on the Crack Growth Rates of Compact-Tension Specimens of Type 304 SS with Different Levels of Sensitization under Low-Frequency, Moderate Stress Intensity, and High-R Loading Conditions at 289°C.

reference water chemistry, i.e., (3), crack growth in the sensitized specimens resumed at the initial rates. Under condition (4), the dissolved-oxygen concentration remained at 0.2-0.3 ppm, but sulfate was not added to the feedwater (a conductivity of 0.16 μS/cm) and crack growth in the sensitized specimens once again ceased, although crack growth in the solution annealed specimen continued at approximately the same rate as before. Condition (4) falls just within the regime of IGSCC for a corrosion potential of +110 mV(SHE) in high-purity water. The benefit of improved water chemistry (i.e., 0.16 vs 0.88 μS/cm conductivity) at the 0.2-0.3 ppm dissolved oxygen level is illustrated in this phase of the experiment. After crack growth resumed under the reference water-chemistry condition, i.e., (5), the oxygen concentration was decreased to 0.002 ppm, and 1.4 ppm hydrogen was added to the feedwater, i.e., condition (6). The steady-state open-circuit corrosion potential of the steel decreased from +120 to -635 mV(SHE) and crack growth ceased in all specimens over a time period of ~1000 h during low-frequency cyclic loading at K_{max} = 34 MPa•m$^{1/2}$. Water-chemistry conditions (2) and (6)

fall below the curve in Fig. 1.21 where IGSCC is not likely to occur. In the last phase of the experiment, the sulfate concentration of the feedwater, containing 0.002 ppm dissolved oxygen and 1.4 ppm hydrogen, was increased from 0.1 to 1 ppm (a conductivity of 8.1 μS/cm). The corrosion potential of the steel increased slightly [-635 to -575 mV(SHE)], primarily owing to the decrease in the pH of the water, and crack growth resumed in the solution annealed and moderately sensitized specimens, but at a relatively low rate ($<3 \times 10^{-11}$ m·s^{-1}). This condition falls on the boundary of the IGSCC regime in Fig. 1.21. Upon moving from a relatively benign environment [e.g., conditions (2) and (4)] to the reference environment [conditions (3) and (5), respectively], significant crack growth occurred in the sensitized specimens within the 170-h time interval for the next compliance measurement. Under almost all water-chemistry conditions, the highest crack growth rates occurred in the solution annealed material. Thus, the superior in-reactor performance of the steel in the annealed condition appears to be related to its resistance to crack initiation rather than to crack propagation. In general, the crack growth results from the fracture-mechanics-type specimens are in agreement with the more extensive CERT data regarding the effects of water chemistry on the SCC susceptibility of the material in high-temperature water.

Observations (a) that measurable changes in crack growth of sensitized Type 304 SS specimens occur rapidly (i.e., within several hours[14] to a day[28]) after changes in bulk feedwater chemistry and (b) that cracks remain dormant for long time periods (>1000 h) under certain water-chemistry conditions in our experiments are consistent with the premise that crack growth is controlled by cathodic reduction processes involving dissolved oxygen and other species at the specimen/bulk-water interface. Under this scenario, the environment at the crack tip could be conducive to crack growth over a wide range of bulk-water chemistries, and thus obviate the apparent requirement to "flush" or deplete the ion-rich crack-tip environment when oxygen and/or impurities are removed from the bulk water in order to mitigate crack growth in the material. The tight, deep nature of stress corrosion cracks implies that diffusional mass transport of ionic species within cracks with large depth-to-width aspect ratios would proceed at relatively low rates compared to electron transport in the metal and adsorption/desorption processes at the specimen surface, as discussed in the previous section.

Figures 1.22-1.24 show the fracture surfaces, the SCC morphology, and the nature of the crack near the tip region for the specimens with different levels of sensitization (EPR = 0, 2, and 20 C/cm^2, respectively). The 1TCT specimens were sectioned vertically, and half of each specimen was split in the plane of the crack at liquid-nitrogen temperature to reveal the SCC fracture surface at low magnification (center micrograph in each figure). The corrosion-product film was removed from the fracture surface by the APAC process[29,30] [i.e., by exposure of the specimens to a gently boiling alkaline permanganate solution (20% NaOH, 3% $KMnO_4$) for 2 h, followed by a hot rinse, and then in a 20% dibasic ammonium citrate solution for 2 h] to reveal the morphology of the underlying metal. The intact portion of the specimen that encompassed the crack was polished and etched to corroborate the mode of crack propagation and also to determine if macrobranching of the crack had occurred during the test. The fracture surface morphology and crack path in the solution annealed specimen (EPR = 0) in Fig. 1.22 indicate that the mode of crack propagation was transgranular, whereas the micrographs in Figs. 1.23 and 1.24 for the lightly (EPR = 2 C/cm^2) and moderately (EPR = 20 C/cm^2) sensitized specimens reveal intergranular cracking. Macrobranching of the cracks was not observed; however, some curvature of the crack front is evident in the three specimens. The fracture morphologies for the three specimens closely resemble those of other specimens that were subjected to similar loading conditions in high-temperature water.[31]

SENSITIZATION:	LOAD CONDITIONS:	WATER CHEMISTRY:
EPR=0 C/cm^2	R=0.95, K_{MAX} 27-34MPa·m$^{1/2}$ f=8 x 10^{-2}Hz, TEMP.=289°C	0.002-0.2 ppm O_2 0.1-1.0 ppm SO_4^{2-}

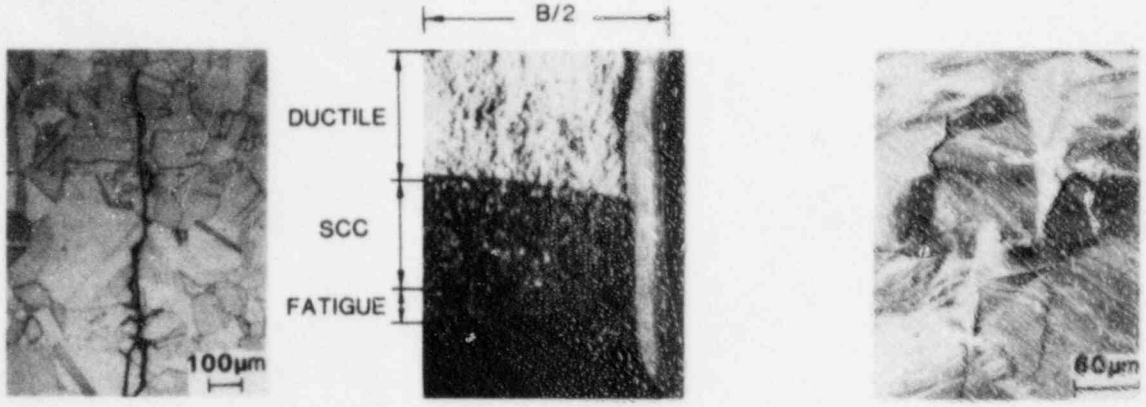

CRACK TIP REGION | FRACTURE SURFACE | SCC FRACTURE MORPHOLOGY

Fig. 1.22. Fracture Surface and SCC Fracture Morphology of a Solution Annealed 1TCT Specimen (No. 27) of Type 304 SS after a Crack Growth Experiment in 289°C Water with Different Simulated BWR Water-Chemistry Conditions.

SENSITIZATION:	LOAD CONDITIONS:	WATER CHEMISTRY:
EPR=2 C/cm^2	R=0.95, K_{MAX} 27-33MPa·m$^{1/2}$ f=8 x 10^{-2}Hz, TEMP 289°C	0.002-0.2 ppm O_2 0.1-1.0 ppm SO_4^{2-}

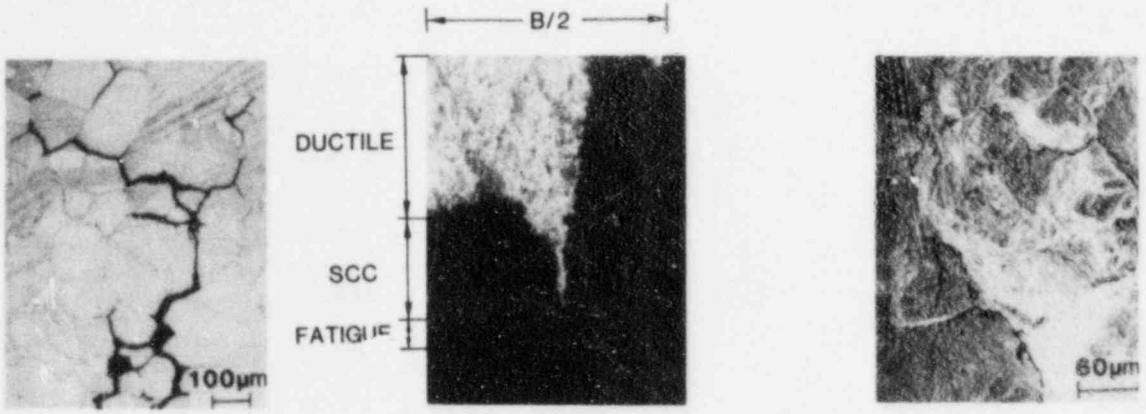

CRACK TIP REGION | FRACTURE SURFACE | SCC FRACTURE MORPHOLOGY

Fig. 1.23. Fracture Surface and SCC Fracture Morphology of a Lightly Sensitized 1TCT Specimen (No. 28) of Type 304 SS after a Crack Growth Experiment in 289°C Water with Different Simulated BWR Water-Chemistry Conditions.

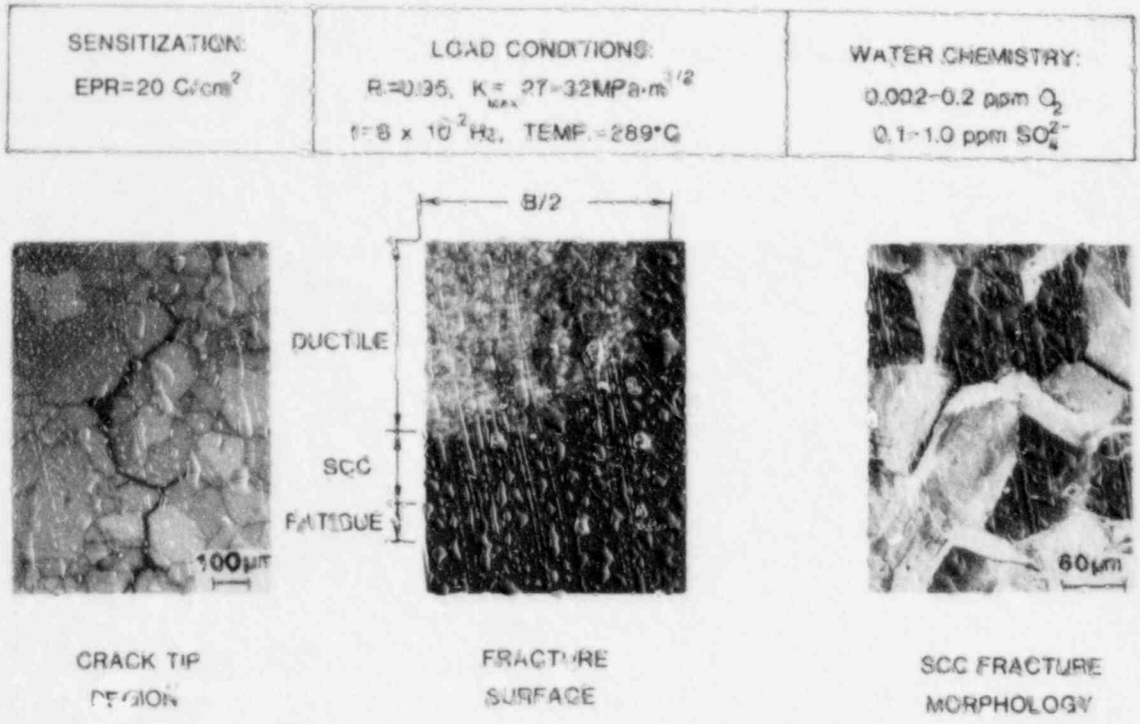

Fig. 1.24. Fracture Surface and SCC Fracture Morphology of a Moderately Sensitized WOL Specimen (No. 29) of Type 304 SS after a Crack Growth Experiment in 289°C Water with Different Simulated BWR Water-Chemistry Conditions.

E. References for Chapter I

1. J. Y. Park and W. J. Shack, in Materials Science and Technology Division Light-Water-Reactor Safety Research Program: Quarterly Progress Report for October-December 1983, NUREG/CR-3689 Vol. IV, ANL-83-65 Vol. IV (August 1984), pp. 26-30.

2. P. S. Maiya and W. J. Shack, in Materials Science and Technology Division Light-Water-Reactor Safety Research Program: Quarterly Progress Report for October-December 1983, NUREG/CR-3689 Vol. IV, ANL-83-65, Vol. IV, (August 1984), pp. 31-50.

3. P. S. Maiya and W. J. Shack, in Environmentally Assisted Cracking in Light Water Reactors: Annual Report for October 1983-September 1984, NUREG/CR-4287, ANL-85-33 (June 1985), pp. 27-61.

4. P. S. Maiya and W. J. Shack, Stress Corrosion Cracking Susceptibility of AISI 316 NG and 316 Stainless Steel in an Impurity Environment, Corrosion 41(11), 30-34 (1985).

5. P. S. Maiya, "Prediction of Environmental and Strain-Rate Effects on the Stress Corrosion Cracking of Austenitic Stainless Steels," in Predictive Capabilities in Environmentally Assisted Cracking, PVP-Vol. 99, The American Society of Mechanical Engineers, ed. Ravi Rungta (1985), pp. 39-54.

6. P. S. Maiya, Observation of Crack Initiation in Low-Cycle Fatigue Specimens of Type 304 Stainless Steel, Scripta Metallurgica 11, 331-334 (1977).

7. P. S. Maiya and W. J. Shack, in Light-Water-Reactor Safety Materials Engineering Research Programs: Quarterly Progress Report for October-December 1984, NUREG/CR-3998 Vol. III, ANL-84-60 Vol. III (October 1985), pp. 14-23.

8. Lars Ljungberg, in SCC Testing in BWR Environment, Report AA TR KM 83-285, SKI Project G.2.1/711/80, EPRI Project RP 1930-4 (1983).

9. M. E. Indig and J. E. Weber, Effects of H_2 Additions on Stress Corrosion Cracking in a Boiling Water Reactor, Corrosion 41(1), 19-30 (1985).

10. L. S. Aubrey et al., "Ferrite Measurement and Control in Cast Duplex Stainless Steels," in Stainless Steel Castings, American Society for Testing and Materials, ASTM STP 756 (1982), pp. 126-164.

11. W. E. Ruther, W. K. Soppet, and T. F. Kassner, in Light-Water-Reactor Safety Materials Engineering Research Programs: Quarterly Progress Report for April-June 1984, NUREG/CR-3998 Vol. II, ANL-84-60 Vol. II (February 1985), pp. 38-47.

12. W. E. Ruther, W. K. Soppet, and T. F. Kassner, Effect of Temperature and Ionic Impurities at Very Low Concentrations on Stress Corrosion Cracking of Type 304 Stainless Steel, Corrosion/85, Boston, MA, March 1985, Paper No. 102.

13. R. B. Davis and M. E. Indig, The Effect of Aqueous Impurities on the Stress Corrosion Cracking of Austenitic Stainless Steels in High-Temperature Water, Corrosion/83, Anaheim, CA, April 1983, Paper No. 128.

14. P. L. Andresen, A Mechanism for the Effects of Ionic Impurities on SCC of Austenitic Iron and Nickel Base Alloys in High-Temperature Water, Corrosion/85, Boston, MA, March 1985, Paper No. 101.

15. W. E. Ruther, W. K. Soppet, and T. F. Kassner, in Materials Science and Technology Division Light-Water-Reactor Safety Research Program: Quarterly Progress Report for October-December 1983, NUREG/CR-3689 Vol. IV, ANL-83-85 Vol. IV (August 1984), pp. 57-75.

16. W. E. Ruther, W. K. Soppet, and T. F. Kassner, in Light-Water-Reactor Safety Materials Engineering Research Programs: Quarterly Progress Report for October-December 1984, NUREG/CR-3998 Vol. III, ANL-84-60 Vol. III (October 1985), pp. 24-36.

17. D. M. Himmelblau, Solubilities of Inert Gases in Water, 0°C to Near the Critical Point, J. Chem. and Engr. Data 5(1), 10-15 (1960).

18. F. H. Sweeton, R. E. Mesmer, and C. F. Baes, Jr., Acidity Measurements at Elevated Temperatures; VII Dissociation of Water, J. Solution Chem. 3(3), 191-214 (1974).

19. W. L. Marshall and E. V. Jones, Second Dissociation Constant of Sulfuric Acid from 25 to 350°C Evaluated from Solubilities of Calcium Sulfate in Sulfuric Acid Solutions, J. Phys. Chem. 70(12), 4028-4040 (1966).

20. C. Wagner and W. Truad, Uber Die Deutung Von Korrosionsvorgangen Durch Uberlagerung Von Electrochemischen Teilvorgangen Und Uber Die Potentialbildung An Mischelektroden, Z. Elektrochem., 44, 391-402 (1938).

21. F. P. Ford, "Stress Corrosion Cracking," in Corrosion Processes, R. N. Parkins, ed., Applied Science Publishers, New York, pp. 271-309 (1982).

22. D. A. Vermilyea, in Proc. Intl. Conf. on Stress Corrosion Cracking and Hydrogen Embrittlement of Iron Base Alloys, R. W. Staehle, J. Hochmann, R. D. McCright, and J. E. Slater, eds., NACE, Houston (1983), p. 208.

23. H. Wendt, Die Kinetik typischer Hydrolsereaktionen Von mehrwertigen Kation, Chimia, 27, 575-588 (1973).

24. C. F. Baes, Jr. and R. E. Mesmer, The Hydrolysis of Cations, John Wiley & Sons, Inc., New York (1976), p. 212.

25. W. E. Ruther, W. K. Soppet, and T. F. Kassner, in Environmentally Assisted Cracking in Light Water Reactors: Annual Report, October 1982-September 1983, NUREG/CR-3806, ANL-84-36 (June 1984), pp. 101-117.

26. K. Arioka, M. Hourai, S. Okamoto, and K. Onimura, The Effects of Boric Acid, Solution Temperature, and Sensitization on the SCC Behavior under Elevated Temperature Water, Corrosion/83, Anaheim, CA, April 1983, Paper No. 135.

27. W. E. Ruther, W. K. Soppet, and T. F. Kassner, in Environmentally Assisted Cracking in Light Water Reactors: Annual Report, October 1983-September 1984, NUREG/CR-4287, ANL-85-33 (June 1985), pp. 93-113.

28. T. A. Prater, W. R. Catlin, and L. F. Coffin, Influence of Dissolved Hydrogen and Oxygen on Crack Growth in LWR Materials, EPRI NP-4183M, Electric Power Research Institute (July 1985).

29. M. T. Jones, Reactor Technology Report, No. KAPL-2000-11 (1960).

30. W. E. Ruther and S. Greenberg, Corrosion of Steels and Nickel Alloys in Superheated Steam, J. Electrochem. Soc. 111(10), 1116-1121 (1964).

31. W. E. Ruther, W. K. Soppet, and T. F. Kassner, in Materials Science and Technology Division Light-Water-Reactor Safety Research Program: Quarterly Progress Report for October-December 1983, NUREG/CR-3689 Vol. IV, ANL-83-85 Vol. IV (August 1984), pp. 75-87.

II. LONG-TERM EMBRITTLEMENT OF CAST DUPLEX STAINLESS STEELS IN LWR SYSTEMS

Principal Investigators:
O. K. Chopra and H. M. Chung

A program is being conducted to investigate the significance of in-service embrittlement of cast-duplex stainless steels under light-water reactor (LWR) operating conditions and to evaluate possible remedies to the embrittlement problem for existing and future plants.

The scope includes the following: (1) characterize and correlate the microstructure of in-service reactor components and laboratory-aged material with loss of fracture toughness and identify the mechanism of embrittlement, (2) determine the validity of laboratory-induced embrittlement data for predicting the toughness of component materials after long-term aging at reactor operating temperatures, (3) characterize the loss of fracture toughness in terms of fracture mechanics parameters in order to provide the data needed to assess the safety significance of embrittlement, and (4) provide additional understanding of the effects of key compositional and metallurgical variables on the kinetics and degree of embrittlement. The relationship between aging time and temperature for onset of embrittlement will be determined by microstructural examination and measurements of hardness, Charpy-impact strength, tensile strength, and J_{IC} fracture toughness. The kinetics and fracture toughness data generated in this program and from other sources will provide the technical basis for assessing the in-service embrittlement of cast stainless steels under LWR operating conditions. Estimates of the degree of embrittlement will be compared with data obtained from examination of material from actual reactor service. Data pertaining to the effects of compositional and metallurgical variables on the embrittlement phenomenon will help in evaluation of the possible remedies for in-service embrittlement of components in existing and future plants.

A. Material Characterization and Mechanical Testing (O. K. Chopra)

Material was obtained from nineteen experimental heats (static-cast keel blocks) and six commercial heats (centrifugally cast pipes and static-cast pump impeller and pump casing ring) of CF-3, -8, and -8M grades of cast duplex stainless steel. Six of the experimental heats were also procured in the form of 76-mm-thick slabs. Charpy-impact specimen blanks were obtained from all heats of material. Blanks for compact tension and tensile specimens were obtained from sections of the cast pipes, pump casing ring, pump impeller, and cast slabs. The specimen blanks are being aged at 450, 400, 350, 320, and 290°C for times up to 50,000 h. Materials from the reactor components and small experimental heats have completed ~11,000 h of aging and cast materials from the large experimental heats (76-mm-thick slabs) have completed ~4000 h of aging. The mechanical test specimens are machined after the thermal aging treatment.

Fractured impact test bars from three heats of aged cast stainless steel, grades CF-8 and CF-8M, were obtained from Georg Fischer Co., Switzerland, for microstructural characterization. The materials are from a previous study of the long-term aging behavior of cast stainless steel.[1] The specimens from CF-8 material (Heats 280 and 278) were aged for 3000, 10,000, and 70,000 h at 300, 350, and 400°C, whereas the specimens from CF-8M material (Heat 286) were aged for 1000 and 10,000 h at 400°C. A cover plate assembly from the recirculation pump of the KRB reactor was also procured. The reactor was in service for ~12 yr. The plate assembly was decontaminated and samples were obtained for microstructural characterization and mechanical testing. The test matrices for the various mechanical tests and microstructural examination have been presented.[2,3]

Data on the chemical composition, ferrite content, hardness, ferrite morphology, and grain structure of the small experimental and commercial heats have been reported.[4,5] During the present quarter, characterization of the six large experimental heats was completed. The heats were static-cast in the form of square (0.61 x 0.61 m) slabs 76 mm thick. All materials were examined in the three orientations as well as in different locations, namely, material from the top, middle, and bottom section of the slabs. The orientation of the

material had little or no effect on either hardness or ferrite content and morphology. The chemical composition, hardness, and ferrite content of the different heats are given in Table 2.1. Small experimental heats (i.e., keel blocks) with chemical composition and ferrite contents equivalent to the large experimental heats are also listed in Table 2.1. The hardness and ferrite content values represent the average values for the three locations.

The grain structures of the large experimental heats are shown in Fig. 2.1. All heats contain a mixed structure of columnar and equiaxed grains. A change from horizontal to vertical growth of the columnar grains was observed near the edges of the cast slabs, e.g., Heat 73. The grain size of Heats 69 (grade CF-3) and 75 (grade CF-8M) is smaller than that for the other heats.

The ferrite morphologies for the large experimental heats are shown in Figs. 2.2-2.4. The CF-8 and -8M grades of cast stainless steels have a lacy morphology, i.e., an interlaced network of ferrite islands. The CF-3 grade of cast steel has a mixture of lacy and acicular morphology. The acicular morphology is characterized by fine needle-like ferrite distributed in the austenite matrix. The ferrite contents and morphologies for the large experimental heats are similar to those observed for the corresponding heats of the keel blocks.

Charpy-impact tests are in progress at room temperature on the various heats of material aged up to 10,000 h at 450, 400, 350, 320, and 290°C. Standard Charpy V-notch specimens were machined from the aged and unaged materials according to ASTM specification E-23. A Dynatup Model 8000A drop-weight impact machine with an instrumented tup and data-readout system was used for the tests. Charpy-impact energies for materials aged for 3000 h at 450, 400, 350, and 320°C are given in Table 2.2. The results indicate that thermal aging of cast duplex stainless steels with >10% ferrite causes a substantial decrease in impact energy. Materials with >20% ferrite show a drastic reduction in impact energy after aging for ~300 h at 450°C or ~3000 h at 400°C. In general, the low-carbon grades of cast stainless steels exhibit greater resistance to embrittlement than the CF-8 and -8M grades.

TABLE 2.1. Chemical Composition and Ferrite Content of Cast Stainless Steel

Heat	Grade	Composition, wt %							Hardness, R_B	Ferrite Content, %	
		Mn	Si	Mo	Cr	Ni	N	C		Calc.[a]	Meas.[b]
					Cast Slabs[c]						
73	CF-8	0.83	1.22	-	19.53	8.94	0.05	0.06	78.8	7.4	7.7
68	CF-8	0.67	1.13	-	20.85	8.08	0.06	0.05	84.6	18.8	23.4
74	CF-8	0.77	1.21	-	20.73	8.17	0.11	0.06	85.8	10.5	18.4
69	CF-3	0.69	1.20	-	20.49	8.43	0.03	0.02	83.7	25.7	23.6
70	CF-8M	0.70	0.74	2.64	19.37	9.13	0.05	0.07	86.5	15.8	18.9
75	CF-8M	0.59	0.67	2.40	21.07	9.02	0.05	0.06	89.5	27.1	27.8
					Keel Blocks[d]						
56	CF-8	0.60	1.16	0.30	19.33	8.93	0.03	0.06	82.5	8.1	10.1
60	CF-8	0.71	1.01	0.26	21.02	8.07	0.05	0.07	86.7	16.9	21.1
51	CF-3	0.66	1.06	0.28	20.36	8.69	0.05	0.02	83.8	17.5	18.0
66	CF-8M	0.71	0.60	2.36	19.41	9.13	0.03	0.06	85.2	17.9	19.9
64	CF-8M	0.70	0.71	2.41	20.87	9.01	0.03	0.05	89.7	32.2	28.4

[a]Calculated from the chemical composition with Hull's equivalent factor.
[b]Measured by ferrite scope Auto Test FE, Probe Type FSP-1).
[c]Chemical compositions obtained from the vendor.
[d]Chemical compositions obtained at Argonne National Laboratory.

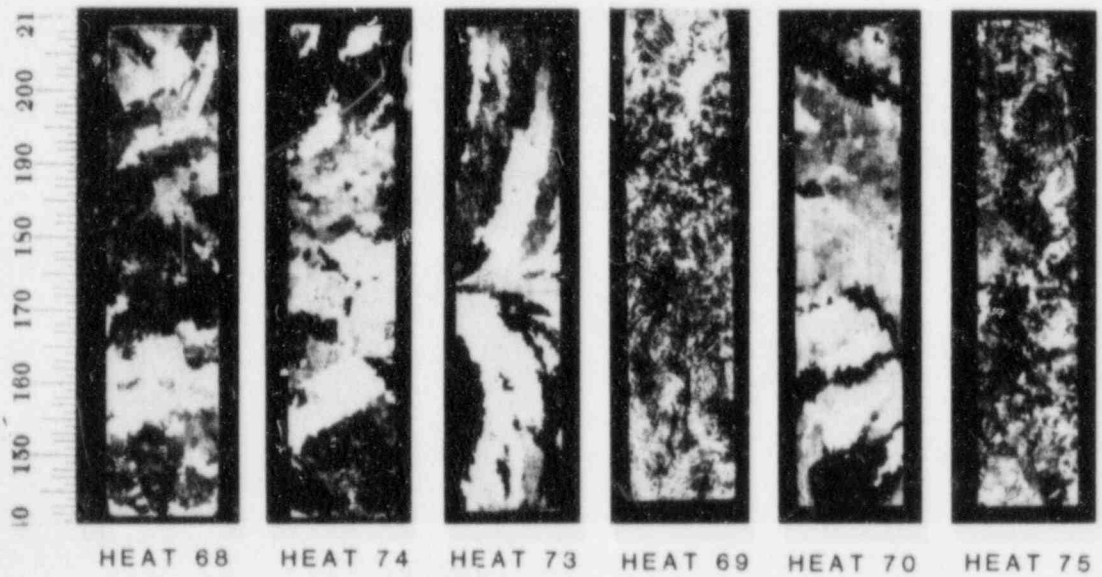

Fig. 2.1. Microstructures Along Verticle Sections of Various Static-Cast Slabs.

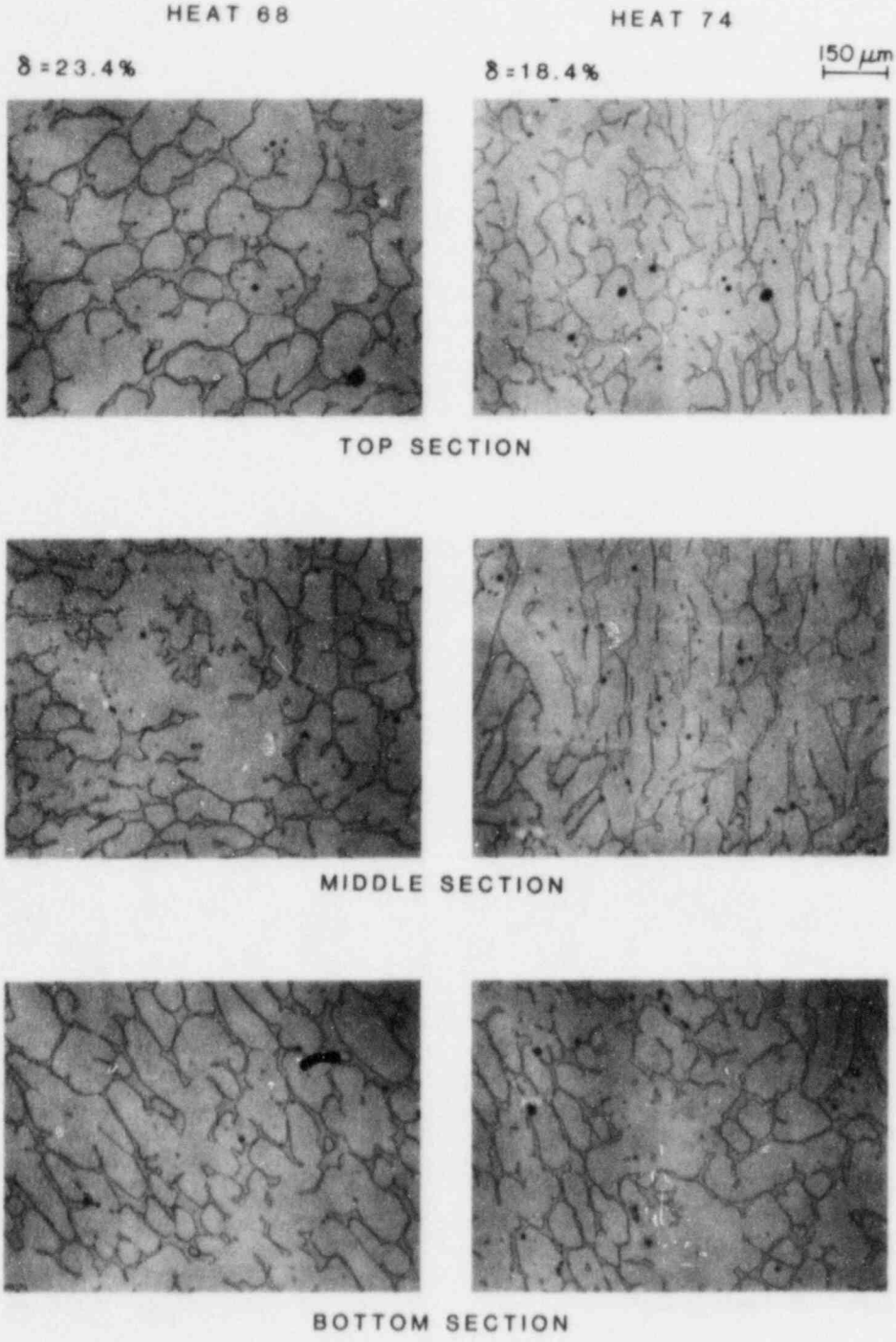

Fig. 2.2. Microstructures from Three Locations in Static-Cast Slabs of CF-8 Stainless Steel with Ferrite Contents of 23.4 and 18.4%.

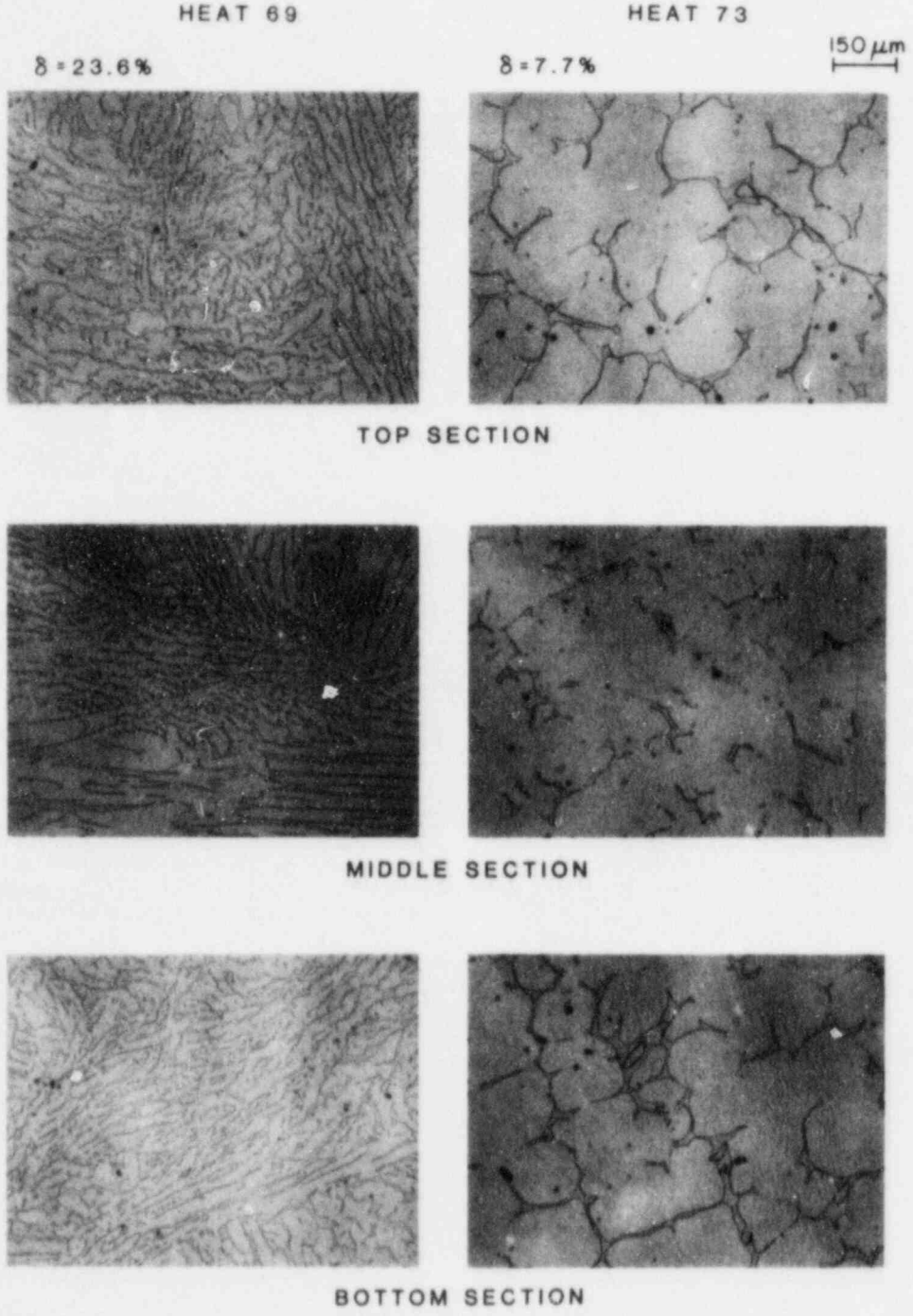

Fig. 2.3. Microstructures from Three Locations in Static-Cast Slabs of CF-3 (Heat 69) and CF-8 (Heat 73) Stainless Steel with Ferrite Contents of 23.6 and 7.7%, Respectively.

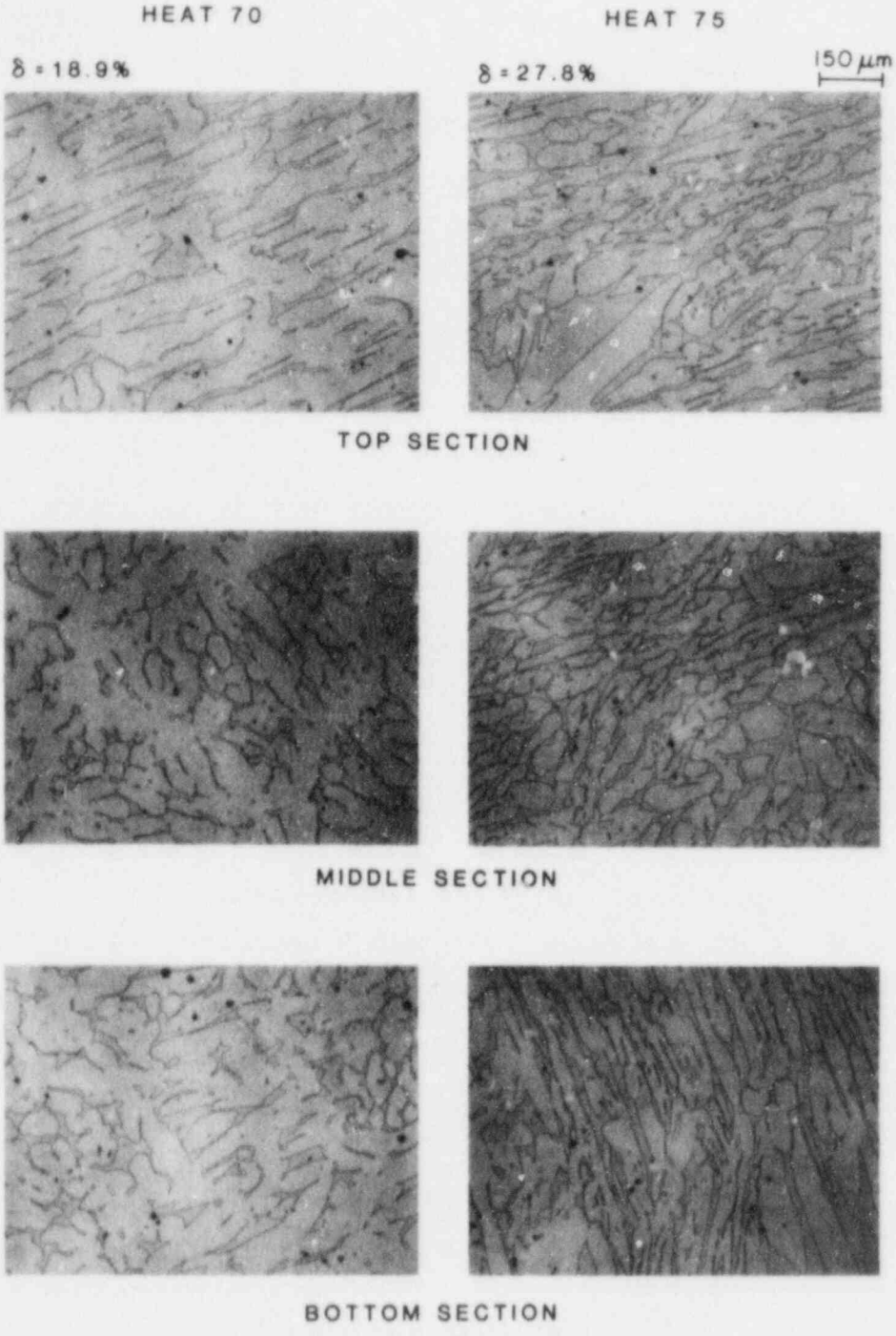

Fig. 2.4. Microstructures from Three Locations in Static-Cast Slabs of CF-8M Stainless Steel (Heats 70 and 75) with Ferrite Contents of 18.9 and 27.8%, Respectively.

TABLE 2.2. Charpy-Impact Data Obtained at Room Temperature for Thermally Aged Cast Stainless Steel

Heat	Ferrite Content, %	Impact Energy,[a] J				
			Aged for 3000 h at			
		Unaged	320°C	350°C	400°C	450°C
			CF-8			
56	10.1	165	151	146	134	105
59	13.5	183	161	135	132	95
61	13.1	201	155	152	148	100
60	21.1	158	150	149	64	51
C1	2.2	47	-	41	46	48
P1	24.1	178	170	158	45	53
			CF-3			
52	13.5	198	175	189	174	146
47	16.3	184	245	179	151	140
51	18.0	161	143	164	131	125
P3	1.9	241	273	225	292	312
P2	15.6	321	357	-	212	158
I	17.1	156	152	156	-	105
			CF-8M			
63	10.4	199	137	166	125	126
66	19.9	177	204	166	113	84
65	23.4	179	147	141	51	51
64	28.4	160	140	120	40	42
P4	10.4	182	198	108	74	36

[a]Tests performed on instrumented drop-weight impact machine with V-notch impact bars (ASTM specification E-23).

Microhardness measurements of the ferrite phase of several thermally aged materials were carried out to evaluate the aging behavior of CF-3 and -8 grades of cast stainless steel. Figure 2.5 shows the influence of thermal aging on the impact energy and microhardness of the ferrite phase of Heat 51 (grade CF-3) and Heat 60 (grade CF-8). The results indicate that the impact energy decreases and the microhardness increases with aging time. For a given aging condition, the microhardness of the ferrite is comparable for Heats 51 and 60. However, the reduction in impact energy is significantly higher for

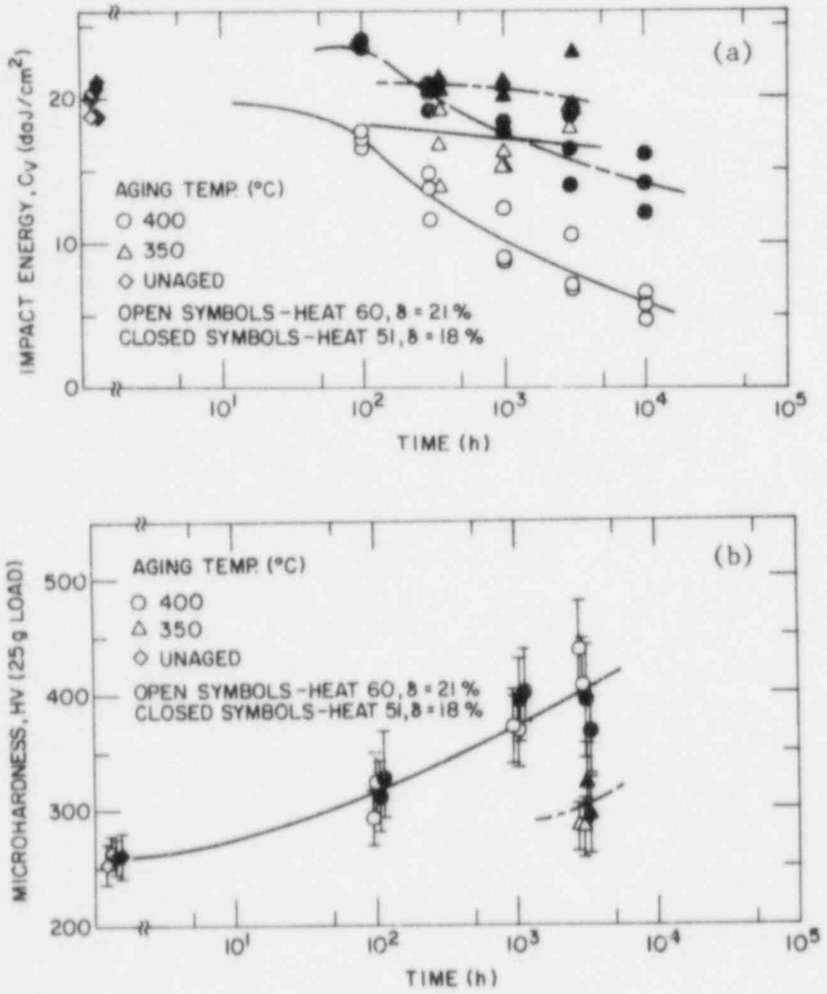

Fig. 2.5. Influence of Thermal Aging on the (a) Room-Temperature Impact Energy and (b) Microhardness of the Ferrite Phase for CF-3 (Heat 51) and CF-8 (Heat 60) Grades of Cast Stainless Steels.

Heat 60 than for Heat 51. The microhardness measurements indicate that the microstructural changes in ferrite matrix are similar for Heats 51 and 60. The difference in impact energy probably arises from the precipitation of carbides at the ferrite/austenite boundaries in Heat 60. Transmission electron microscopy (TEM) examination of the fractured Charpy specimens is in progress to characterize the microstructure of thermally aged materials.

Figure 2.6 shows the load-time curves for Heat 60 in the unaged condition and after aging for 300, 3000, and 10,000 h at 400°C. Two important features are evident, namely, thermal aging leads to a reduction in impact energy and

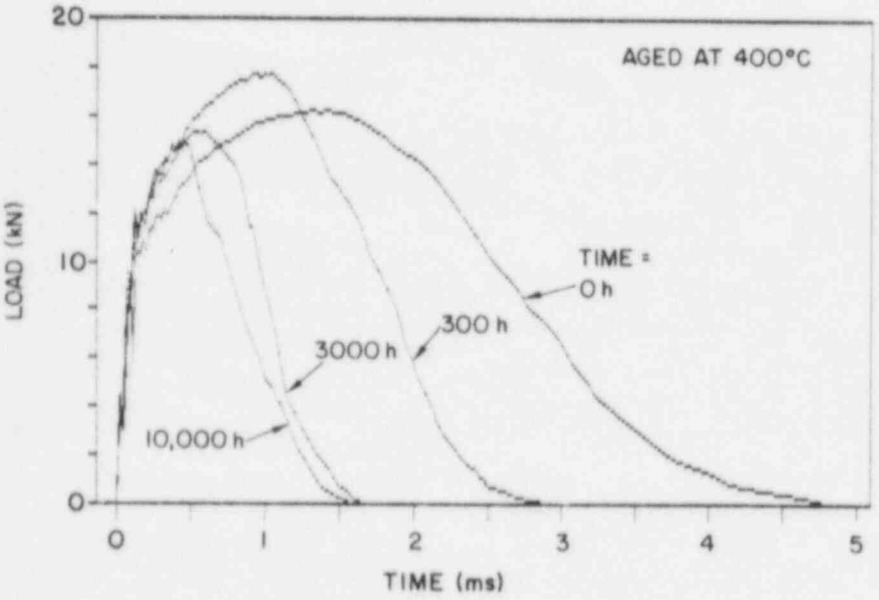

Fig. 2.6. Room-Temperature Load-time Curves for Charpy V-Notch Specimens of Heat 60.

an increase in the strain hardening rate of the material. The strain hardening rate increases after aging for a relatively short time (i.e., ~300 h) and does not change significantly with further aging. The maximum load for the specimen aged for 300 h is greater than that for the unaged specimen. The higher strain hardening rates for the aged material are associated with precipitation in the ferrite matrix. The load-time curve for the specimen that was aged for 10,000 h exhibits a sudden drop in load, indicative of a brittle fracture mode. Such load-time curves were typical for all heats with >20% ferrite.

B. Microstructural Investigation (H. M. Chung)

1. Introduction

Microstructural characteristics of the aged impact-tested specimens have been investigated by TEM, scanning-electron microscopy (SEM), optical microscopy, and small-angle neutron scattering (SANS) techniques. The results of the microstructural examination of the Georg Fischer (GF) materials and the KRB pump cover plate have been reported previously.[3-5] In this reporting

period, microstructures of the KRB pump cover as well as several laboratory-aged heats of cast duplex stainless steel (with compositions similar to those of the KRB material) have been examined further. The microstructural characteristics were correlated with the fracture behavior of the impact specimens to provide a better understanding of the embrittlement mechanism(s) of cast duplex stainless steels.[6] The results showed that three phases were responsible for embrittlement of the ferrite phase. Precipitation on the ferrite/austenite phase boundary was also identified, which leads to weakening of the phase boundary. Precipitates that are responsible for degradation of the impact-failure resistance of the G. Fischer, KRB pump cover, and several other heats of cast duplex stainless steel are described below.

2. Precipitates Associated with the Ferrite Phase Embrittlement

The characteristics of the three precipitates, i.e., G-phase, Type-X, and the chromium-rich α', are summarized below.

G-Phase

Figure 2.7 shows the characteristic morphology and selected-area diffraction (SAD) patterns of the G-phase observed in the GF material after aging at 400°C for 7.6 yr. The precipitates were also observed in the reactor-aged pump cover material, which was exposed to the coolant at ~274°C for ~12 yr. Volume fractions of the G-phase in the KRB pump material or in GF Heats 280 and 278, aged at 300°C for ~8 yr, were not large enough to produce distinct reflections in the diffraction patterns [similar to those of Figs. 2.7(B) and (C)]. Although 400°C aging produced precipitates of the G-phase in the ferrite grains as well as on the grain boundaries [Fig. 2.7(A)], no grain boundary precipitation was observed after aging at $\leq$300°C. During lower temperature aging, the precipitates were observed primarily in association with dislocations in the ferrite; this observation indicates a dislocation pinning effect. The nearly spherical precipitate is ~5 nm in size. The diffraction patterns are similar to those of the $M_{23}C_6$ phase, but with a slightly larger lattice parameter. The precipitates also had a cube-on-cube orientation relative to the bcc ferrite matrix, which would be unusual for the $M_{23}C_6$ phase. (400) reflections were characteristically weak or absent in the

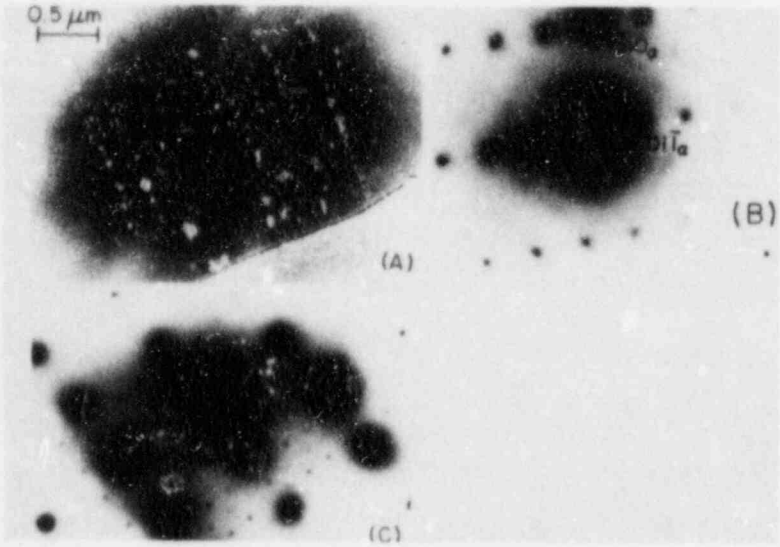

Fig. 2.7. (A) Dark-Field Morphology and (B and C) Characteristic SAD Patterns of the G-Phase Silicide Observed in CF-8 Cast Duplex Stainless Steel after Aging at 400°C for 7.6 yr.

diffraction patterns [Fig. 2.7(C)]. Energy-dispersive x-ray analysis showed an enrichment of Ni and Si in the precipitates. From these results, the precipitates were identified as the G-phase (a phase rich in Ni and Si), which has been observed in an Fe-12Cr-4Ni alloy after aging at 450°C[7] and in commercial EM-12 (9Cr-2Mo), HT-9 (12Cr-1Mo), and AISI 416 (13Cr) ferritic steels after irradiation at temperatures of <425°C.[8]

Type-X Precipitates

In both the KRB pump material and GF Heats 280 and 278, aged at 300°C for 8 yr, the unidentified (Type-X) precipitate was always observed on dislocations. The precipitates observed in the KRB pump material, which are interwoven with the dislocations, have been shown in Fig. 2.3 of Ref. 3. Apparently, the precipitates were very effective in pinning dislocation motion in the material aged for a long time near 300°C. The precipitate reflections in the SAD patterns were weak, diffuse, and streaked, owing to a low volume fraction and small particle size. In typical SAD patterns containing the Type-X precipitates, only extremely weak precipitate reflections with a d-spacing of 0.218 nm were detected. The weak reflections could not be detected on the microscope screen. No cross-grid patterns could be obtained.

α' Precipitate

Chromium-rich α' precipitates in the ferrite were observed in the KRB pump-cover material [Fig. 2.8(A)]. The extremely small (~2 nm) α' precipitates could not be resolved by TEM either under a strong bright-field or under a dark-field imaging condition. The precipitates could be resolved only under a weak-beam bright-field imaging condition. The mottled morphology characteristic of the α' was difficult to resolve in the GF material after aging at 300°C for 8 yr. However, optimum weak-beam imaging[9] at a magnification of 20-40 thousand times revealed α' precipitates 1-1.5 nm in size when the negatives were developed and examined on a lighted table with a magnifying glass. Negatives taken under a normal bright- or dark-field imaging condition did not reveal any α' precipitates in the GF materials. Figure 2.8(B) shows the α' in the ferrite of Heat 60 (Table 2.1) after aging at 400°C for 1.2 yr. The precipitate size and morphology are similar to those of the KRB reactor-aged material.

3. Precipitate Characterization by Small-Angle Neutron Scattering

Although the very fine α' in the GF materials, aged either at 300°C for 8 yr or at 400°C for 7.6 yr, could be resolved by the weak-beam TEM technique, the results from the small-angle neutron scattering experiments showed no distinct intensity peak at ~1-nm diameter, which corresponds to the size of α' in the materials. However, an intensity peak corresponding to the G-phase, which exhibits a distinct phase boundary (relative to the ferrite matrix) and a size an order of magnitude larger than the α', was observed as shown in Fig. 2.9.[10] The diameters of the most populous scattering centers shown in Figs. 2.9(A) and (B), i.e., ~1.6 and ~5.5 nm, are in good agreement with the sizes of the G-phase observed by TEM for the two aging conditions, i.e., GF Heat 278 aged at 400°C for 1.2 and 7.8 yr, respectively. A comparison of Figs. 2.9(A) and (B) shows an Ostwald ripening of the G-phase after aging at 400°C for 7.6 yr. The absence of an intensity peak corresponding to the α' size (1-2 nm) in Fig. 2.9 is not surprising since a distinct phase boundary is not expected between the chromium-rich α' and the chromium-depleted ferrite phase in the materials.

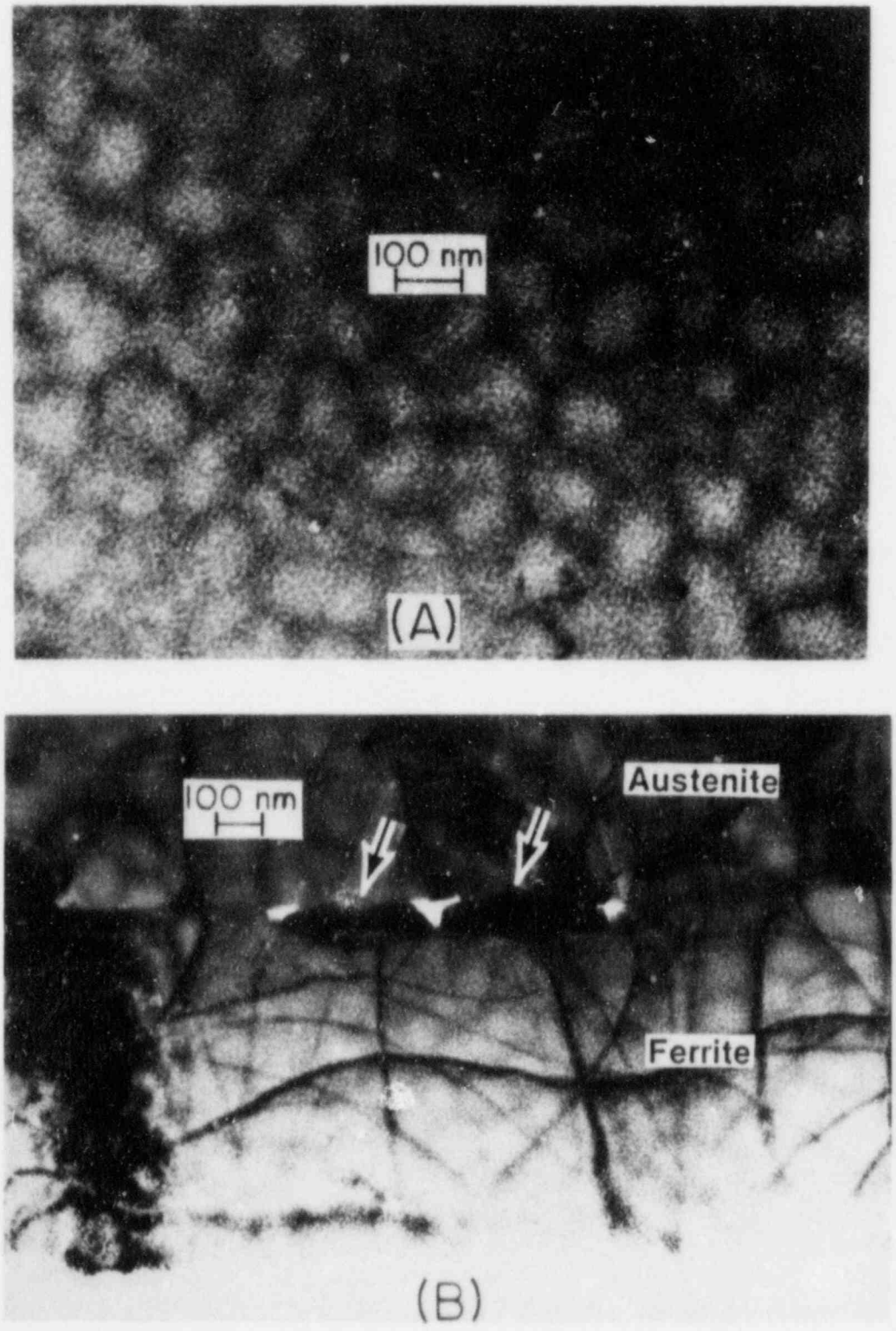

Fig. 2.8. Morphologies of α' in the Ferrite Phase of the Reactor Pump Cover (A) and Heat 60 of Cast Duplex Stainless Steel after Aging at 400°C for 10,000 h (B). $M_{23}C_6$ precipitates on the phase boundary are denoted by arrows in (B).

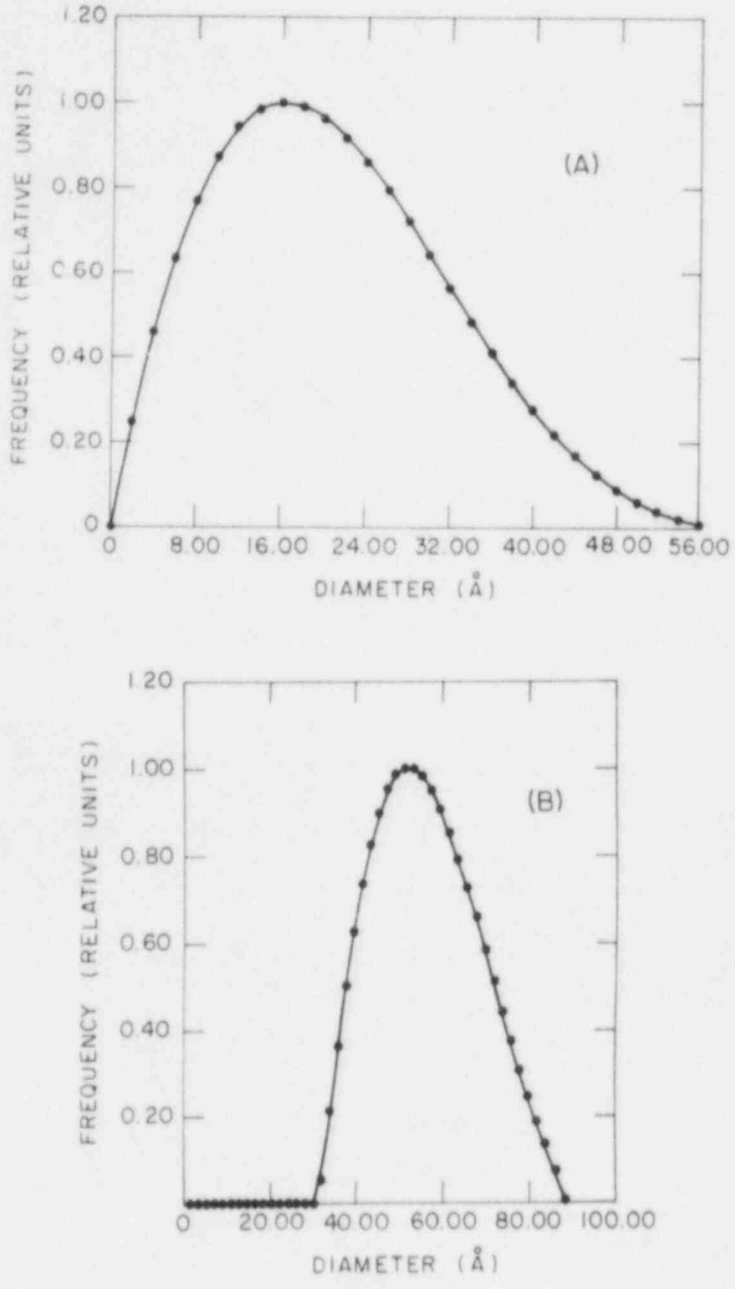

Fig. 2.9. Relative Population of Precipitates vs Guinier Diameter Obtained by Small-angle Neutron Scattering Technique for the G. Fischer Cast Duplex Stainless Steel Heat 278 after Aging at 400°C for (A) 1.2 yr and (B) 7.6 yr.

4. Grain Boundary Precipitate

A distinct difference between the microstructures of the laboratory-aged GF materials and the reactor pump-cover material involves precipitation of a grain boundary phase in the latter. Bright- and dark-field morphologies and a SAD pattern of the grain boundary phase observed in the KRB pump cover have been reported previously.[3] The phase was observed on the boundary between the austenite and ferrite grains. Several different zone axes of the SAD patterns were obtained. Indexing of the diffraction patterns showed that the grain boundary precipitates were $M_{23}C_6$ carbides (fcc, lattice constant observed ~1.065 nm), which had cube-on-cube orientation relative to austenite. The overall distribution of the grain boundary phase could be more clearly observed in low-magnification optical micrographs. For example, in the KRB pump material, ~60% of the austenite-ferrite grain boundaries are decorated by the phase; this observation indicates a possible weakening of the grain boundaries.[3] Aging of Heat 60 also yielded grain boundary precipitation of the $M_{23}C_6$ carbide [Fig. 2.8(B)]. The chemical composition of Heat 60 is very similar to that of the reactor pump material. However, the grain boundary $M_{23}C_6$ carbide was not observed in the low-carbon Heat 51 after aging at 400°C for ~1.2 yr. The absence of grain-boundary carbide precipitates in Heat 51 and the GF materials, i.e., Heats 280 and 278, is most likely related to the low-carbon contents (Table 2.1) compared to the higher carbon contents of the reactor pump cover and Heat 60 materials.

The precipitation of grain boundary carbides appears to be responsible for the rapid reduction in the impact energy for the high-carbon Heat 60 compared to that for Heat 51 [Fig. 2.5(a)]. However, the microstructural characteristics of the ferrite matrix are similar for the two heats and, as expected, the hardnesses of the ferrite phase are comparable [Fig. 2.5(b)]. The grain-boundary $M_{23}C_6$ precipitation in Heat 60 was significantly smaller after aging at 350°C for 10,000 h than after aging at 400°C for similar times. This is believed to be one of the factors that contribute to the higher impact energies for Heat 60 aged at 350°C relative to those aged at higher temperatures. However, the lower hardness of the ferrite phase for the material aged

at 350°C indicates that other factors, viz., the microstructural characteristics of the ferrite matrix, also contribute to the overall embrittlement behavior.

5. SEM Fractography

Comparative fracture surface morphologies of the laboratory-aged GF materials and the reactor pump-cover material were evaluated by SEM after room-temperature impact tests. The fracture surface morphology of the ferrite phase of the reactor pump cover and the GF material aged at 300°C for 8 yr or at 400°C for 1.2 yr was invariably cleavage-type (Fig. 2.10), which means negligible ductility of the phase. Undoubtedly, the ferrite was generally embrittled by one or more combinations of the above-mentioned precipitates, i.e., G-phase, Type-X, and α'. It was, in fact, possible to map the cleavage-ferrite and ductile-austenite portions of a given fracture surface. The cleavage map of the reactor pump cover indicated that ~50-60% of the overall fracture surface was ferrite, although the ferrite volume fraction was only ~30%. Although not conclusive, this finding indicates preferential crack propagation along the ferrite phase under the impact condition. There was also some indication of decohesion along the grain boundary of the reactor pump-cover material, as shown in Fig. 2.10(B). The relatively smooth morphology shown in Fig. 2.10(B) appears to correspond to grain boundaries that are partly covered by ductile tears. However, for the laboratory-aged GF materials, the austenite fracture surface morphology invariably showed transgranular ductile failures, as in Fig. 2.10(A). The intergranular decohesion of aged cast duplex stainless steel, associated with the austenite/ferrite boundary carbide precipitation, may have been observed by other investigators.[11]

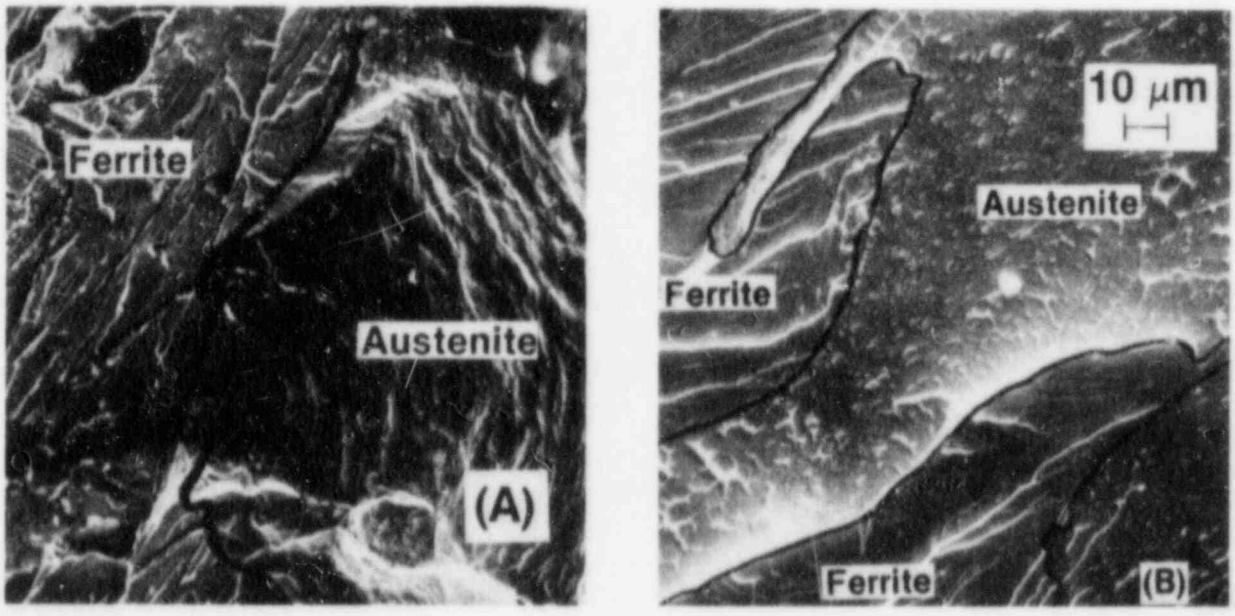

Fig. 2.10. Comparison of Fracture Surface Morphologies of (A) the Room-Temperature Impact-tested Specimens of the G. Fischer Material Aged at 300°C for 8 yr and (B) the Reactor Pump Cover Material after 12 yr of Service in a Boiling-Water Reactor.

C. References for Chapter II

1. A. Trautwein and W. Gysel, "Influence of Long Time Aging of CF-8 and CF-8M Cast Steel at Temperatures Between 300 and 500 deg. C on the Impact Toughness and the Structure Properties," Spectrum, Technische Mitteilungen aus dem+GF+Konzern, No. 5 (May 1981); Stainless Steel Castings, eds. V. G. Behal and A. S. Melilli, ASTM STM 756 (1982), p. 165.

2. O. K. Chopra and G. Ayrault, Long-Term Embrittlement of Cast Duplex Stainless Steels in LWR Systems: Annual Report, October 1982-September 1983, NUREG/CR-3857, ANL-84-44 (July 1984); Nucl. Eng. Des. 86, p. 69 (1985).

3. O. K. Chopra and H. M. Chung, in Materials Science and Technology Division Light-Water-Reactor Safety Research Program: Quarterly Progress Report, October-December 1984, NBUREG/CR-3998 Vol. III, ANL-84-60 Vol. III (October 1985), pp. 48-61.

4. O. K. Chopra and G. Ayrault, in Materials Science and Technology Division Light-Water-Reactor Safety Research Program: Quarterly Progress Report, October-December 1983, NUREG/CR-3689 Vol. IV, ANL-83-85 Vol. IV (August 1984), pp. 129-151.

5. O. K. Chopra and H. M. Chung, in Materials Science and Technology Division Light-Water-Reactor Safety Materials Engineering Research Programs: Quarterly Progress Report, January-March 1984, NUREG/CR-3998 Vol. I, ANL-84-60 Vol. I (September 1984), p. 52.

6. H. M. Chung and O. K. Chopra, "Microstructure of Cast-Duplex Stainless Steel after Long-Term Aging," in Proc. Second Intl. Symp. on Environmental Degradation of Materials in Nuclear Power Systems - Water Reactors, September 9-12, 1985, Monterey, CA, to be published.

7. G. T. Brown and R. T. Allsop, Embrittlement of a 12%Cr-4Ni Steel, J. Iron Steel Inst. (1960), p. 435.

8. D. S. Gelles and L. E. Thomas, "Effects of Neutron Irradiation on Microstructure in Commercial and Experimental Ferritic Alloys," presented at Topical Conf. on Ferritic Alloys for Use in Nuclear Energy Technologies, June 19-23, 1983, Snowbird, UT.

9. D. J. H. Cockayne, "The Weak-Beam Method of Electron Microscopy," in Diffraction and Imaging Techniques in Material Science, S. Amelinckx, R. Gevers, and J. Van Landuyt, eds., North Holland, 1978, Vol. I, pp. 153-183.

10. J. E. Epperson, J. S. Lin, and S. Spooner, "The Fine Scale Microstructure in Cast and Aged Duplex Stainless Steels Investigated by Small Angle Neutron Scattering," to be published.

11. J. R. Donati, Electricité de France, France, private communication.

Distribution for NUREG/CR-4490 Vol. I (ANL-85-75 Vol. I)

Internal:

R. Avery
O. K. Chopra
H. M. Chung
L. W. Deitrich
D. R. Diercks
F. Y. Fradin
B. R. T. Frost
D. M. Gruen
P. R. Huebotter
T. F. Kassner (10)
K. L. Kliewer
D. S. Kupperman
P. S. Maiya
V. A. Maroni
K. Natesan
F. A. Nichols
J. Y. Park
W. E. Ruther
R. A. Scharping
W. J. Shack (5)
W. K. Soppet
E. M. Stefanski (2)
C. E. Till
R. A. Valentin
R. W. Weeks
H. Wiedersich
ANL Patent Dept.
ANL Contract File
ANL Libraries (2)
TIS Files (5)

External:

NRC, for distribution per R5 (350)
DOE-TIC (2)
Manager, Chicago Operations Office, DOE
R. Dalton, DOE-CH
Materials Science and Technology Division Review Committee:
C. B. Alcock, U. Toronto
A. Arrott, Simon Fraser U.
M. H. Cohen, Exxon Research and Engineering Co., Annandale, N. J.
R. C. Dynes, AT&T Bell Labs., Murray Hill
A. G. Evans, U. California, Santa Barbara
E. Kay, IBM San Jose Research Lab.
M. B. Maple, U. California, San Diego
P. G. Shewmon, Ohio State U.
J. K. Tien, Columbia U.
J. W. Wilkins, Cornell U.
R. B. Adamson, General Electric Co., Vallecitos Nuclear Center, P. O. Box 460, Pleasanton, Calif. 94566
P. L. Andresen, General Electric Corporate Research and Development, Schenectady, N. Y. 12301
G. A. Arlotto, Office of Nuclear Regulatory Research, USNRC, Washington
D. Atteridge, Battelle Pacific Northwest Lab., P. O. Box 999, Richland, Wash. 99352
W. H. Bamford, Structural Materials Engineering, Westinghouse Electric Corporation, WNES, Box 355, Pittsburgh, Pa. 15230
W. Berry, Battelle-Columbus Labs., 505 King Ave., Columbus, O. 43201
C. Y. Cheng, Office of Nuclear Reactor Regulation, USNRC, Washington
W. J. Collins, Office of Inspection and Enforcement, USNRC, Washington
A. Cowan, Risley Nuclear Power Development Labs., U. K. Atomic Energy Authority, Risley, Warrington, WA3 6AT, England
G. Cragnolino, Brookhaven National Lab., Upton, N. Y. 11973
R. M. Crawford, NUTECH Engineers, 225 N. Michigan Ave., Chicago, Ill. 60601
D. Cubiciotti, Electric Power Research Inst., P. O. Box 10412, Palo Alto, Calif. 94303
W. H. Cullen, Materials Engineering Associates, Inc., 9700 B. George Palmer Highway, Lanham, Md. 20706
J. C. Danko, AWTAC, New Topside Rd., Route 4, Box 90, Louisville, Tenn. 37777
B. J. L. Darlaston, CEGB, Berkeley Nuclear Labs., Berkeley, Glos., England
H. Domian, Alliance Research Center, Babcock & Wilcox Co., Alliance, O. 44601
B. J. Elliot, Office of Nuclear Reactor Regulation, USNRC, Washington
M. Fox, Route 2, Box 252, Athens, Ala. 35611
Y. S. Garud, S. Levy, Inc., 1901 S. Bascom Ave., Campbell, Calif. 95008
J. H. Gittus, Springfields Nuclear Power Development Labs., U. K. Atomic Energy Authority, Springfields, Salwick, Preston PR4 ORR, England

M. Guttmann, Electricite de France, Les Renardieres Roule de Sens, 77 Ecuelles, France
W. Gysel, Georg Fischer, Ltd., Schaffhausen, Switzerland
D. O. Harris, 750 Welch Rd., Palo Alto, Calif. 94303
W. S. Hazelton, Office of Nuclear Reactor Regulation, USNRC, Washington
P. Hedgecock, APTECH Engineering Services, Inc., 795 San Antonio Rd., Palo Alto, Calif. 94303
B. Hemsworth, HM Nuclear Installations Inspectorate, Thames House North, Millbank, London SW1P 42J, England
M. E. Indig, General Electric Co., P. O. Box 460, Pleasanton, Calif. 94566
R. E. Johnson, Office of Nuclear Reactor Regulation, USNRC, Washington
W. V. Johnston, Office of Nuclear Reactor Regulation, USNRC, Washington
R. L. Jones, Electric Power Research Inst., P. O. Box 10412, Palo Alto, Calif. 94303
J. Kass, General Electric Co., 175 Curtner, San Jose, Calif. 95125
P. M. Lang, Office of Converter Reactor Deployment, USDOE, Washington, D. C. 20545
L. Ljungberg, ASEA-ATOM, Box 53, S-721 04, Västerås, Sweden
J. Muscara, Office of Nuclear Regulatory Research, USNRC, Washington
D. M. Norris, Electric Power Research Inst., P. O. Box 10412, Palo Alto, Calif. 94303
D. R. O'Boyle, Commonwealth Edison Co., P. O. Box 767, Chicago, Ill. 60690
R. A. Oriani, U. Minnesota, Minneapolis, Minn. 55455
S. Ranganath, General Electric Co., 175 Curtner, San Jose, Calif. 95125
J. T. A. Roberts, Battelle Pacific Northwest Lab., P. O. Box 999, Richland, Wash. 99352
E. J. Rowley, Commonwealth Edison Co., P. O. Box 767, Chicago, Ill. 60690
E. F. Rybicki, Dept. of Mechanical Engineering, U. Tulsa, Tulsa, Okla. 74110
C. Z. Serpan, Office of Nuclear Regulatory Research, USNRC, Washington
L. Shao, Office of Nuclear Regulatory Research, USNRC, Washington
V. K. Sikka, Oak Ridge National Lab., P. O. Box X, Oak Ridge, Tenn. 37830
R. D. Silver, Office of Nuclear Reactor Regulation, USNRC, Washington
G. Slama, Framatome, Tour FIAT, Cedex 16, 92084 Paris la Defense, France
P. Smerd, Combustion Engineering, Inc., P. O. Box 500, Windsor, Conn. 06095
S. Smialowska, Dept. of Metallurgical Engineering, Ohio State U., Columbus, O. 43210
L. J. Sobon, NUTECH Engineers, 6835 Via del Oro, San Jose, Calif. 95119
A. A. Solomon, School of Nuclear Engineering, Purdue U., West Lafayette, Ind. 47907
H. D. Solomon, General Electric, P. O. Box 43, Schenectady, N. Y. 12301
D. M. Stevens, Lynchburg Research Center, Babcock & Wilcox Co., P. O. Box 239, Lynchburg, Va. 24505
A. Taboada, Office of Nuclear Regulatory Research, USNRC, Washington
L. Taylor, National Nuclear Corp., Cambridge Rd., Whetstone, Leicester LE8 3LH, England
R. A. Walker, The Welding Inst., Abington Hall, Abington, Cambridge, CB1 6AL, England
J. R. Weeks, Brookhaven National Lab., Upton, N. Y. 11973
K. R. Wichman, Office of Nuclear Reactor Regulation, USNRC, Washington

NRC FORM 335 (2 84) NRCM 1102 3201 3202

U.S. NUCLEAR REGULATORY COMMISSION

BIBLIOGRAPHIC DATA SHEET

SEE INSTRUCTIONS ON THE REVERSE

1 REPORT NUMBER (Assigned by TIDC and Vol. No. if any)

NUREG/CR-4490 Vol. I
ANL-85-75 Vol. I

2 TITLE AND SUBTITLE

Light-Water-Reactor Safety Materials Engineering Research Programs: Quarterly Progress Report, January-March 1985

3 LEAVE BLANK

4 DATE REPORT COMPLETED

MONTH | YEAR

5 AUTHOR(S)

W. J. Shack et al.

6 DATE REPORT ISSUED

MONTH: March | YEAR: 1986

7 PERFORMING ORGANIZATION NAME AND MAILING ADDRESS (Include Zip Code)

Argonne National Laboratory
9700 South Cass Avenue
Argonne, Illinois 60439

8 PROJECT/TASK/WORK UNIT NUMBER

9 FIN OR GRANT NUMBER

A2212, A2243

10 SPONSORING ORGANIZATION NAME AND MAILING ADDRESS (Include Zip Code)

Division of Engineering Technology
Office of Nuclear Regulatory Research
U. S. Nuclear Regulatory Commission
Washington, D. C. 20555

11a TYPE OF REPORT

Quarterly

b PERIOD COVERED (Inclusive dates)

January-March 1985

12 SUPPLEMENTARY NOTES

13 ABSTRACT (200 words or less)

This progress report summarizes the Argonne National Laboratory work performed during January, February, and March 1985 on water reactor safety problems related to out-of-core materials. The research and development areas covered are Environmentally Assisted Cracking in Light Water Reactors and Long-Term Embrittlement of Cast Duplex Stainless Steels in LWR Systems.

14 DOCUMENT ANALYSIS - a KEYWORDS/DESCRIPTORS

Crack growth
Embrittlement cast stainless steel
Low-temperature aging
Phase precipitation and identification
Sensitization
Stress corrosion cracking
Water chemistry
Weld overlays

b IDENTIFIERS/OPEN ENDED TERMS

15 AVAILABILITY STATEMENT

unlimited

16 SECURITY CLASSIFICATION

(This page) unclassified

(This report) unclassified

17 NUMBER OF PAGES

80

18 PRICE